Design of a 3D Printed, Man-portable, Unmanned Aerial Vehicle

a project presented to
The Faculty of the Department of Aerospace Engineering
San José State University

in partial fulfillment of the requirements for the degree

Master of Science in Aerospace Engineering

by

Aaron M. Do

May 2025

approved by

Dr. Yawo Ezunkpe

Faculty Advisor

ABSTRACT

Design of a 3D Printed, Man-portable, Unmanned Aerial Vehicle

Aaron Do

3D printing is a manufacturing technology that has revolutionized the production of goods. It allows for increased flexibility in design, a faster developmental timeline, and reduced costs. In the aerospace industry, 3D printing is being used to manufacture vital components in the engines of some of the most modern passenger airliners the world has ever seen. Another development in the industry is the proliferation of UAVs, with many companies developing and utilizing both fixed-wing and rotor-based drones. This project hopes to combine the two developments together. The design that came out is a flying-wing aircraft, with a wingspan of 1250 mm, a length of 700 mm, and an estimated weight of 2.5 kg.

ACKNOWLEDGEMENTS

I would like to express my heartfelt gratitude to my mother and father for their unwavering support throughout my entire life. Without them, I would not be the person I am here today. I am also deeply thankful to my sister Amanda for constantly pushing me to do my best, and my other sister, Audrina, for always reminding me to take breaks and care for myself. Special thanks to Dr. Yawo Ezunkpe and the faculty in San Jose State University, whose guidance and feedback were invaluable throughout the course of this project. Finally, I am forever grateful to my uncle, Tom Bien Nguyen, for showing me the wonders of 3D printing.

Table of Contents

List of Figures

Chapter 12 —Weight and Balance

Chapter 13 — Flight Components

Chapter 14 — Subsystem Arrangement

Chapter 15 — 3D Printing Preparations

Chapter 16 — 3D Printing Settings and Process

Chapter 18 — Assembly

Chapter 19 — Closing Remarks

List of Tables

List of Symbols

Symbol	Definition	Unit (SI)	Unit (Imperial)
AR	Aspect ratio	-	
AR_{wetted}	Wetted aspect ratio	-	
b	Wingspan	m	ft
BMF	Battery mass fraction	-	
c	Chord length	m	ft
C_D	Coefficient of Drag	-	
C_L	Coefficient of Lift	-	
C_M	Coefficient of Moment	-	
E	Endurance	hr	
E_{sb}	Energy of Battery	Wh/kg	-
E_T	Total Energy	-	
g	Gravity	m/s^2	ft/s^2
h	Altitude	m	ft
L/D_{max}	Max lift-to-drag ratio	-	
m_b	Mass of battery	lbs	kg
m_i	Mass of component	lbs	kg
m_{total}	Total mass	lbs	kg
MAC	Mean aerodynamic chord	m	ft
NP	Neutral point	m	ft
p	Pressure	-	
P_{used}	Power used	kW	-
P_r	Prandtl Number	-	
q	Heat flux	-	
R	Range	m	ft
R_e	Reynold's Number	-	
S	Reference wing area	m^2	ft^2
$\frac{S_{wet}}{S_{ref}}$	Wetted area ratio	-	
SM	Static margin	m	ft
u	u-component of velocity	-	
v	v-component of velocity	-	
V	Horizontal Velocity	m/s	ft/s
V_V	Vertical Velocity	m/s	ft/s
w	w-component of velocity	-	
W_0	Weight @ takeoff	kg	lbs
$W_{Payload}$	Weight of Payload	kg	lbs
X_{cg}	Center of gravity @ x-axis	m	ft
x_i	Location (x-axis) of component	m	ft
Y_{cg}	Center of gravity @ y-axis	m	ft
y_i	Location (y-axis) of component	m	ft

Greek			
η_{b2s}	Efficiency from battery to system	-	
η_p	Efficiency of propeller	-	
λ	Taper ratio	-	
ρ	Density	kg/m^3	$slugs/ft^3$
μ	Dynamic viscosity of fluid	m^2/s	ft^2/s
τ	Stress	-	

Chapter 1 — Introduction

1.1 Introduction

One of the most important advancements in aviation is the recent rise in the use of Unmanned Aerial Vehicles (UAVs), commonly referred to as drones. These drones can perform a variety of tasks, from aerial photography to package delivery. The most common drone type being used are quadcopters, due to their ability to hover and move with precision. Fixed-wing drones offer higher speeds and a heavier payload but are harder to control. Another important advancement is the proliferation of 3D printers. Compared to traditional methods, 3D printing has a lower barrier to entry for individuals, while also being easier to operate than a lathe or a CNC machine.

1.2 Literature Review.

Resources are split into four sections, an overview of 3D printing in the aerospace industry, the usage of flying wings, the steps to fabricate small drones, and a look at other small flying-wing drones on the market. These sections are going to be vital in the development of the flying-wing RC-UAV.

1.2.1 Overview of Additive Manufacturing in the Aerospace Industry

The aerospace industry is one of the first industries to utilize additive manufacturing, commonly referred to as 3D Printing. According to Fu et al, additive manufacturing, allows a user to manufacture geometrically complex components [1]. This is done by creating the component layer by layer, millimeters at a time. Additive manufacturing can also use a large variety of materials which include metals, polymers, composites, and ceramics. The main reason why the aerospace industry has embraced additive manufacturing is due to the promised weight reductions the technology provides, without sacrificing safety.

One of the earliest examples of this is General Electric's usage of additive manufacturing to develop a new fuel nozzle injector [2]. In 2003, GE was having issues with a new injector they were developing. Early injectors were made from 20 different parts that had to be welded and machined together. Mass production of these components was going to be difficult and expensive. So, the company initiated a project with Morris Technologies, an early additive manufacturing company, to develop a way to manufacture the injector. By 2005, Morris Technologies was able to successfully build a new injector that combined all 20 separate parts into 1 single component, while also reducing weight by 25% and being 5 times more durable [3]. By 2012, Morris and GE developed manufacturing parameters to mass-produce the injector. Currently, the injector is used by GE in its LEAP engine, which is on the Airbus A320neo, Boeing 737 MAX, and Comac C919.

Figure 1.1 – Morris Technologies's 3D printed fuel nozzle [2]

Although printing with metal is used in high-end applications, polymers are still the most popular material to print with [4]. Unlike metal, polymers have a relatively low melting temperature, meaning they don't require a lot of heat to manipulate. Plastics usually have a melting temperature range from 200° C to 400° C, while metals have a melting temperature of 1100°C to 1400° C. The lower melting temperature polymers use not only decreases the complexity of the polymer printer, making prices low when compared to metallic printers, but is also extremely useful for rapid prototyping, as print times as quicker on polymer printers. The most common filament used is polylactic acid (PLA) followed by (acrylonitrile butadiene styrene (ABS) [5].

Additive manufacturing provides the user unparalleled flexibility when compared to conventional manufacturing. Currently, hospitals are creating custom biomedical implants for their patients, while clothing companies are utilizing additive manufacturing to develop clothing that is fitted to any body type [6]. The ability to create parts on-site is therefore a large advantage, as cutting inventory and shortening supply chains would lower costs overall. Additive manufacturing is expected to produce $2 trillion worth of components by 2030.

The usage of additive manufacturing would allow the creation of a single-print wing, with an integrated wing structure already built [7]. Traditionally, a wing would be made up of a series of ribs and spars to maintain the wing's shape, with a skin on top of the structure for aerodynamics. With additive manufacturing, however, a small wing can be formed that has a lattice structure inside for structural support. Seung et al experimented with a 3D Kagome structure, a hexagonal diamond structure, and a 3D pyramidal structure for the wing. The research Seung et al conducted determined that the Kagome structure was able to withstand high compression stress the best.

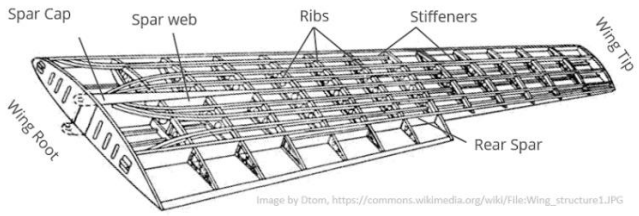

Figure 1.2 – Internal structural of a semi-monocoque aircraft wing [8]

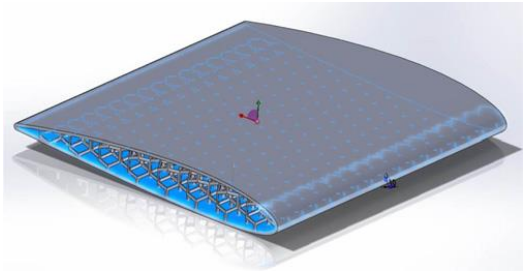

Figure 1.3 – Seung et al's CAD model of proposed reinforced wing with Kagome reinforcements [7]

1.2.2 Overview of Flying Wings

Flying wing designs date to the earliest days of aviation. Even back then, scientists and engineers were enamored with the potential for more efficient aircraft. In 1933, Walter and Reimar Horten began testing flying wing gliders, before transitioning to a jet-powered flying wing during 1944, with the Horton Ho-229 [9]. On the other side of the war, the Northrop Corporation were developing their own flying wings, in the N-1M, which had its first flight in 1940. Northrop was also developing the XB-35 long-range flying wing bomber during the war, but production issues delayed its first flight until 1946. The four contra-rotating propellers that power the XB-35 was outdated in the post-war years. So, Northrop replaced the four propellers with eight jet engines in the YB-49, which took first flight in 1947 [10] Another famous flying-wing was the Avro Vulcan took its first flight in 1952. The Vulcan bomber eventually grew to backbone of the UK's nuclear bomber fleet for most of the Cold War [11]. The most famous flying wing however, is the Northrop B-2 Stealth Bomber, which took its first flight in 1989 [2].

Figure 1.4 – Northrop N-1M [13]

The benefits of a flying wing design have always been well understood. In theory, a high lift-to-drag ratio could be achieved reducing the amount of parasitic drag the aircraft faces, a job flying wings are designed for. The Northrop B-2 is believed to have a lift-to-drag ratio of 22 [14]. A successful flying wing design is expected to reduce the required runway length the aircraft uses for takeoff and landing and improve fuel efficiency by 15-20% [15]. However, balancing the aspect ratio and the wing area is necessary to ensure an optimal lift-to-drag ratio during flight.

The potential downsides of a flying wing are also well understood. Due to the tailless design of the concept, the aircraft's longitudinal controllability would be at risk, due to the aircraft lacking a horizontal stabilizer. Most flying wings also fly without a vertical stabilizer, meaning that the aircraft is unstable in yaw. On the B-2, the aircraft uses a series of elevons to control both roll and pitch, while also using a split rudder to control yaw [16]. To control both the longitudinal and lateral stability of the aircraft, control systems must be implemented to ensure controllability of the aircraft throughout its flight

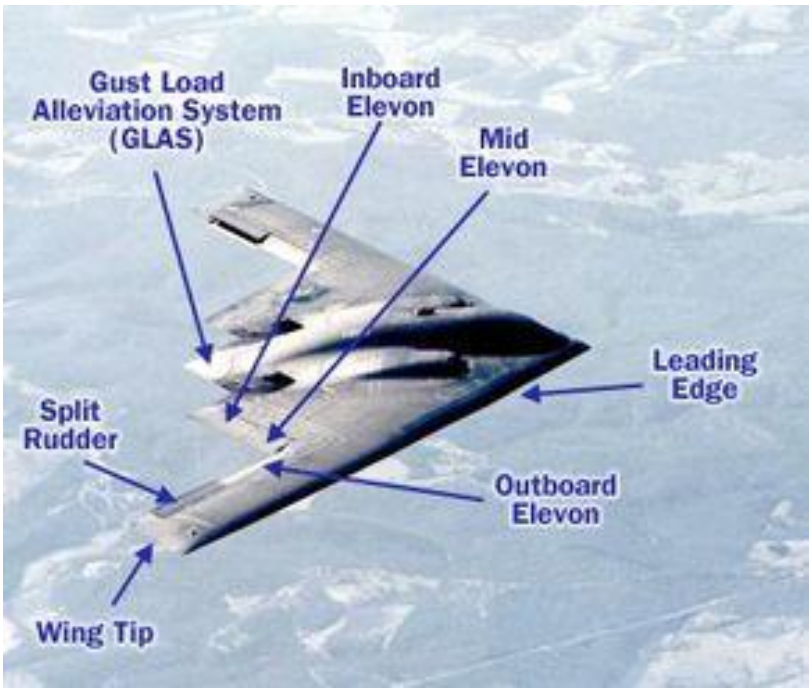

Figure 1.5 – Control surfaces of a B-2 stealth bomber [17]

1.2.3 Fabrication of Fixed-Wing Drones

The fabrication of fixed-wing drones is a well-studied subject in aerospace. Currently, the design of a drone can be split into three main phases: the conceptual design, the preliminary design, and the detailed design [18]. In the conceptual design phase, market research is done to identify the feasibility of an aircraft. The wing shape, position, fuselage, empennage configuration, propulsion system, and landing gear is identified early in the development cycle. The preliminary design occurs when constraints are put upon the aircraft, as stated by the potential mission. For example, a Short-Takeoff-and-Landing (STOL) aircraft might have a minimum take-off distance of 100 ft, while a passenger airliner must be able to carry 150 passengers. A matching graph is used to identify an optimal thrust-to-weight ratio and wing loading, comparing a variety of parameters. During the detailed-design phase, the wing airfoil, motor, are chosen. To choose the airfoil, XFLR5 is used to simulate and analyze the aircraft's performance with different airfoils at different flight regimes, giving the engineer a list of airfoils which would be able to perform the given mission [19]. Depending on the engineering team though, the conceptual design phase and the preliminary design phase are combined, as seen in Panagiotopoulos et al's team [20].

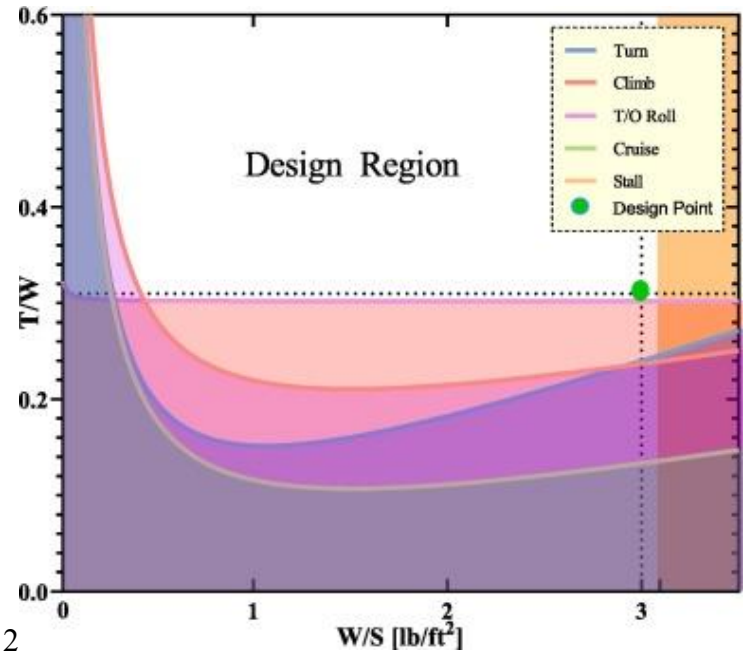

2

Figure 1.6 – El Adawy et al's matching graph [18]

After the design phase is finalized, construction can finally begin. Traditionally, aluminum, wood, and steel used in the industry [21]. However, the 21st century saw the introduction of composites, such as carbon fiber, as a leading material in aviation, due to their increased strength while being lighter than the traditional materials. Chung et al's flying wing drone utilized laser-cutting to create ribs made from balsa wood to create the internal structure of UAV. Meanwhile, a carbon-fiber, glass-fiber, and epoxy mix was used to create the skin [22]. As a result, Chung's team was able to develop a drone with a wingspan of 3.0 m, a length of 1.2 m, and a weight of the drone is 8.62 kilograms.

Figure 1.7 – Chung et al's drone [22]

1.2.4 Examples of Man-portable Flying Wing Drones

The Skywalker X8 UAV is a man-portable flying wing drone. Developed by Skywalker Technology Co., based in Wuhan, China, the aircraft has a wingspan of 212 centimeters and a length of 79 centimeters. The aircraft is made of composites and EPO foam and has a gross weight of 3-6 kilograms. The aircraft has a maximum flight time of 25 minutes and a maximum airspeed of 70 km/h. The drone can take off from a catapult launch, or hand thrown.

Figure 1.8 – Skywalker X8 UAV [23]

The Super Stingray is a 3D-printed flying wing UAV developed by Flightory and has a wingspan of 113 centimeters and a length of 70 centimeters. The aircraft is made of LW-PLA and PETG polymers and has a gross weight of 1-2.5 kilograms. When equipped with the recommended electronics, the drone has nearly 3 hours of flight time and a max airspeed of 90 km/h. The drone needs to be tossed into the air to take off.

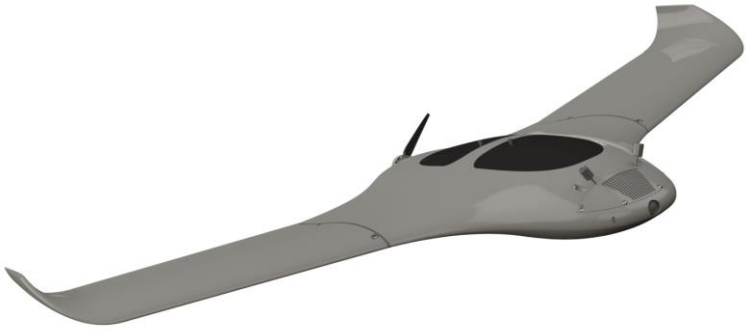

Figure 1.9 – Super Stingray UAV [24]

The Eclipson EGW-80 “Graywing” is a 3D-printed FPV flying wing designed by Eclipson Airplanes. The Graywing is designed to be fast and agile with a wingspan of 80 centimeters, and a total length of 75 centimeters. When printing the aircraft, the user can use either LW-PLA or PLA. If the user decides to use PLA, then the aircraft weighs 750 grams.

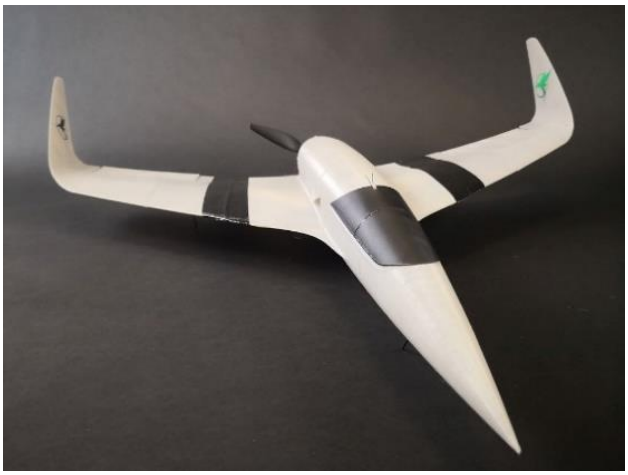

Figure 1.10 – Eclipson EGW-80 “Graywing” [25]

1.3 Project Objective

The objective of this project is to develop and prototype a man-portable, flying-wing RC-UAV, named Beansky. The airframe of the UAV is going to be 3D printed, utilizing a commercial 3D printer. The servos, motors, battery, and electronics that are used to control the aircraft are going to be sourced from the market. The man-portable requirement will be fulfilled by having two requirements: the aircraft must weigh less than 2.5 kilograms and it must be carried by a single person when not it is not in use. A way to make it more man-portable, while having a large wing is to be able to tear-down the aircraft when it's not in use. When the pilot needs to the use the aircraft, they should be able to prepare the aircraft as quickly as possible.

1.3.1 Deliverables

In addition to obligatory reports, the most important deliverables are as follows:

- A .rar file that contains the required 3D printing files
- A 3D printed mock-up with electronics

1.3.2 Evaluation Metrics

Success in this endeavor will be measured by the following evaluation metrics:

- Ability to print components
- Transportability
- Ease of assembly and disassembly in-field

1.4 Methodology

A preliminary design of the Beansky will be developed using other 3D printed aircraft to determine the general size of the aircraft. The current plan is for the aircraft to utilize a flying wing design, due to the promised performance increase have during low-speed regimes. To create a CAD model of the preliminary design, SolidWorks is going to be used. To determine the best airfoil to use, XFLR5 will be used. CFD testing will also be conducted on the preliminary design to confirm the aircraft's flight performance. After the CFD work is complete, the final aircraft design can be completed, which includes the files used to print out the aircraft. After the mock-up is completed, tests will be conducted to determine how easy or difficult it is to set up the aircraft. Flight tests will not be conducted due to the high costs of electronics and risk of damages to the airframe.

Chapter 2 — Mission Requirements

2.1 Mission Description

Beansky is designed to be an adaptable flying wing, prop driven aircraft capable of many missions, from land surveillance to search-and-rescue missions. The aircraft is intended to be hand-launched, allowing the user to launch the UAV anywhere, without any infrastructure. To recover the UAV, Beansky must conduct a belly landing. This can potentially damage the aircraft, due to the potential landing site being too hard. Therefore a choice of a wire skid to be installed later can be used to cushion the aircraft. While landing, the aircraft's propeller is expected to be damaged, therefore the pilot would need to replace it.

2.2 Mission Profile

The mission profile that the aircraft is expected to fulfill depends on the sensors installed on the aircraft. In this example, Beansky will be equipped with a thermal camera and a GPS to conduct aerial search and rescue missions and map landmarks for first responders. The mission profile is as follows:

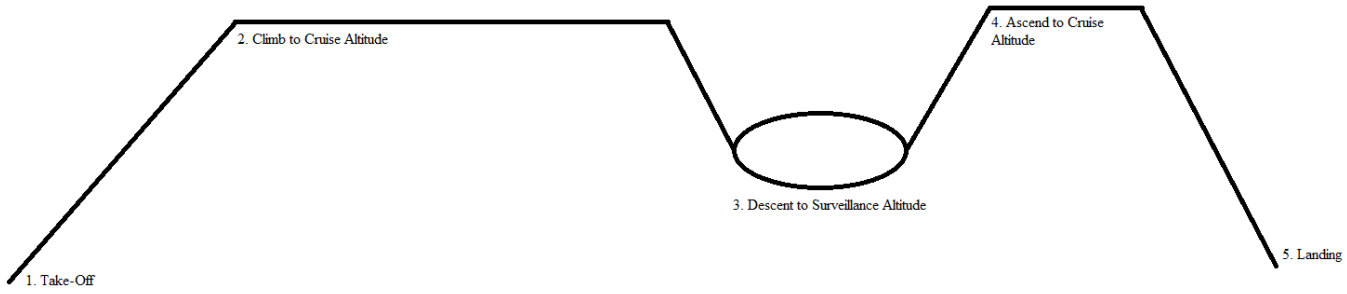

Figure 2.1 – Beansky mission profile for surveillance

2.3 Aircraft Requirements

A key requirement for Beansky is that it must be man-portable. This means that a single person must be able to configure the aircraft for flight, set up communications, fly, and store the aircraft without external assistance. To do so, the wings will be detachable from the aircraft. The electronics and sensors on the aircraft must also be easily accessible and configurable by the pilot. Another requirement is that as stated before, the aircraft must be hand-launched and be recoverable by the user, to reduce the amount of infrastructure required. In terms of flight performance, Beansky's aerial endurance is prioritized.

Chapter 3 — Similar Aircraft Comparison

The following is a comparison of small, man-portable, flying-wing UAVs, made out of a variety of materials.

Table 3.1 – Aircraft propulsion comparison [23, 24, 25]

	Skywalker X8	Flightory Super Stingray	Eclipson EGW-80 “Graywing”
Propulsion	Dualsky XM4255EA V3 (KV520)	AS2317 3S-4S LongShaft 3D Trainer Airplane Brushless Motor (KV1250)	Sunnysky X2212 2S-4S Brushless Motor (KV1250)
ESC	Flyfun V 6S-14S ESC	T-Motor F35A 3-6S ESC	Aerostar 30A ESC (3S)
# of Engines	1	1	1
Max Power	1344 W	596 W	100 - 300 W
Battery	16000mAH 6S 22.2V LiPo Pack	5000mAH 4S 14.8V LiPo Pack	2200mAH 3S 11.1V LiPo Pack
# of Propeller Blades	2	2	2
Propeller Diameter	14 in	10 in	8 in

Table 3.2 – Aircraft performance [23, 24, 25]

		Skywalker X8	Flightory Super Stingray	Eclipson EGW-80 “Graywing”
Takeoff Method		Hand-launch/ Catapult	Hand-launch	Hand-launch
Landing Method		Belly Landing/ Parachute	Belly Landing	Metal Wires
Stall Speed				35 km/h
Optimal Speed		65-70 km/h	70-90 km/h	
Endurance		25 min	3 hrs	

Table 3.3 – Geometry/Dimensions comparison [23, 24, 25]

	Skywalker X8	Flightory Super Stingray	Eclipson EGW-80 “Graywing”
Wingspan	212.2 cm	113 cm	80 cm
Wing Aspect Ratio	~5.62	3.7	3.5
Wing Loading	~37.5 g/dm^2	32-70 g/dm^2	57 g/dm^2
Wing Airfoil	NACA 65-209 mod	Selig S5020	
Total Length	79 cm	70 cm	75 cm
Wing Area	80 dm^2	31 dm^2	13 dm^2

Material	Composites + EPO Foam	LW-PLA + PETG	PLA
Takeoff Weight	2500 – 3000 g	1000 – 2500 g	750 g

Chapter 4 — Initial Weight Estimate

Raymer's equations are going to be used to calculate the initial weight of the aircraft. These results would then be compared with similar aircraft discussed in Chapter 3 to determine if the sizing is correct.

4.1 Raymer Hand Calculations

4.1.1 Assumptions

Table 4.1 – Flying wing and their aspect ratios

Platform	Aspect Ratio (b^2/S)
Northrop B-2 Spirit	5.76
Northrop Grumman X-47B	4.04
Horten Ho 229	5.35
Skywalker X8	5.62
Flightory Super Stingray	3.7
Eclipson EGW-80 "Graywing"	3.5

Before starting hand calculations, preliminary values need to be obtained. To choose Beansky's aspect ratio, comparisons were made with similar aircraft. Given Beansky's flying wing configuration, an aspect ratio of 4 was chosen.

The next step is to determine Beansky's assumed L/D_{max}. This is determined by first using Fig. 4.1 to determine the aircraft's wetted area ratio. A wetted area ratio of 2 was chosen because of the flying wing configuration of Beansky.

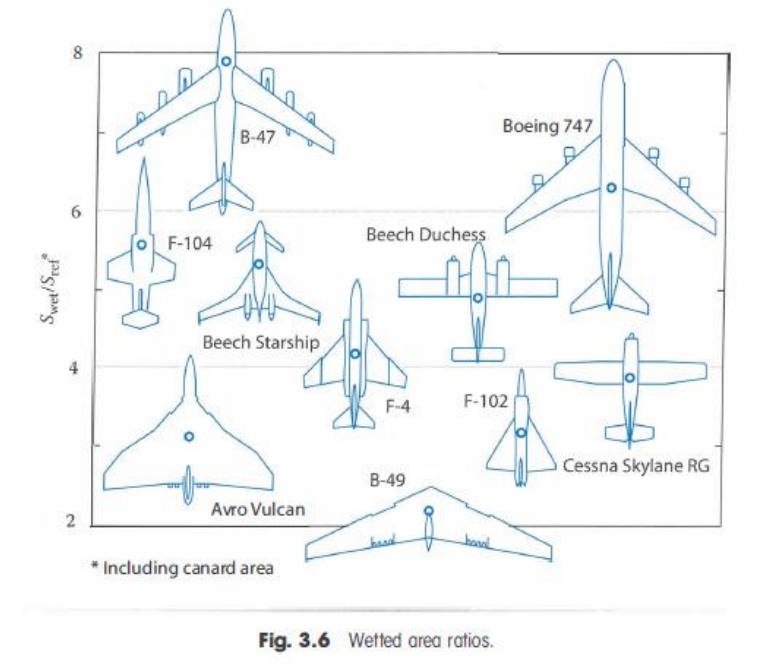

Fig. 3.6 Wetted area ratios.

Figure 4.1 – Raymer's wetted area ratio comparison graph [26]

From the wetted area ratio, a wetted aspect ratio can be obtained by using equation 4.1. Afterwards, the wetted aspect ratio is determined by using the following equation:

$$AR_{Wetted} = AR/(\frac{S_{wet}}{S_{ref}}) \quad (4.1)$$

With an AR_{Wetted} of 2 and by following the retractable prop aircraft line in Fig 4.2., the L/D_{max} can be estimated to be 15. This was reduced to 10 in testing, due to fears of inefficiency due to the home-built nature of the aircraft.

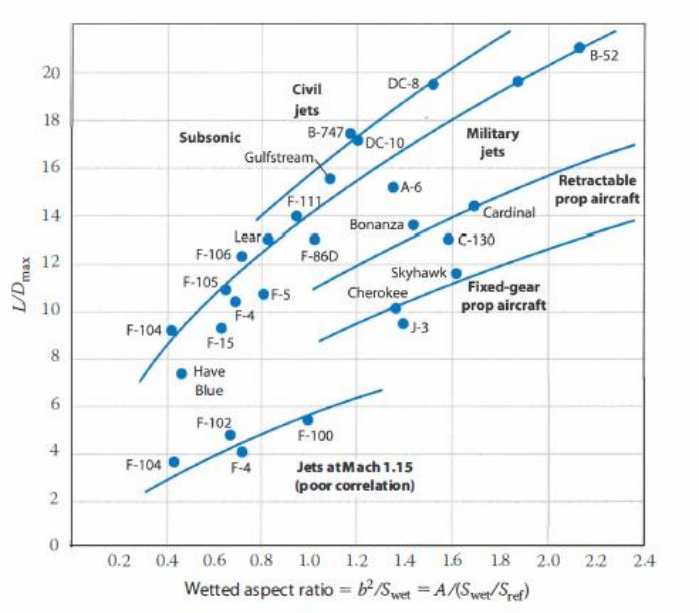

Figure 4.2 – Raymer's maximum lift-to-drag ratio trends based on aircraft [26]

Furthermore, due to Beansky being a small UAV, Table 4.2 shows how the W_e/W_0 is determined.

Table 4.2 – Raymer's empty weight fraction vs W_0 (Table 3.1) [26]

$W_e/W_0 = AW_0^C K_{vs}$	A	C
Sailplane (unpowered)	0.86	-0.05
Sailplane (powered)	0.91	-0.05
Homebuilt (metal/wood)	1.19	-0.09
Homebuilt (composite)	1.15	-0.09
General aviation (single-engine)	2.36	-0.18
General aviation (twin-engine)	1.51	-0.10
Agricultural aircraft	**0.74**	-0.03
Twin turboprop	0.96	-0.05
Flying boat	1.09	-0.05
Jet trainer	1.59	-0.10

Jet fighter	2.34	-0.13
Military cargo/bomber	0.93	-0.07
Jet transport	1.02	-0.06
UAV (tac recce & UCAV)	1.67	-0.16
UAV (high altitude)	2.75	-0.18
UAV (small)	0.97	-0.06

($K_{vs} = variable\ sweep\ constant = 1.04\ if\ varaiable\ sweep = 1.00\ if\ fixed\ sweep$

4.1.2 Raymer's Hand Calculations

According to Raymer, the final weight of the aircraft can be defined as:

$$W_0 = \frac{W_{Payload}}{1 - BMF_{total} - \frac{W_e}{W_0}} \tag{4.2}$$

To estimate the total battery mass fraction (BMF_{total}), the sum of multiple BMFs per mission segment is needed:

$$BMF_{Loiter} = \frac{E\ V\ g}{3.6\ E_{sb}\ \eta_{b2s}\ \eta_p\ L/D} \tag{4.3}$$

$$BMF_{LevelFlight} = \frac{R\ g}{3.6\ E_{sb}\ \eta_{b2s}\ \eta_p\ L/D} \tag{4.4}$$

$$BMF_{Climb} = \frac{h}{3.6\ V_V\ E_{sb}\ \eta_{b2s}} \frac{P_{used}}{m} \tag{4.5}$$

The endurance, range, and vertical velocity needs to be solved to find the BMF per mission segment:

$$E = 3.6 \frac{L}{D} \frac{E_{sb}\ \eta_{b2s}\ \eta_p}{g\ V} \frac{m_b}{m} \tag{4.6}$$

$$R = 3.6 \frac{L}{D} \frac{E_{sb} \eta_{b2s} \eta_p}{g} \frac{m_b}{m} \tag{4.7}$$

$$V_V = \frac{1000\ \eta_p}{g} \frac{P_{used}}{m} - \frac{V}{3.6\ L/D} \tag{4.8}$$

By using an iterative method on equation 4.2, the gross weight of the aircraft can be determined.

Table 4.3 – List of assumptions made

Inputs	Units
$W_{Payload}$	10 [N]
g	9.8 [m/s^2]
m_b	0.178 [kg]
E_{sb}	200 Wh/kg
η_{b2s}	0.9

η_p	0.7
P_{used}	0.028 [kW]
L/D Ratio	10
V	70 [km/h]
h	100 [m]

The aircraft is determined to have a gross weight of 56.45 N, or 5.7 kg.

4.2 Conclusion

The Skywalker X8, Flightory Super Stingray, and Eclipson EGW-80 “Graywing”, has a maximum takeoff weight of 3 kg, 2.5 kg, and 0.75 kg respectively. This makes the calculated weight of Beansky almost twice as heavy as its contemporaries. However, those aircraft utilize extremely lightweight materials, such as foam LW-PLA, and PETG. It is believed that utilizing PLA in the design, Beansky will be able to reduce its weight by nearly a half, as Raymer’s methods assume that the aircraft utilize aluminum and steel in its construction.

Chapter 5 — Preliminary Design

5.1 Introduction

By utilizing the Skywalker X8, Super Stingray, and Blackwing EBW-160 UAVs discussed in Chapter 3 as a baseline, a preliminary design of Beansky can be developed. The Beansky will have a wingspan of roughly 120 cm and a total length of roughly 70 cm. As the aircraft has a flying-wing design, it is not expected to have a horizontal tail for pitch control. Therefore, elevons must be used to control the aircraft. Similarly to the other aircraft, Beansky will not have a rudder system to control the yaw. However, to promote yaw stability, the aircraft will be equipped with winglets at the wingtips.

5.2 Aircraft Subsections

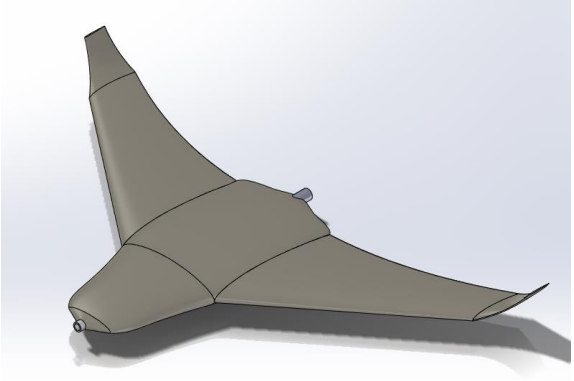

Figure 5.1 – Preliminary Beansky design

5.2.1 Nose

The nose of the aircraft is where the electronics that run the aircraft are located. This includes the flight computer, battery, servo connectors, communication systems, and GPS. By having all the electronics in the front, the aircraft's center of mass would be pushed forward, giving the aircraft longitudinal stability. The camera is going to be integrated within the nose. Ballasts are going to be installed in the nose if required.

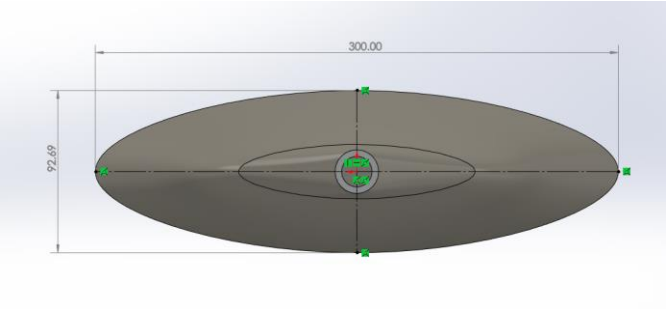

Figure 5.2 – Nose front view (mm)

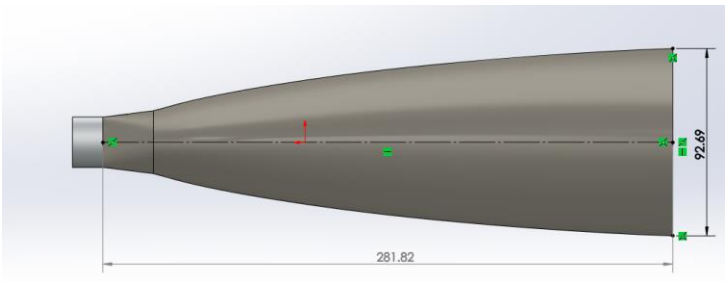

Figure 5.3 – Nose side view (mm)

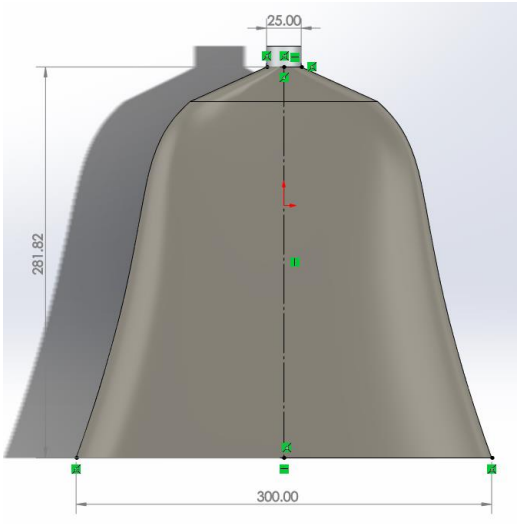

Figure 5.4 – Nose top view (mm)

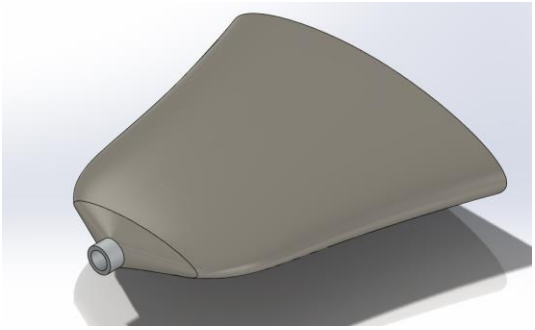

Figure 5.5 – Nose isometric view

5.2.2 Rear Fuselage

The aircraft's fuselage houses the motor used to propel the UAV forward. The wings are also going to be attached to the fuselage, making it vital for flight. To ensure that the wings are properly attached, carbon-fiber rods might be used to create an attachment point for the wings. The nose

and fuselage are blended to create a streamlined structure. The total length of the aircraft is going to be roughly 70 cm.

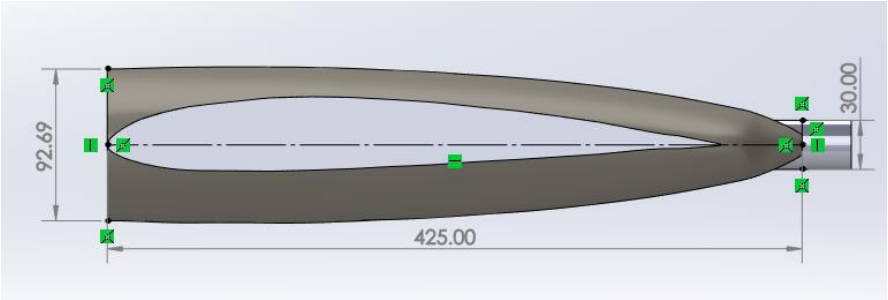

Figure 5.6 – Rear fuselage side view (mm)

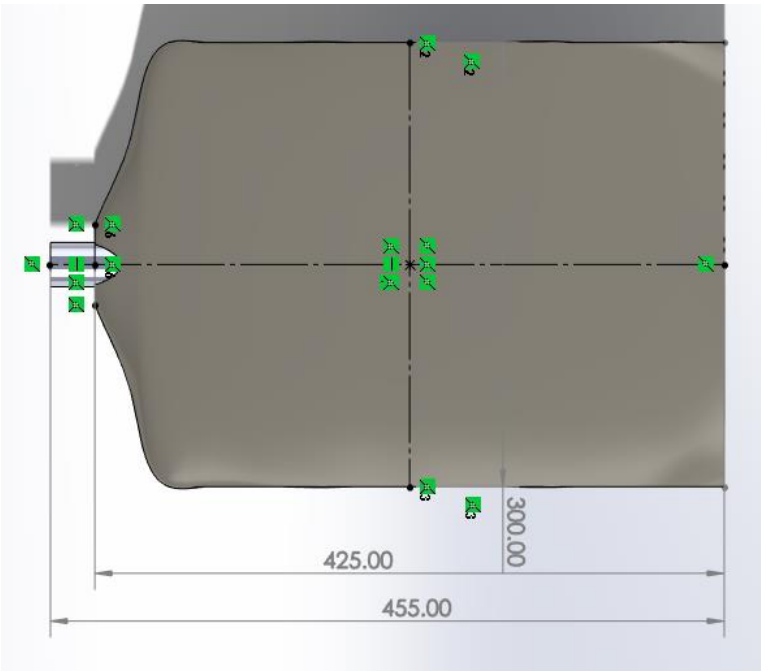

Figure 5.7 – Rear fuselage top view (mm)

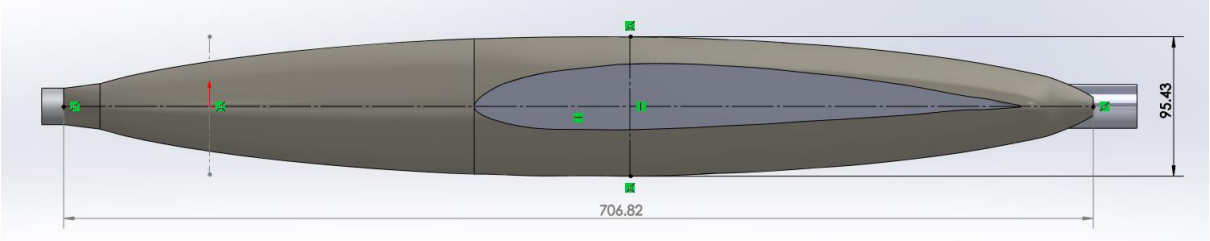

Figure 5.8 – Full fuselage side view (mm)

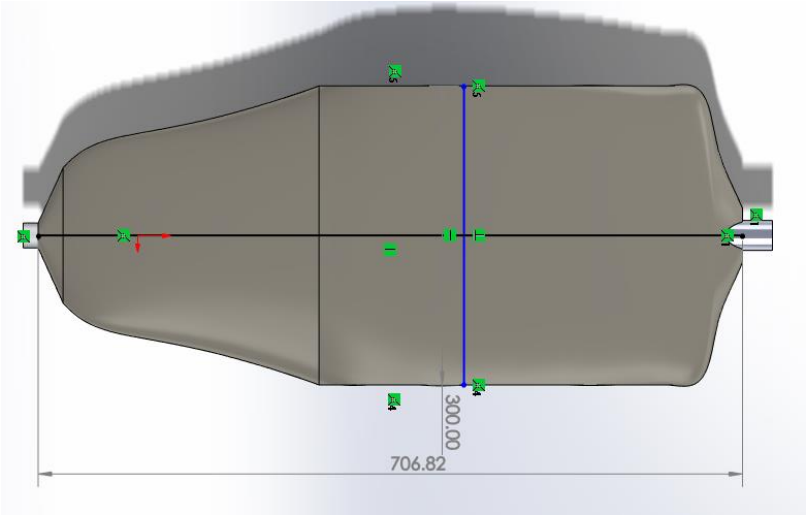

Figure 5.9 – Full fuselage top view (mm)

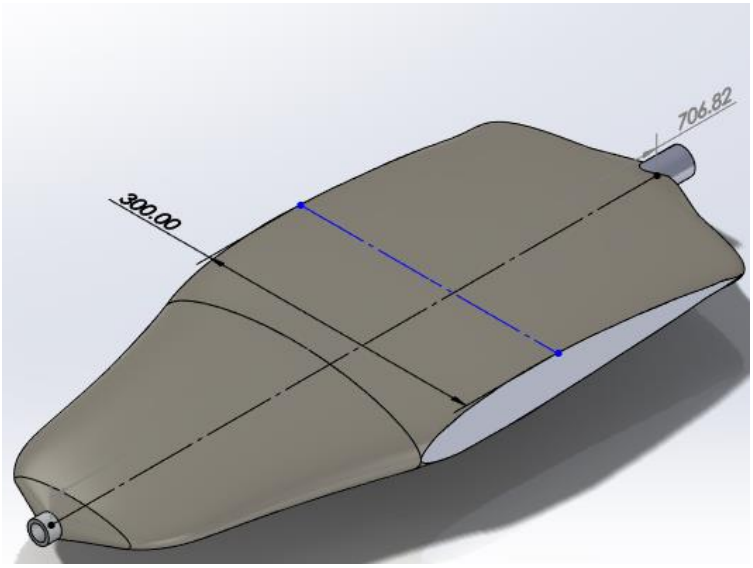

Figure 5.10 – Full fuselage isometric view (mm)

5.2.3 Wings

The aircraft is going to utilize a swept wing, to reduce drag while also moving the center of lift back. The NACA 2412 airfoil that the preliminary design is currently utilizing is a placeholder. As such, an airfoil optimized for speeds of 70 km/h (43.5 mph) will be used in the final design. The aircraft has a total wingspan of 1250 millimeters, because when compared to our baseline, the total wingspan falls in the middle range. The chord of the wing root is 375 millimeters, while the chord of the wing tip is 150 millimeters.

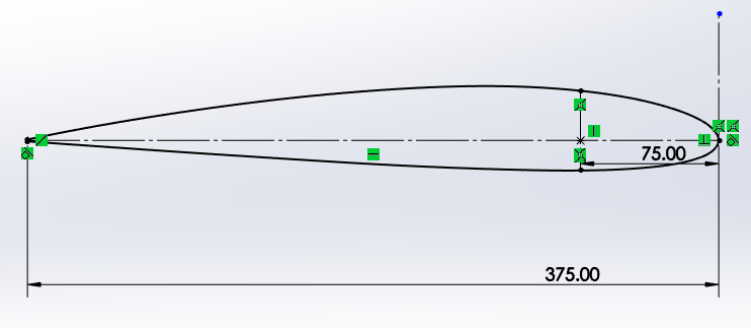

Figure 5.11 – NACA 2412 airfoil @ Wingroot (mm)

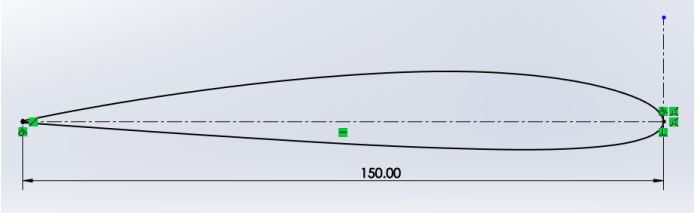

Figure 5.12 – NACA 2412 airfoil @ wingtip (mm)

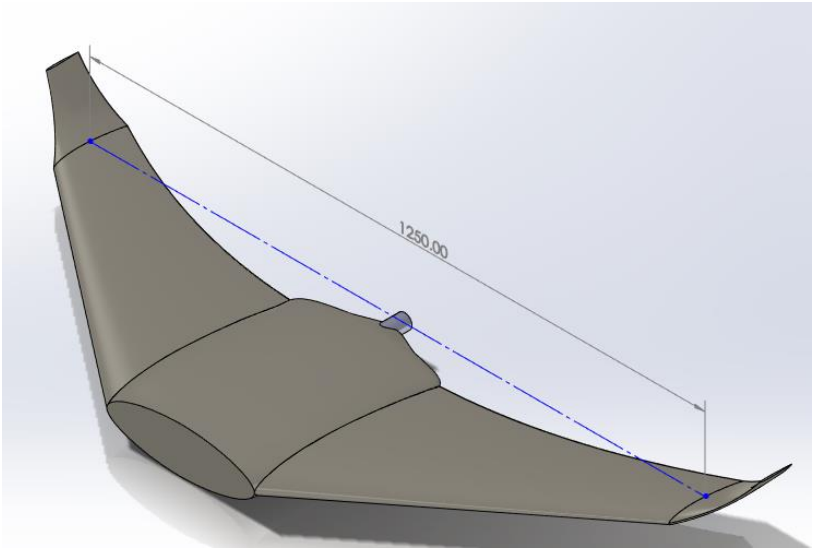

Figure 5.13 – Wing isometric view (mm)

Chapter 6 — Final Fuselage Design

6.1 Introduction

The fuselage of the aircraft is a vital component of the aircraft, as it not only acts as the central spine of the aircraft, but also where all the electronics are located. Due to the nature of the aircraft being 3D printed, the entire structure can be designed using SolidWorks and later printed as separate pieces that could later be attached together during final assembly using glue. To assist with lining up the aircraft, each 3D printed part of the fuselage has attachment nodes that are used to guide the neighboring part to its proper position.

6.2 Nose Design

The nose cone of the aircraft has a vertical distance of 30 cm (11.8 in), and a horizontal distance of 17.5 cm (6.89 in). It has a square mount in the nose of the aircraft which is where the camera is located. On top of the aircraft are three distinct antenna holes, which is where both the video transmitter and radio receiver both emit and receive signals. The current plan is for the battery to be placed in the nose to assist with weight and balancing.

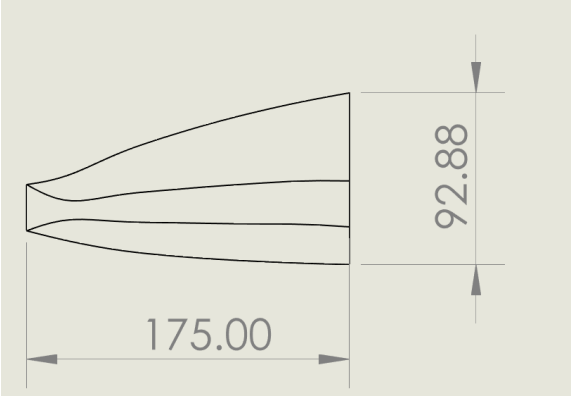

Figure 6.1 – Nose side-view

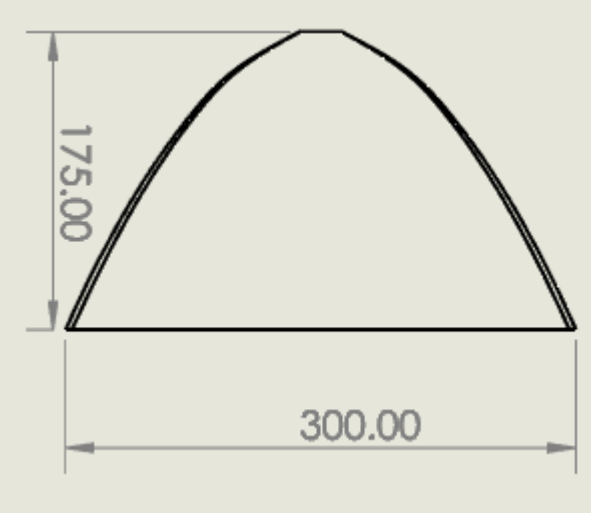

Figure 6.2 – Nose top-view

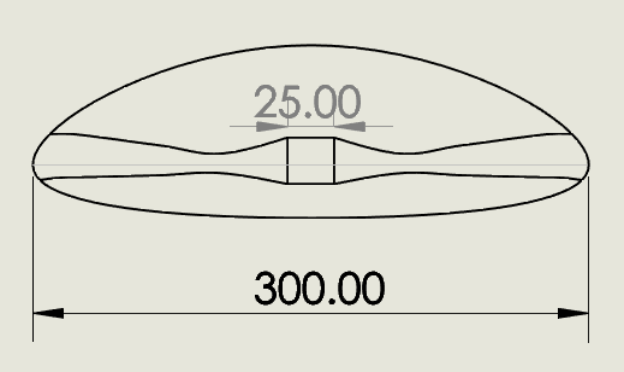

Figure 6.3 – Nose front-view

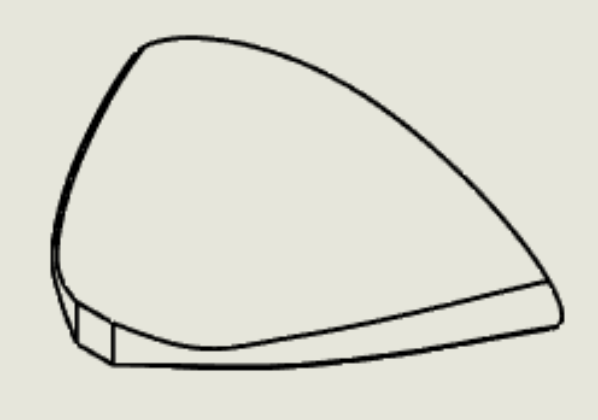

Figure 6.4 – Nose isometric-view

6.3 Fuselage Layout

The central fuselage has a maximum length of 47.5 cm, a maximum width of 30 cm, and a maximum height of nearly 10.5 cm. The motor is going to be mounted on the rear of the central fuselage. The chosen airfoil, the MH60 airfoil, is integrated with the fuselage and will be further discussed in chapter 5.

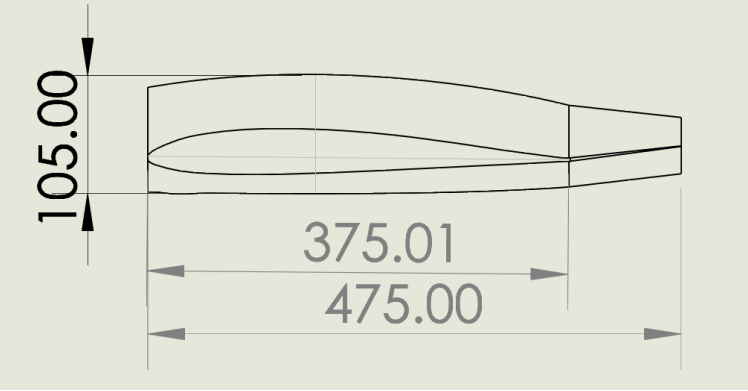

Figure 6.5 – Central fuselage side view

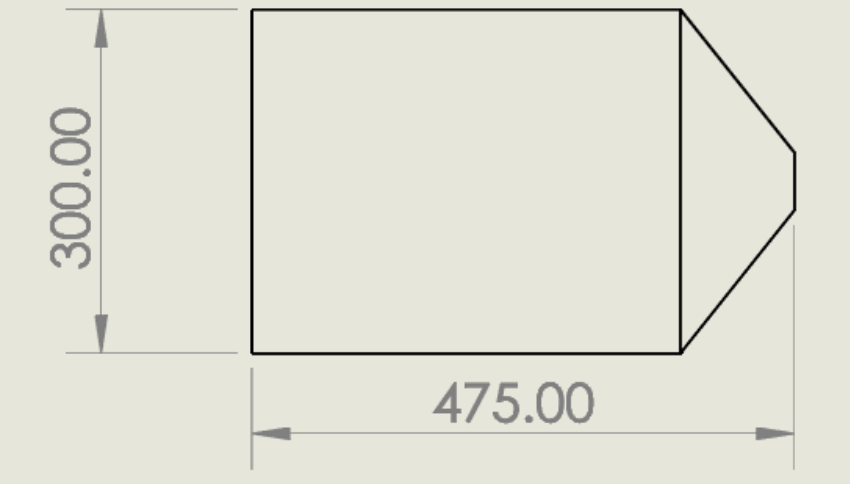

Figure 6.6 – Central fuselage top-view

Figure 6.7 – Central fuselage front-view

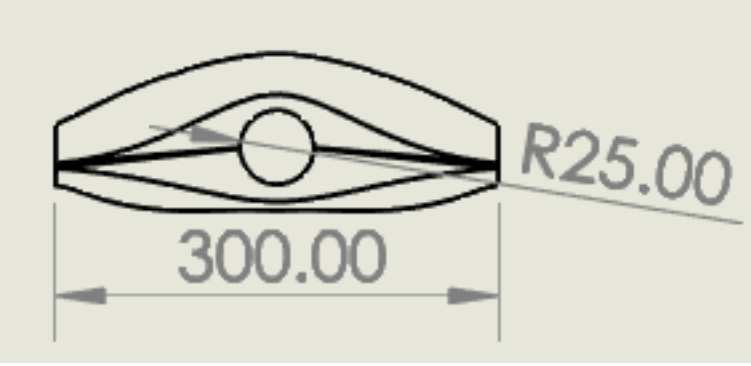

Figure 6.8 – Central fuselage rear-view

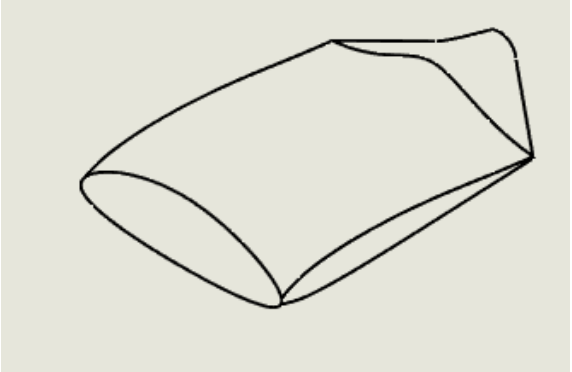

Figure 6.9 – Central fuselage isometric-view

6.4 Conclusion

By combining the nose and central fuselage, the total length of the fuselage is 65 cm, while the total width being 30 cm and total height being 10.5 cm. For the time being, the fuselage design in adequate for the scope of the project.

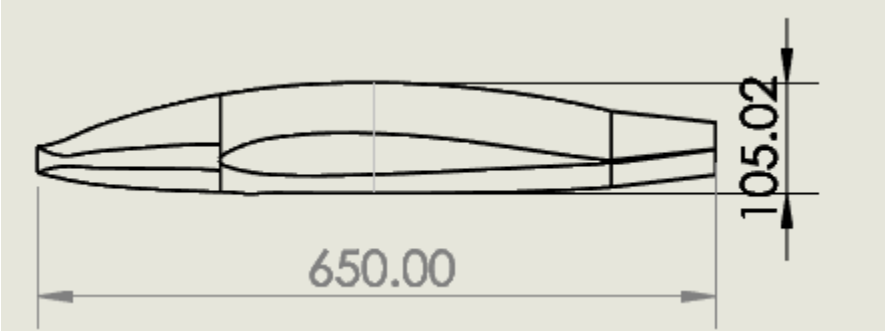

Figure 6.10 – Full fuselage side-view

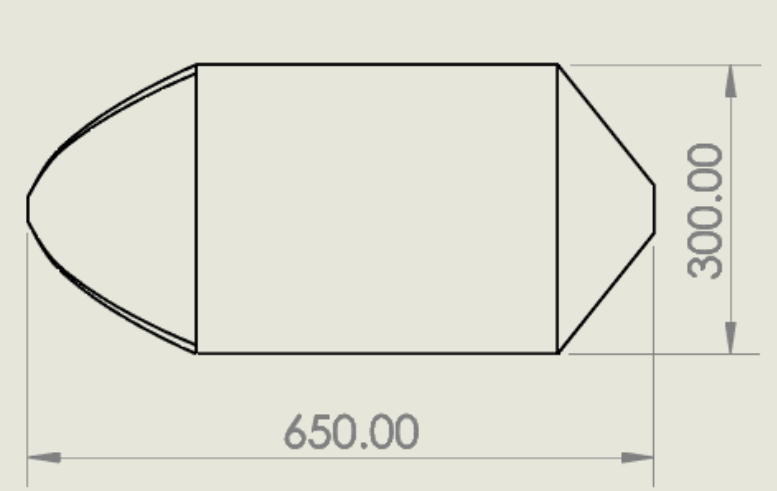

Figure 6.11 – Total fuselage side-view

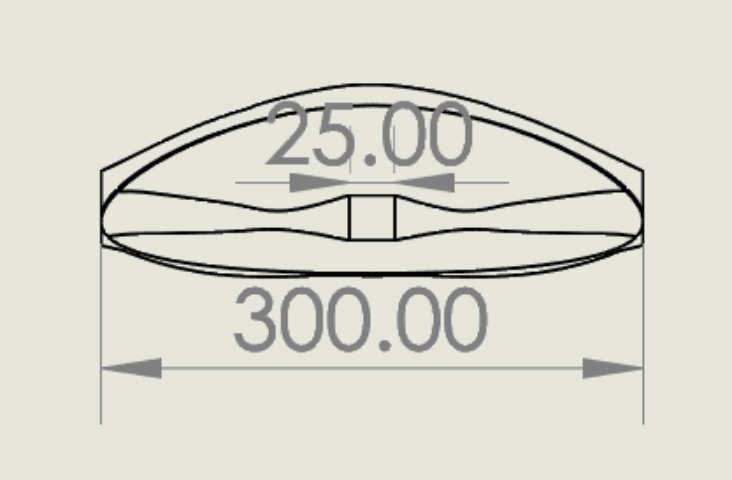

Figure 6.12 – Total fuselage front-view

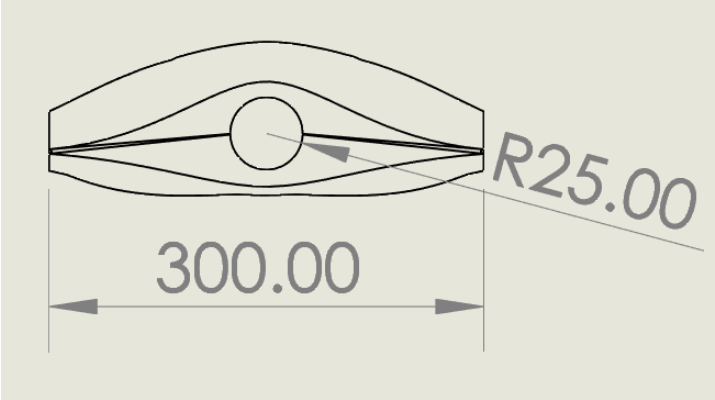

Figure 6.13 – Total fuselage rear-view

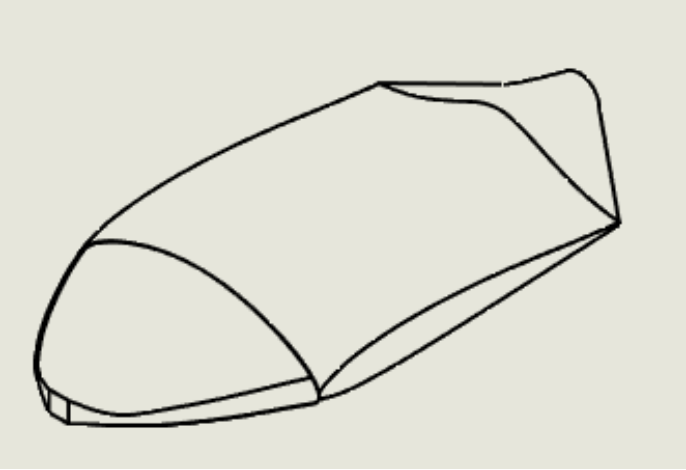

Figure 6.14 – Total fuselage isometric-view

Chapter 7 — Final Wing Design

7.1 Wing Design Evaluation

Although there are no immediate pass/fail criteria that drives wing design, the hand-tossed and flying wing design of the Beansky makes it a necessity for the aircraft to produce as much lift as possible as low speeds to ensure takeoff, while also having as little pitching moment as possible.

To determine the fluid flow over the wings, the Reynolds number is determined using the following equation:

$$R_e = \frac{\rho u c}{\mu} \tag{7.1}$$

The Reynolds number used to calculate the optimal flight characteristics is 400000. Furthermore, to assist with static stability, the wing must also be swept back to have a reasonable aerodynamic center.

7.2 Wing Planform

With the requirements identified, a swept wing with a high lift and low pitching moment is selected. The calculated aerodynamic center is 298.81 mm from the front leading edge.

Table 7.1 – Wing parameters

Parameter	Millimeter	Metric	Imperial
Reference Wing Area (S)	371875 mm^2	0.371875 m^2	4.002 ft^2
Aspect Ratio (AR)	4.2		
Taper Ratio (λ)	0.3371		

The mean aerodynamic chord of the aircraft can be calculated as:

$$MAC = \frac{2}{3} c_{root} \frac{1+\lambda+\lambda^2}{1+\lambda} \tag{7.2}$$

The MAC is calculated to be 321.88. From there, the aerodynamic center is assumed to be a quarter value of the MAC, meaning that is 80.47 mm along it. This equates to being 298.81 mm away from the top of the wing.

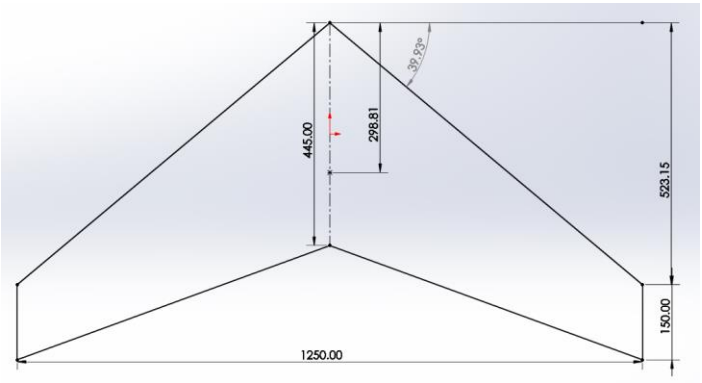

Figure 7.1 – Wing planform

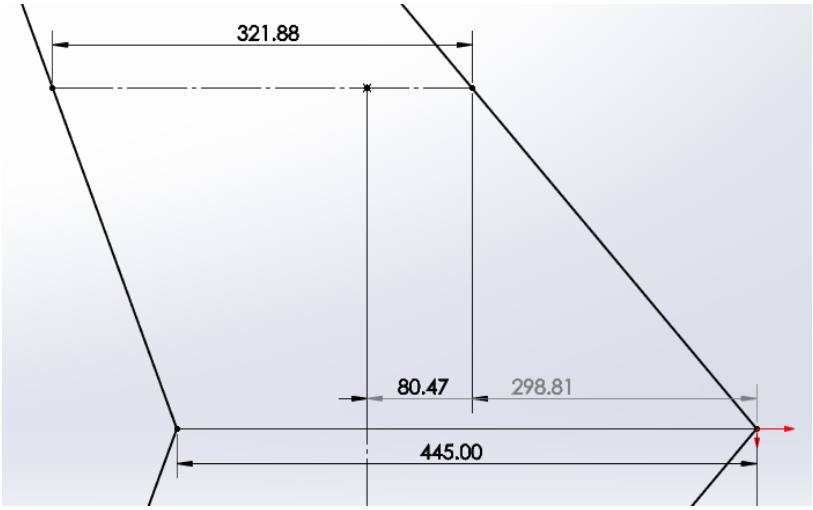

Figure 7.2 – Wing MAC

7.3 Airfoil Selection

The tailless nature of Beansky means that the overall pitching moment of the aircraft cannot be compensated with a horizontal stabilizer. As a result, a lot of strain is put onto the horizontal control surface. To reduce this strain, the airfoil chosen must have a low pitching moment coefficient. When comparing the MH60 airfoil to other airfoils, it produces more lift at low speeds while also less pitching moments than the NACA 2412. The final airfoil has its trailing edge smoothed out with a semicircle of 3 mm. The root and tip chord lengths are the same as the preliminary design.

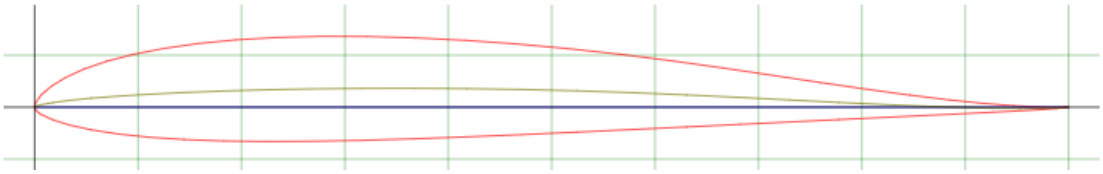

Figure 7.3 – Wing MAC

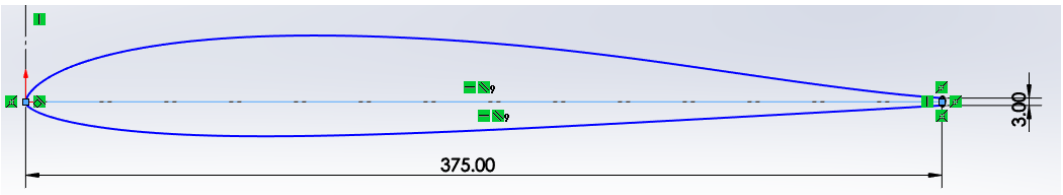

Figure 7.4 – MH60 wing root airfoil

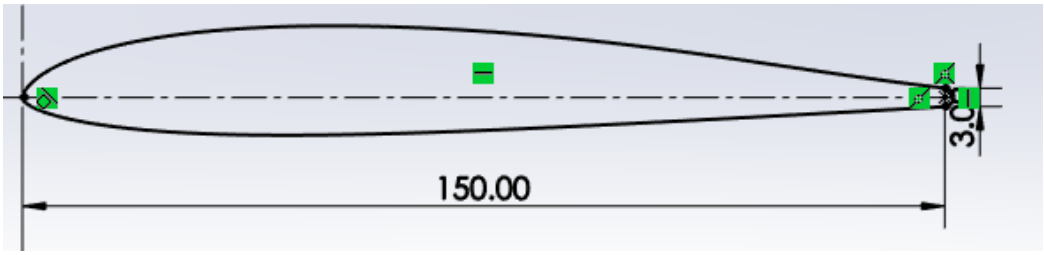

Figure 7.5 – MH60 wing tip airfoil

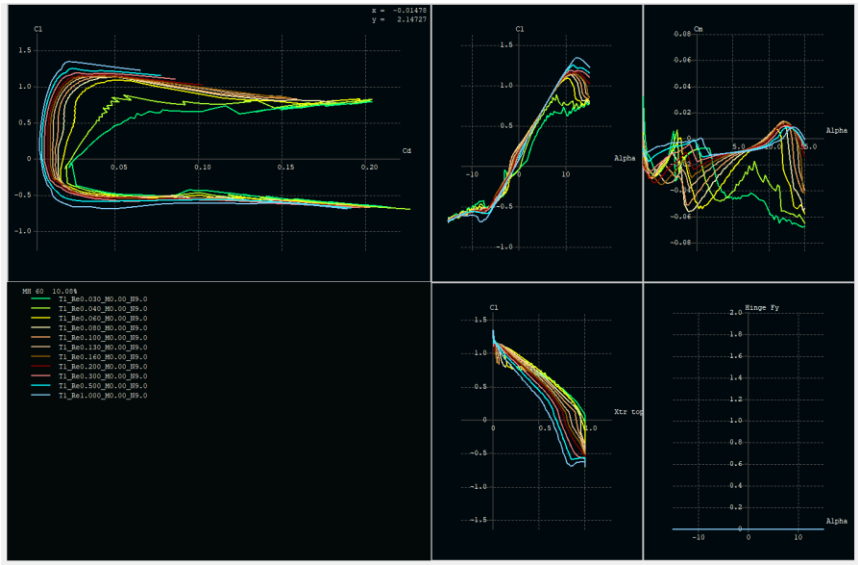

Figure 7.6 – MH60 airfoil XFLR5 analysis

7.4 Control Surfaces

To provide the aircraft with both longitudinal and lateral controls, flying wings utilize elevons, which is a combination of the elevator and the aileron, giving the aircraft the ability to both roll and pitch. In this case, the elevons are seen in figure 5.6. The center rectangle is reserved for the fuselage.

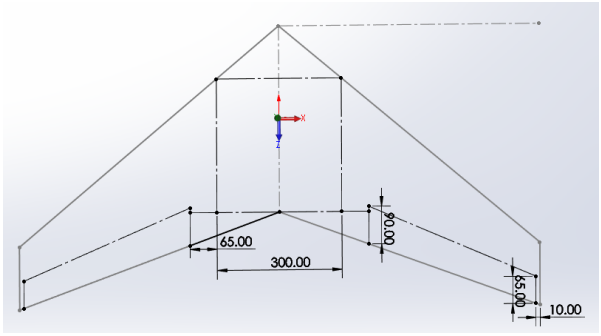

Figure 7.7 – Elevon location

Chapter 8 — Final Empennage Design

8.1 Introduction

As this is a flying wing aircraft, Beansky does not have a horizontal stabilizer. It does have winglets at the wingtips, giving the aircraft lateral stability. However, as there are no control surfaces on the winglets, lateral control of the aircraft will be dependent on the elevons.

8.2 Fin Airfoil

The vertical fins that are utilized for the vertical fin is the NACA 0012. The NACA 0012 airfoil was chosen due to its optimized flight characteristics at a low Reynold's numbers (R_e=400000).

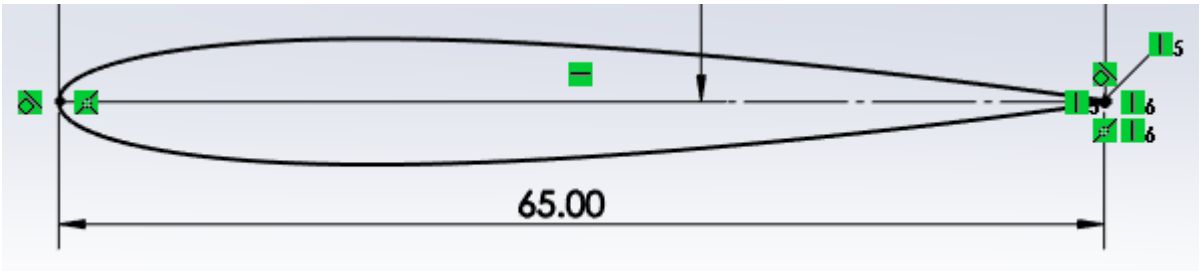

Figure 8.1 – NACA 0012 wing fin airfoil

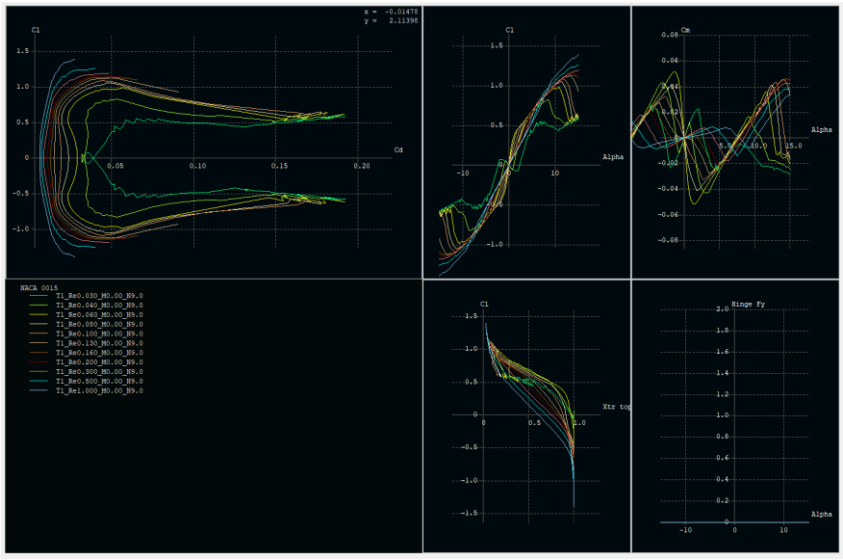

Figure 8.2 – NACA 0015 airfoil XFLR5 analysis

8.3 Winglet Design

The winglet must transition from the MH60 airfoil from the wing, to the NACA 0012 at the tip, while also transitioning 90°. The winglet has a total vertical height of 125 mm, while only extending the wing horizontally 50 mm.

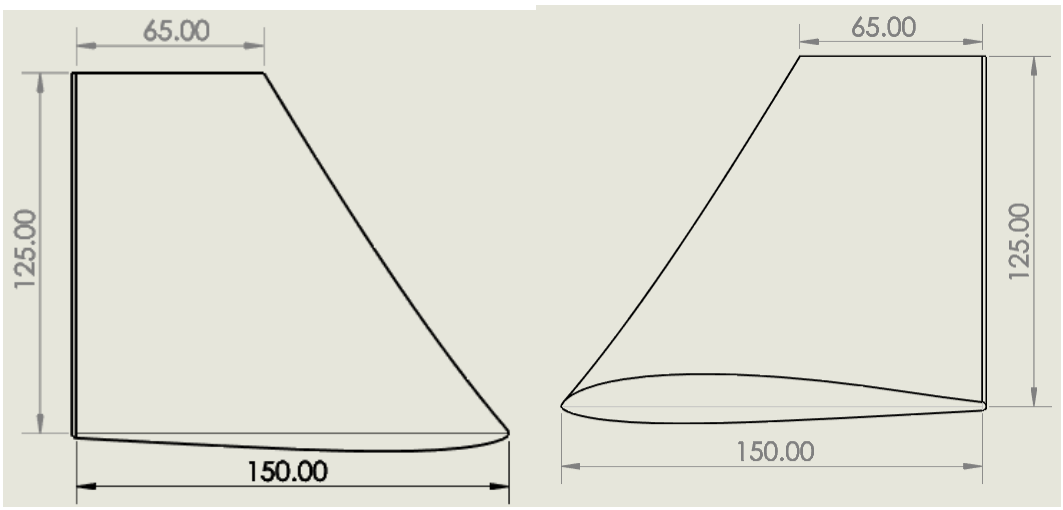

Figure 8.3 – Right winglet right & left view

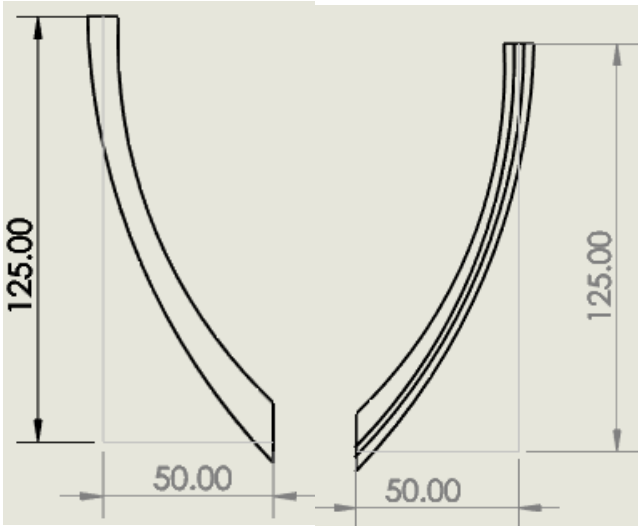

Figure 8.4 – Right winglet front & rear view

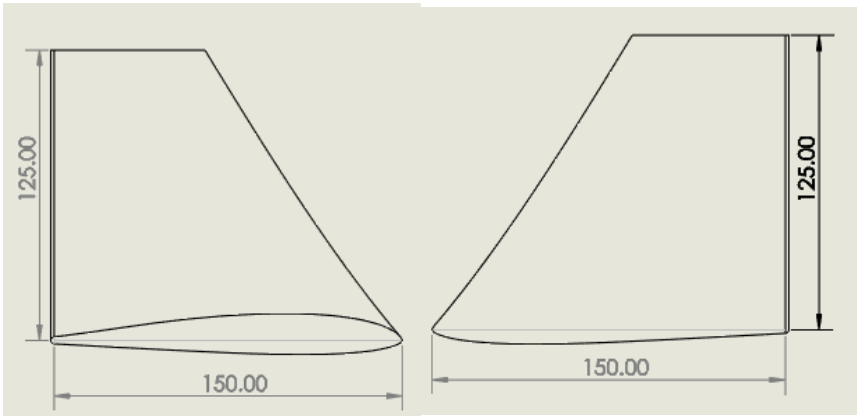

Figure 8.5 – Left winglet right & left view

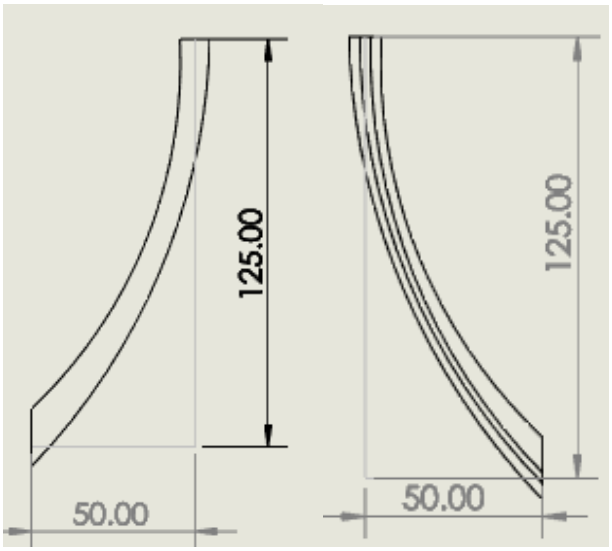

Figure 8.6 – Left winglet front & rear view

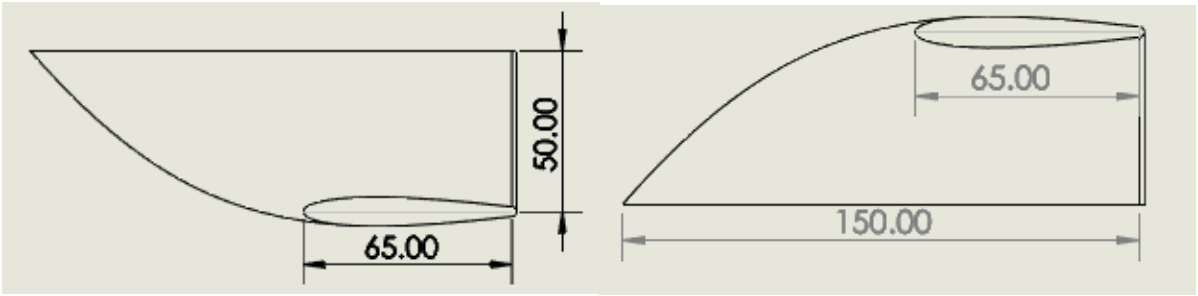

Figure 8.7 – Left & right winglet top-view

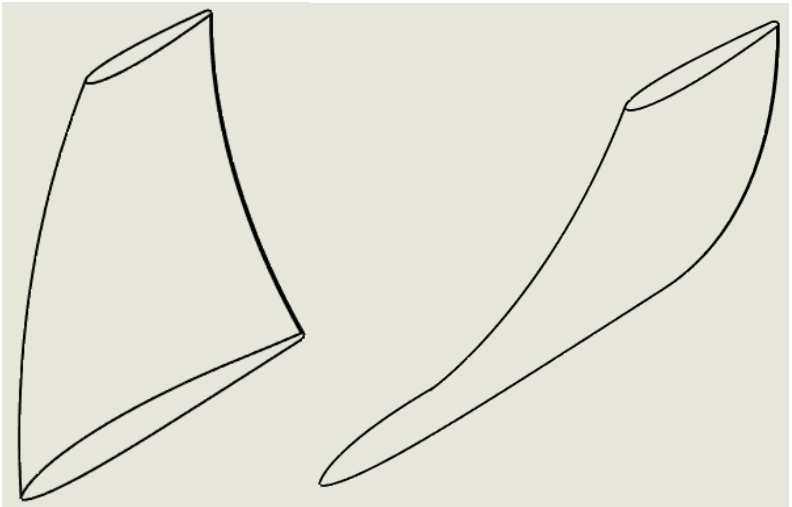

Figure 8.8 – Right & left winglet isometric-view

8.4 Conclusion

Although the lack of a vertical control surface is concerning, it is not an unproven design. The Flightory Super Stingray for example, utilizes only the two elevons to control flight. A redesign on the winglet to create a rudder system can be developed in the future to give the pilot more control.

Chapter 9 — Final Landing Gear

9.1 Introduction

Initially, the design of Beansky did not involve landing gear, as the plan was to belly-land the aircraft. However, after seeing how much damage a belly landing would have on the airframe, it was decided to search for landing gear. It was decided to utilize landing skids as seen on helicopters, due to their ease of installation and how little it effects the aerodynamics of the aircraft.

9.2 Skid Design

To simplify the construction of the landing gear, the skid was designed to be as simple as possible, while also strong enough to withstand the stresses of landing. A design goal of the skid is to be able to clear a 14 in diameter propeller that the aircraft would be equipped with. A 14 inch diameter propeller was chosen due to that being the propeller for the Skywalker X8. The landing skid must also be able to be attached to the aircraft, requiring changes to the wing design.

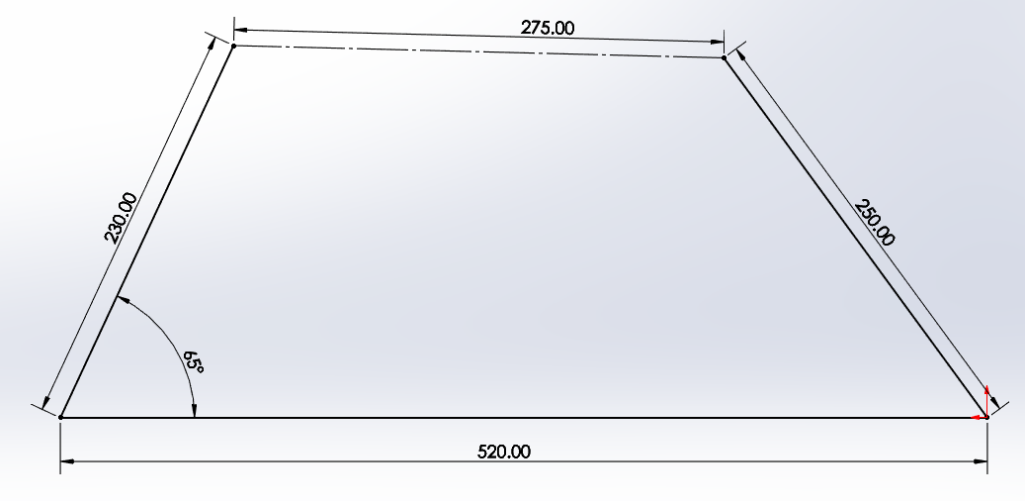

Figure 9.1 – Landing skid

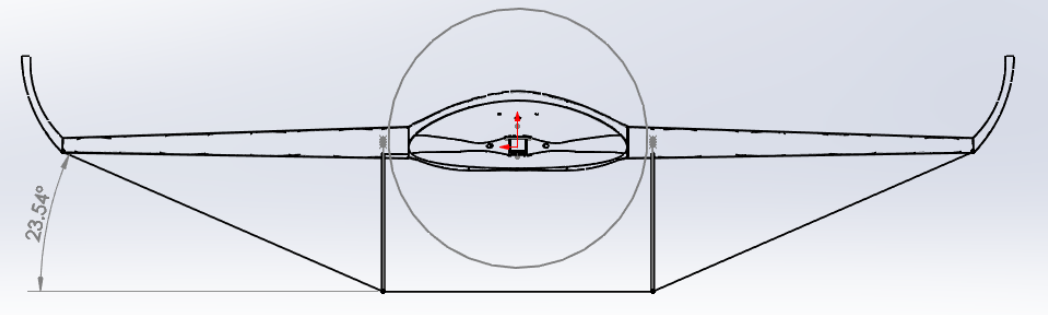

Figure 9.2 – Beansky front view w/ landing gear

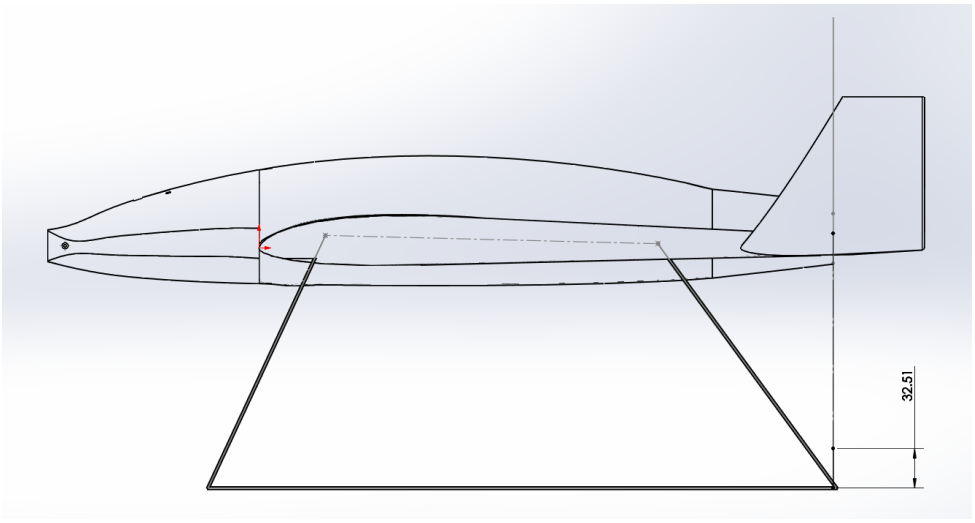

Figure 9.3 – Beansky propeller clearance (mm)

To attach the landing gear to the airframe, two holes are built into each wing that can hold the landing gear in place. The skids are located 35 mm away from the wing root, giving clearance to both the propeller and a wide base. Glue can be used to reenforce the landing gear-wing joint.

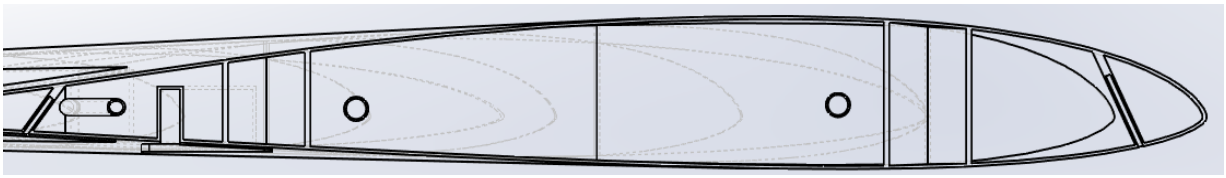

Figure 9.4 – Beansky landing gear attachment location cross-section (left wing)

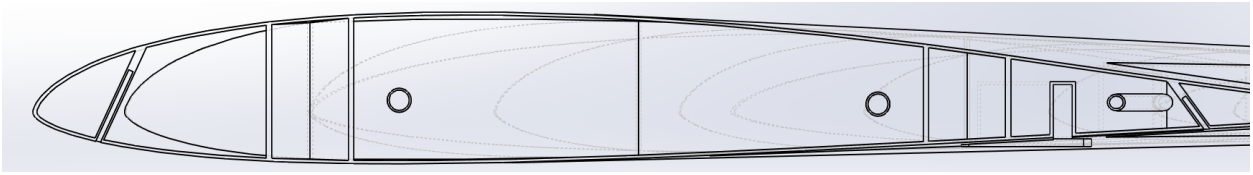

Figure 9.5 – Beansky landing gear attachment system cross-section (right wing)

9.3 Conclusion

Although the usage of a skid to cushion a landing is intriguing, due to the “disposable” nature of the drone, as well as the original plan to conduct belly landings if needed, the landing gear design is not as optimized for Beansky as other components.

Chapter 10 — CFD Simulation

10.1 Background

Computation Fluid Dynamics (CFD) is a analytical method that uses mathematical algorithms to solve problems that involve fluid flow. In this case, the bedrock that makes up CFD are the Navier-Stokes equation, which describes how the velocity, pressure, temperature, and density of a fluid relate. The Navier-Stokes equations rely heavily on the conservation of mass, conservation of momentum (in u, v, and w directions), and conservation of energy [27]:

$$\frac{\partial \rho}{\partial t} + \frac{\partial (\rho u)}{\partial x} + \frac{\partial (\rho v)}{\partial y} + \frac{\partial (\rho w)}{\partial z} = 0 \tag{10.1}$$

$$\frac{\partial (\rho u)}{\partial t} + \frac{\partial (\rho u^2)}{\partial x} + \frac{\partial (\rho uv)}{\partial y} + \frac{\partial (\rho uw)}{\partial z} = -\frac{\partial \rho}{\partial x} + \frac{1}{Re}\left[\frac{\partial (\rho \tau_{xx})}{\partial x} + \frac{\partial (\rho \tau_{xy})}{\partial y} + \frac{\partial (\rho \tau_{xz})}{\partial z}\right] \tag{10.2}$$

$$\frac{\partial (\rho v)}{\partial t} + \frac{\partial (\rho uv)}{\partial x} + \frac{\partial (\rho v^2)}{\partial y} + \frac{\partial (\rho vw)}{\partial z} = -\frac{\partial \rho}{\partial x} + \frac{1}{Re}\left[\frac{\partial (\rho \tau_{xy})}{\partial x} + \frac{\partial (\rho \tau_{yy})}{\partial y} + \frac{\partial (\rho \tau_{yz})}{\partial z}\right] \tag{10.3}$$

$$\frac{\partial (\rho w)}{\partial t} + \frac{\partial (\rho uw)}{\partial x} + \frac{\partial (\rho vw)}{\partial y} + \frac{\partial (\rho w^2)}{\partial z} = -\frac{\partial \rho}{\partial x} + \frac{1}{Re}\left[\frac{\partial (\rho \tau_{xz})}{\partial x} + \frac{\partial (\rho \tau_{yz})}{\partial y} + \frac{\partial (\rho \tau_{zz})}{\partial z}\right] \tag{10.4}$$

$$\frac{\partial (E_T)}{\partial t} + \frac{\partial (uE_T)}{\partial x} + \frac{\partial (vE_T)}{\partial y} + \frac{\partial (wE_T)}{\partial z} = -\frac{\partial (up)}{\partial x} - \frac{\partial (vp)}{\partial y} - \frac{\partial (wp)}{\partial z} - \frac{1}{R_e P_r}\left[\frac{\partial q_x}{\partial x} + \frac{\partial q_y}{\partial y} + \frac{\partial q_z}{\partial z}\right] + \frac{1}{R_e}\left[\frac{\partial}{\partial x}\left(u\tau_{xx} + v\tau_{xy} + w\tau_{xz}\right) + \frac{\partial}{\partial y}\left(u\tau_{xy} + v\tau_{yy} + w\tau_{yz}\right) + \frac{\partial}{\partial z}\left(u\tau_{xz} + v\tau_{yz} + w\tau_{zz}\right)\right] \tag{10.5}$$

In this case, by utilizing CFD software to interpret the Navier-Stokes equations, aerospace engineers are able to analyze the flight characteristics of an aircraft, without the usage of a wind tunnel or flight testing, saving both time, money, and materials.

10.2 Introduction

To confirm the aircraft's ability to fly, the model was put into a Fluid Analysis to observe how the aircraft would react during flight. By doing so, the amount of lift and drag the aircraft faces can be calculated, as well as the bending moment and torsional moment. Two models will be simulated, one at 72 km/h (20 m/s), which is the maximum cruise speed, and 28.8 km/h (8 m/s), which will is the estimated stall speed.

10.3 Fluid Domain

The fluid domain surrounding the aircraft is a 3.25 m x 1 m x 2 m box, with the aircraft's origin being 1 m away from the inlet boundary condition. By using a Boolean subtract function, the aircraft can be separated from the domain, allowing the aircraft to be meshed.

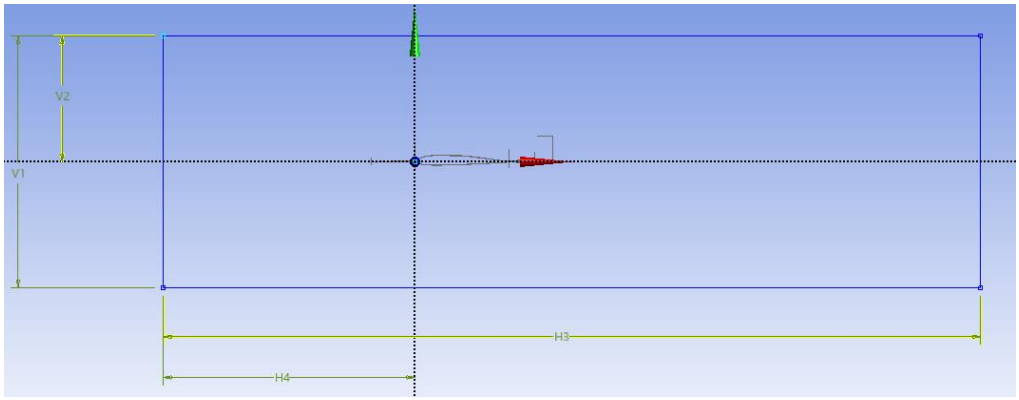

Figure 10.1 – Fluid domain (3.5 m x 1 m x 2 m)

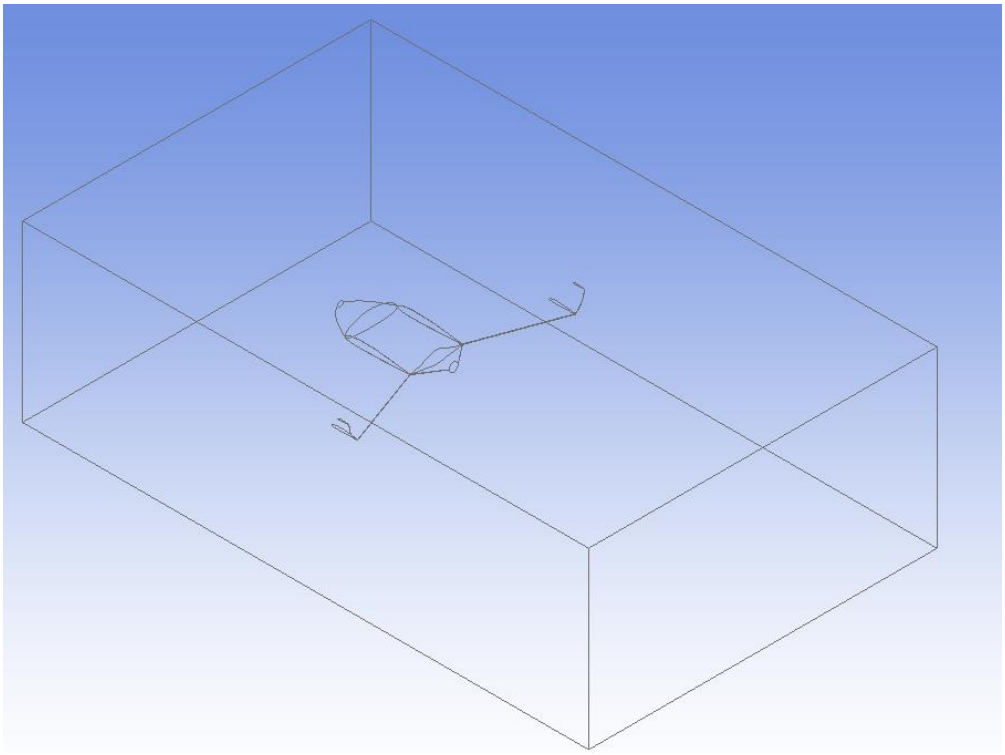

Figure 10.2 – Isometric view of fluid domain

10.4 Mesh

A face sizing mesh was used on the simulation, with a default element size of 0.2 m and a growth rate of 1.2. As a result of the mesh, 167722 nodes and 943948 elements were created.

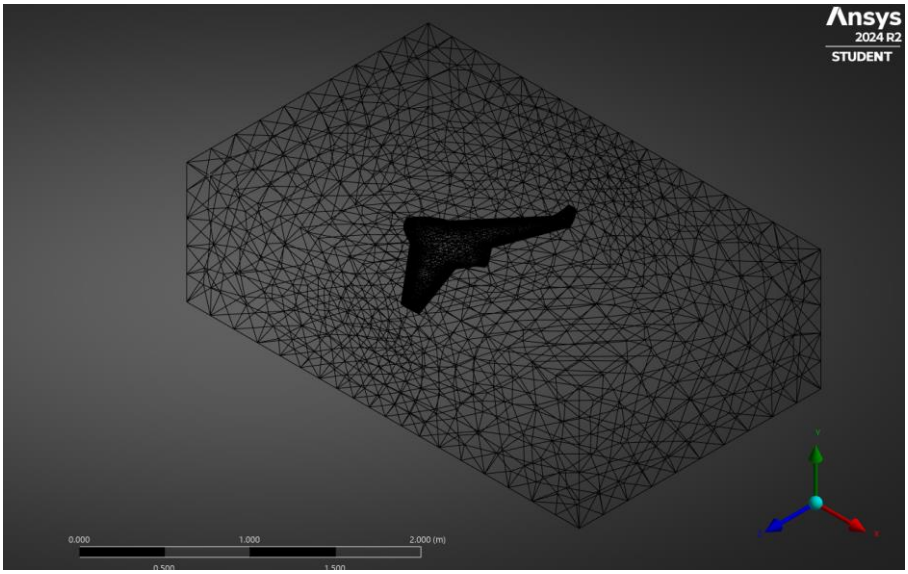

Figure 10.3 – Simulation mesh

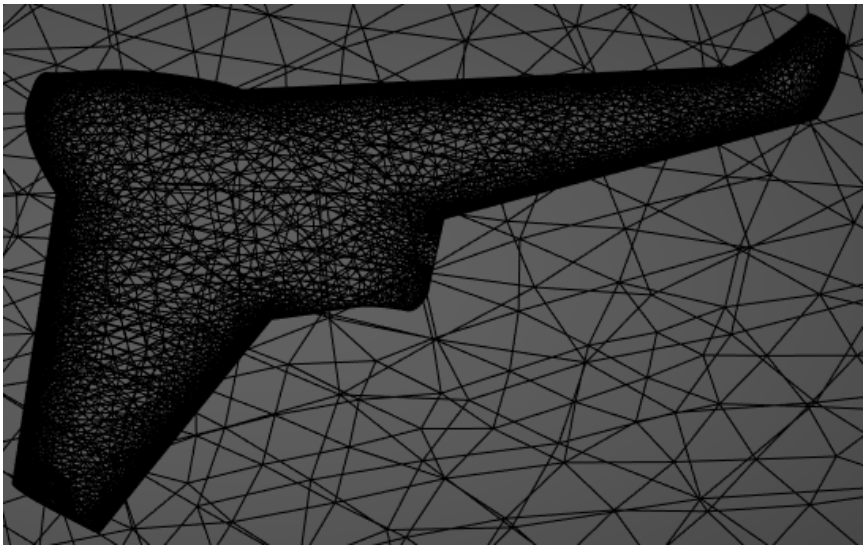

Figure 10.4 – Aircraft mesh

10.5 CFD Physics

The model used for the simulation is a k-omega turbulence model. The fluid used in the simulation is air, with a density of 1.225 kg/m^3, and a viscosity of 1.789E-5 kg/(m s). The boundary conditions of the simulation are as follows: the inlet with an x-velocity of 72 km/h (20 m/s) or 30 km/h (8.33 m/s) depending on the simulation, and a pressure outlet at the rear of the simulation. The aircraft is defined as a wall boundary condition. The lift, drag, coefficient of lift, and coefficient of drag of the aircraft are calculated.

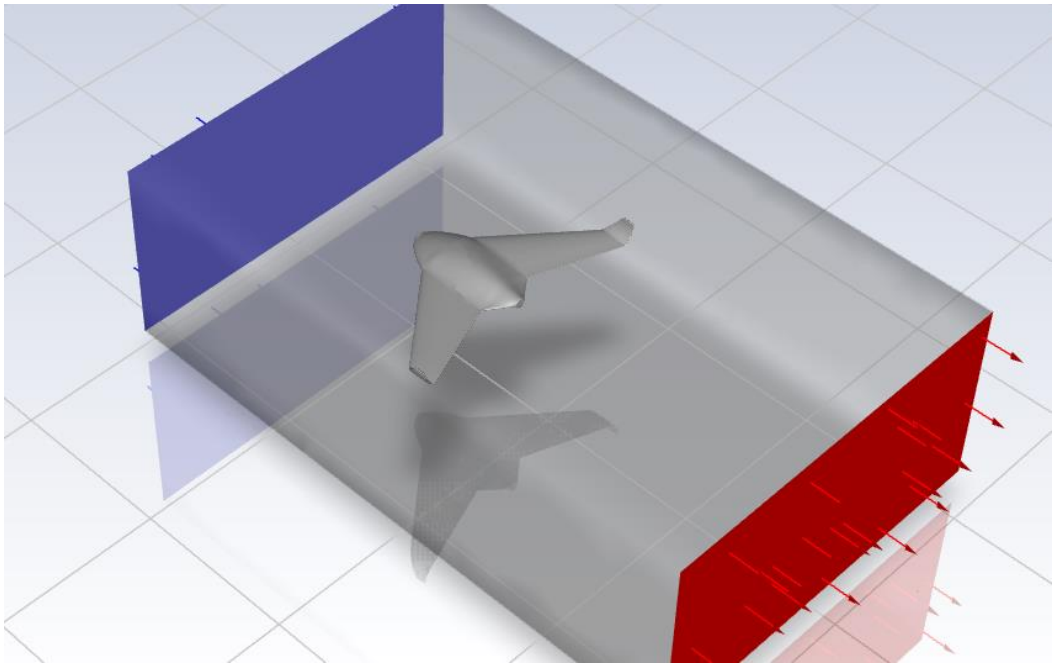

Figure 10.5 – Aircraft simulation

10.6 Results

As a result, the lift, drag, and pitching moment at the aerodynamic center can be found. The coefficients of lifts, drag, and pitching moment can be calculated using the following formulas:

$$C_L = \frac{2 \times L}{\rho \times S \times v^2} \tag{10.6}$$

$$C_D = \frac{2 \times D}{\rho \times S \times v^2} \tag{10.7}$$

$$C_M = \frac{2 \times M}{\rho \times S \times c \times v^2} \tag{10.8}$$

When subjected to a 72 km/h airflow, the aircraft produces 9.5059 N of Lift, experiences 1.6859 N of Drag, and a pitching moment of 1.0702 Nm around the aerodynamic center. Likewise, when subject to a 30 km/h airflow the simulation shows that 1.6721 N of Lift was produced, faces 0.3572 N of Drag, and has a pitching moment of 0.1835 Nm. Using both values we can determine a range for the overall lift, drag, and moment coefficients. In this case, the C_L ranges from 0.09551 – 0.09677, the C_D from 0.01694 - 0.02067, and the C_M from 0.02980 - 0.03016.

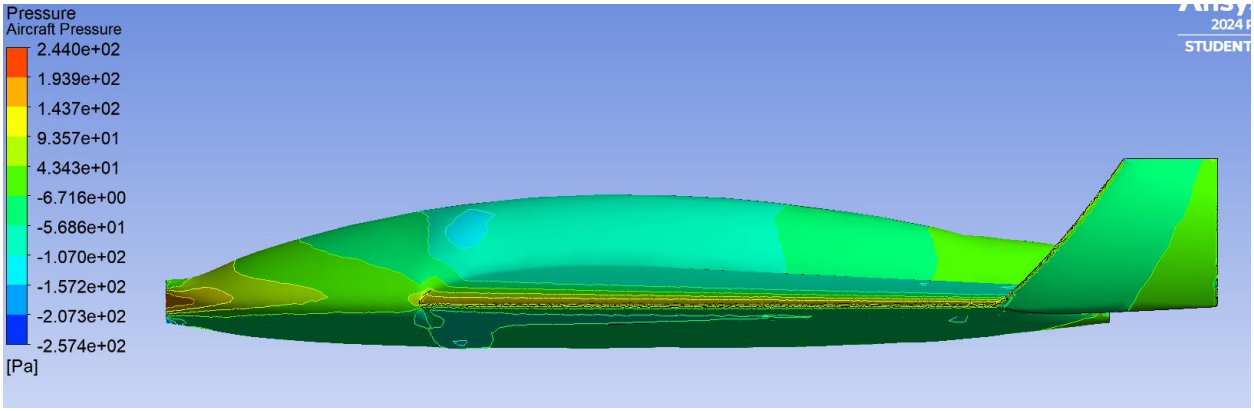

Figure 10.6 – Aircraft side view pressure distribution (72 km/h)

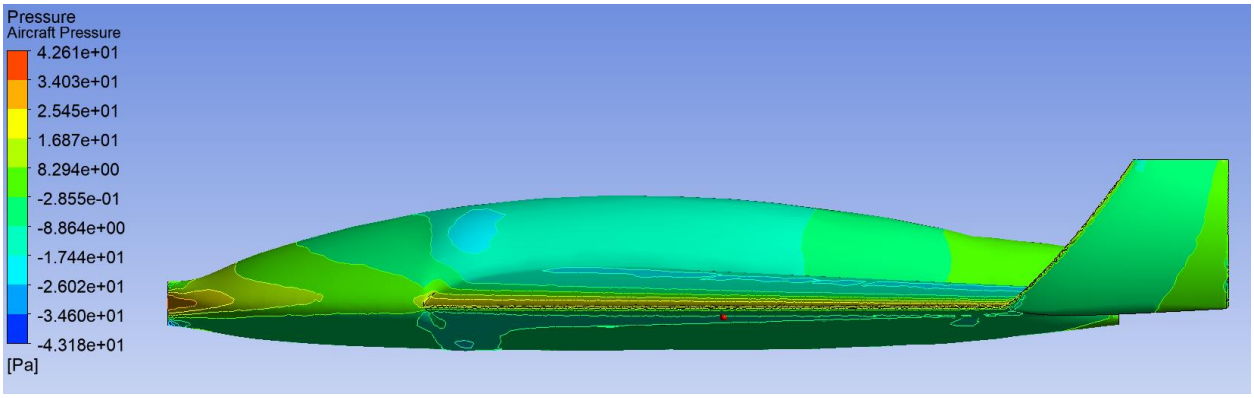

Figure 10.7 – Aircraft side view pressure distribution (30 km/h)

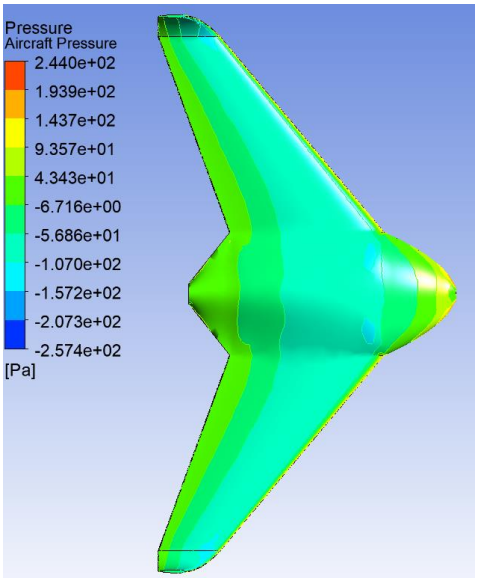

Figure 10.8 – Aircraft top view pressure distribution (72 km/h)

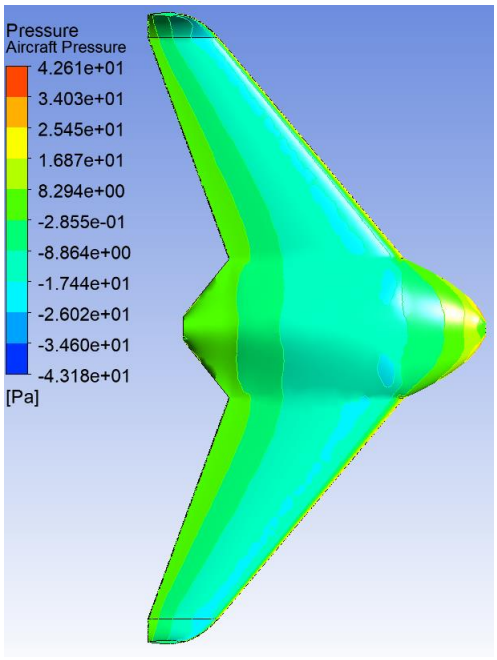

Figure 10.9 – Aircraft top view pressure distribution (30 km/h)

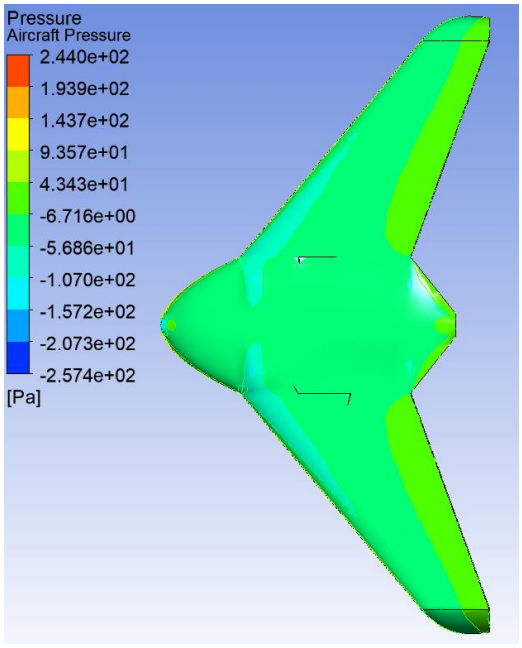

Figure 10.10 – Aircraft bottom view pressure distribution (72 km/h)

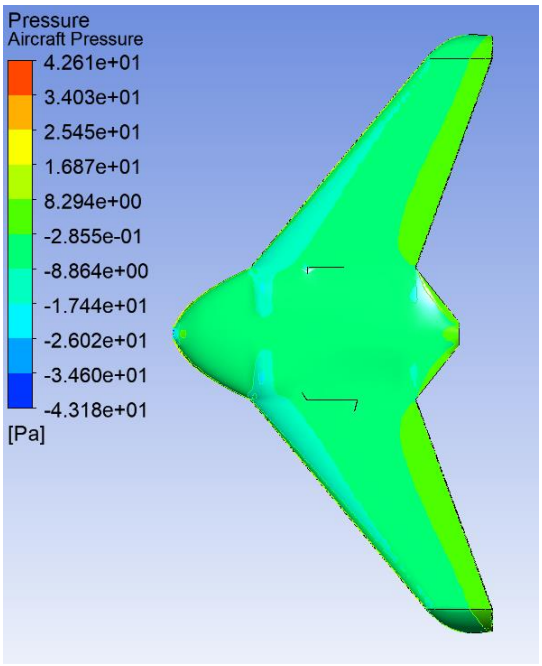

Figure 10.11 – Aircraft bottom view pressure distribution (30 km/h)

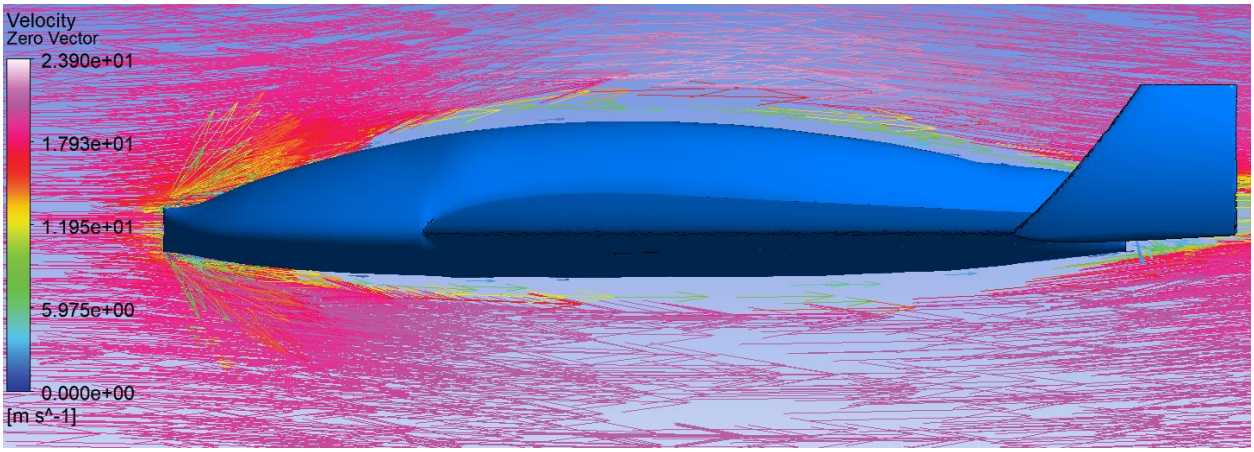

Figure 10.12 – Airflow side view (@ center plane) (72 km/h)

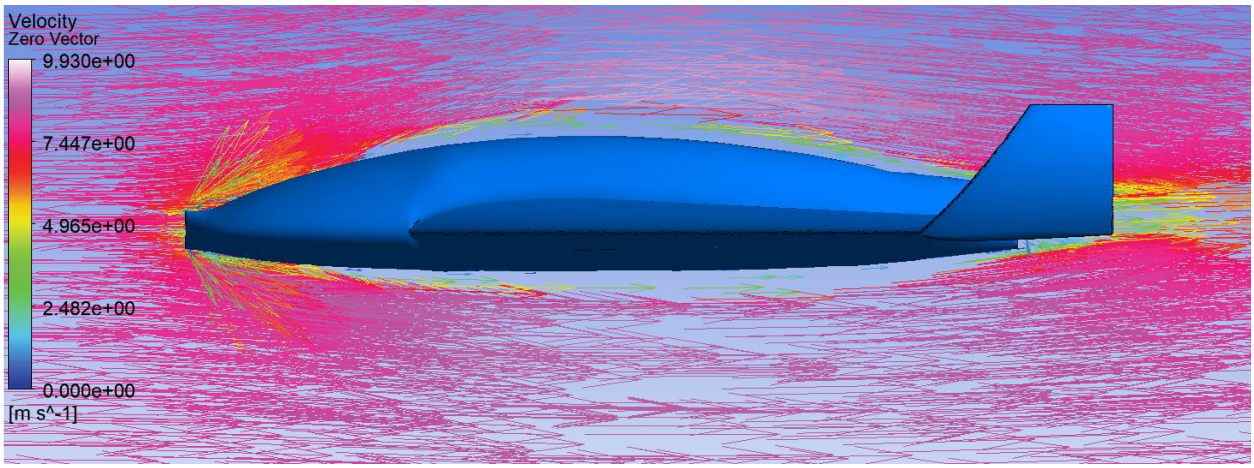

Figure 10.13 – Airflow side view (@ center plane) (30 km/h)

Figure 10.14 – Airflow side view (0.25 m from center plane) (72 km/h)

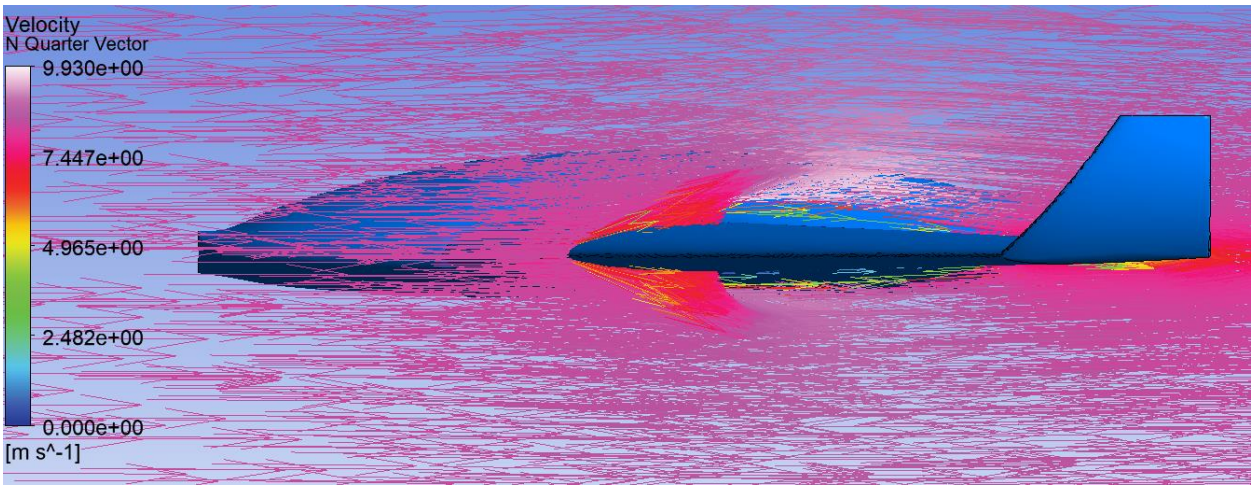

Figure 10.15 – Airflow side view (0.25 m from center plane) (30 km/h)

Figure 10.16 – Airflow side view (0.5 m from center plane) (72 km/h)

Figure 10.17 – Airflow side view (0.5 m from center plane) (30 km/h)

Chapter 11 — Internal Structure

11.1 Central Fuselage Structure

The fuselage structure is made up of a central horizontal spine that acts as the “floor” of the aircraft, being the location where the electronics are located. The central spine is located 5.75 mm below the origin, which is based on the location of the airfoil. Twin vertical supports also run throughout the length of the fuselage and are 67.50 mm away from the origin. A smaller vertical support also runs through the bottom of the aircraft, connecting with the central spine to give it some support. There are two gaps that run in between the wall of the fuselage and the vertical support, which exists to reduce the overall weight of the structure without compromising safety. The two divots made in the center of the central spine exist to easily attach electronics to the aircraft with the usage of zip ties.

Figure 11.1 – Origin location

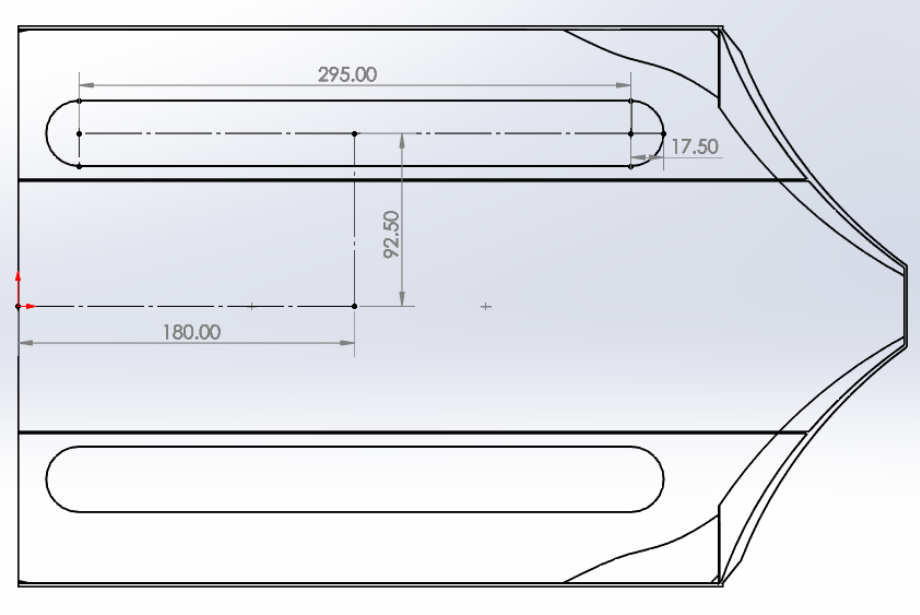

Figure 11.2 – Central fuselage internal structure top-view

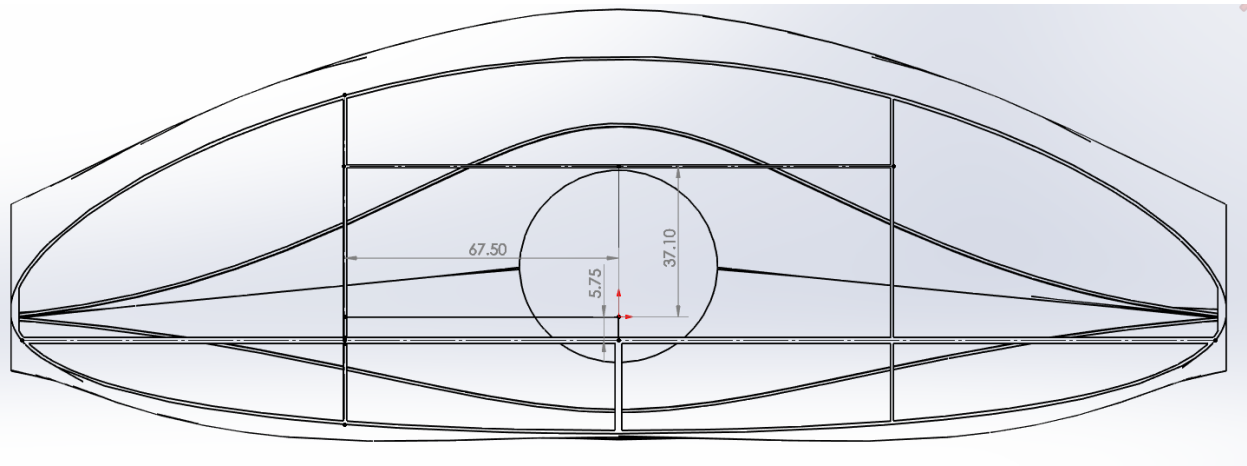

Figure 11.3 – Central fuselage internal structure location

There also exists a top spine, whose primary purpose is to assist with the 3D printing process as well as give the structure some support. It only runs in between the two vertical supports. The thickness of the structure can be seen in Fig. 9.4.

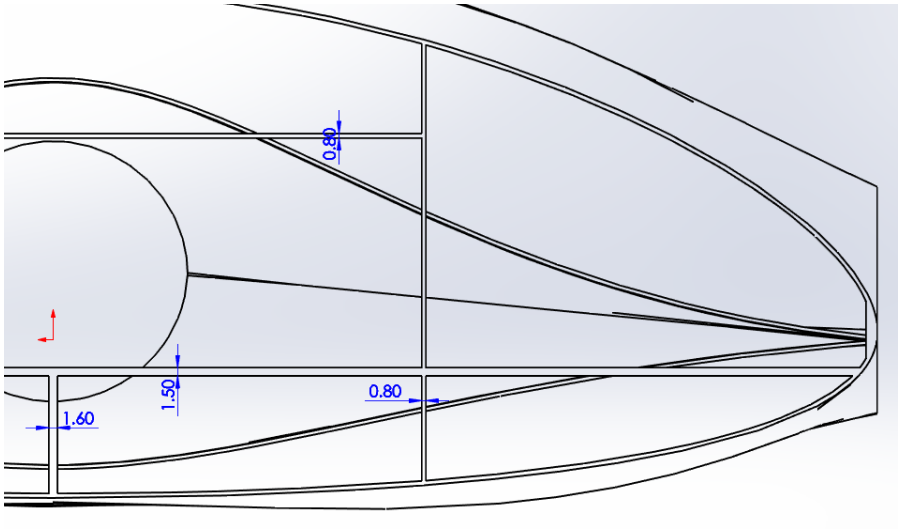

Figure 11.4 – Internal structure sizing

11.2 Nose Structure

The internal structure of the nose is similar to the internal structure of the central fuselage. Both the central spine and the twin vertical supports are present. The central spine also gives the flight electronics a location where the electronics can be mounted too. Similar to the internal structure of the central fuselage, there are gaps in the central spine to save weight that run parallel to the fuselage. Smaller holes to mount sensitive electronics are present in the nose, while the electronics in the central fuselage will only rely on zip-ties. The nose and the central fuselage share the same origin.

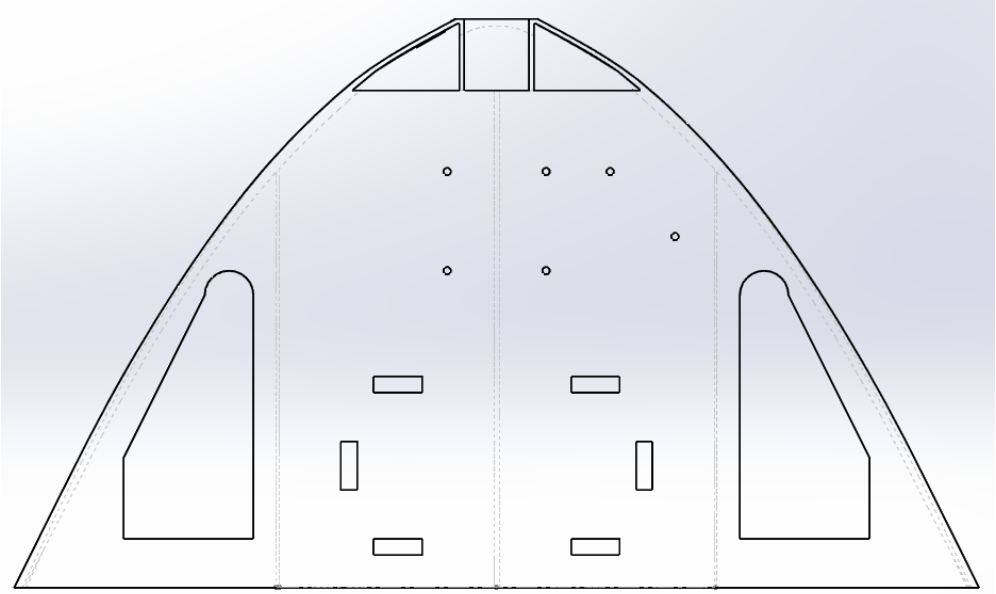

Figure 11.5 – Nose internal structure top-view

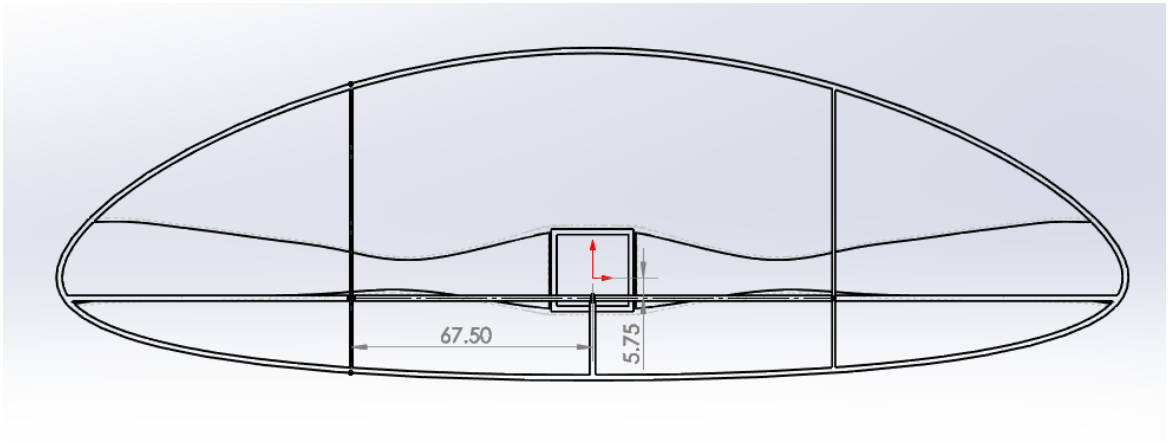

Figure 11.6 – Nose internal structure location

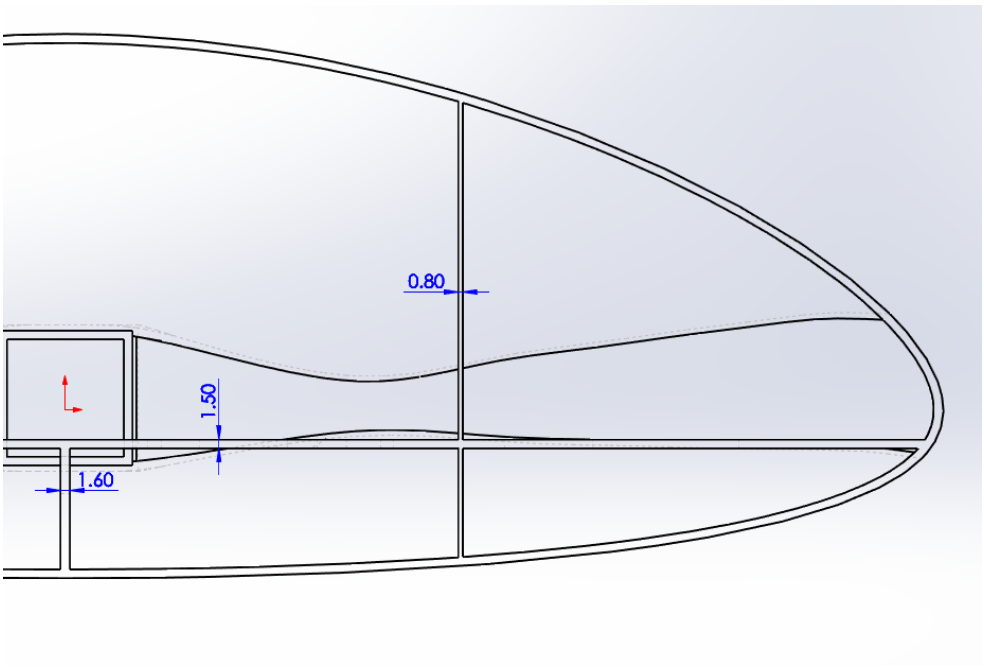

Figure 11.7 – Nose internal structure sizing

11.3 Wing Structure

Internally, the wing is held up by a lattice pattern of ribs, each displaced by 80 mm vertically, and crossing the horizontal by 25°. Each rib has a thickness of 0.6 mm and supports the wing throughout the flight. The wing is reinforced this way to take advantage of 3D printing, as this technique is impossible using traditional methods. By doing so, overall weight of the wing would be reduced, while still giving the wing rigidity against bending moments.

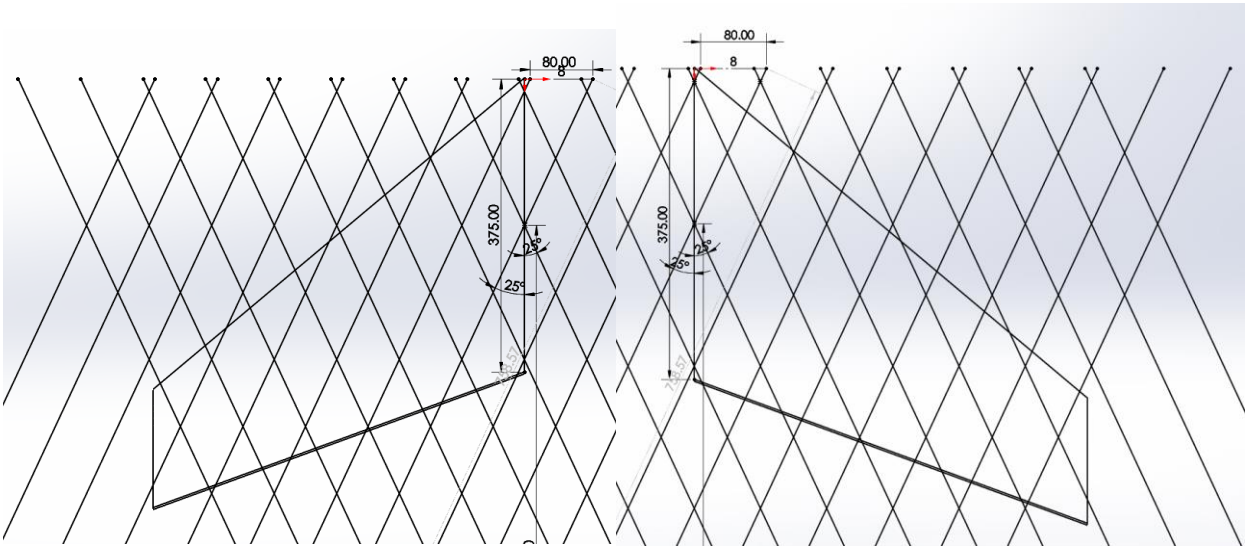

Figure 11.8 – Left & right wing rib setup

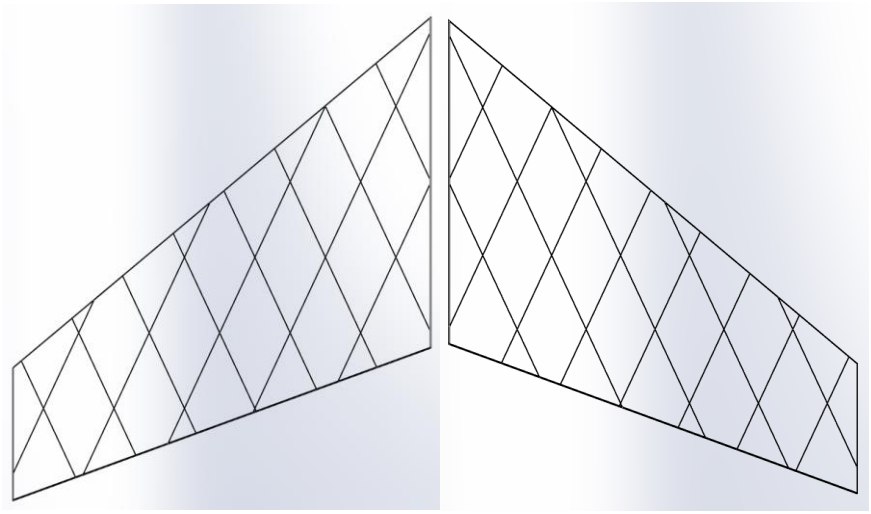

Figure 11.9 – Full left & right wing w/ visible ribs

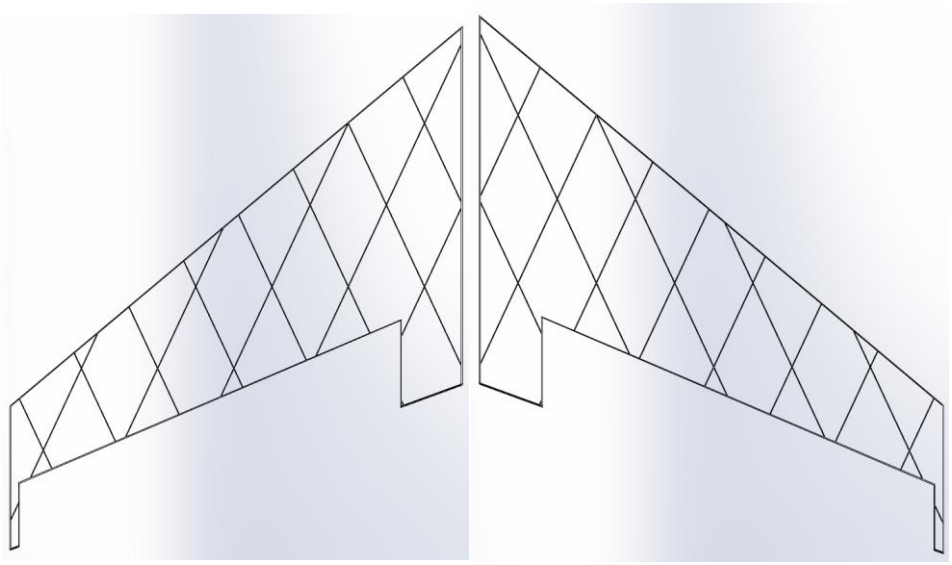

Figure 11.10 – Final left & right wing w/ visible ribs

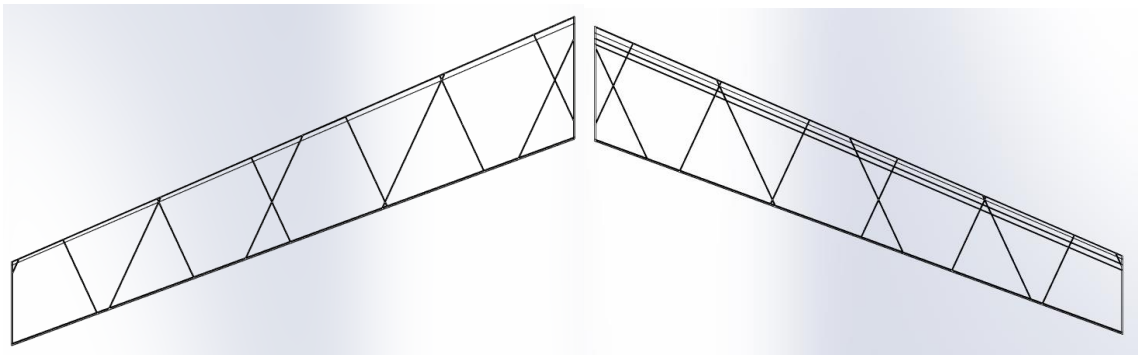

Figure 11.11 – Left & right elevon w/ visible ribs

11.4 Winglet Structure

Unlike the internal of the fuselage and wings, the internal structure was supposed to be hollow, however when the 3D printing program attempted to use the winglet, the system would fail. It was decided to allow the 3D printer to infill the winglet, create its own structure. the 3D printing program taking advantage of the system to infill, creating a lightweight structure for it.

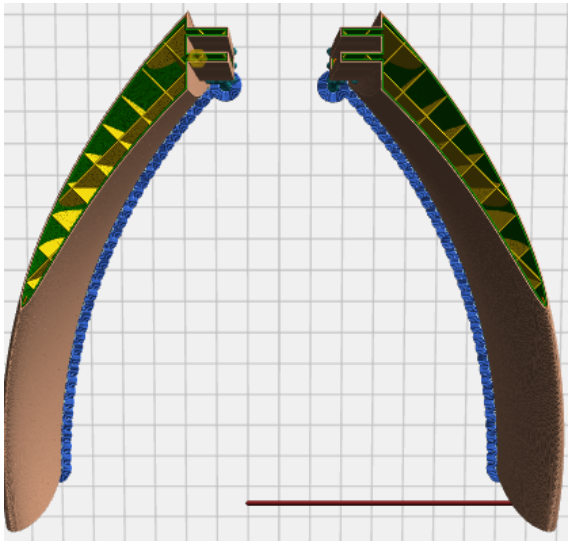

Figure 11.12 – 3D printed winglet w/ internal rib cross-section

Chapter 12 — Weight and Balance

12.1 Introduction

In any aircraft, the weight and location of every component and every piece of equipment is essential to maintain the stability of the aircraft. When the center of mass of the aircraft shifts such as, when cargo slides to the rear, then control of that aircraft becomes impossible and it would crash. To determine the weight and balance of the aircraft, Solidworks is used to estimate the structural Center of Mass, while each electric component will act as point mass. By using these two, the center of mass can be determined. To simplify matters, wires and PCB-based electronics such as the Flight Controller, GPS module, etc. are to be ignored as well as the servo due to its lightweight making it negligible. Furthermore, it is assumed that the aircraft is symmetrical on the x-axis.

12.2 Structure Center of Mass

After identifying all the materials as PLA, the center of mass is seen as:

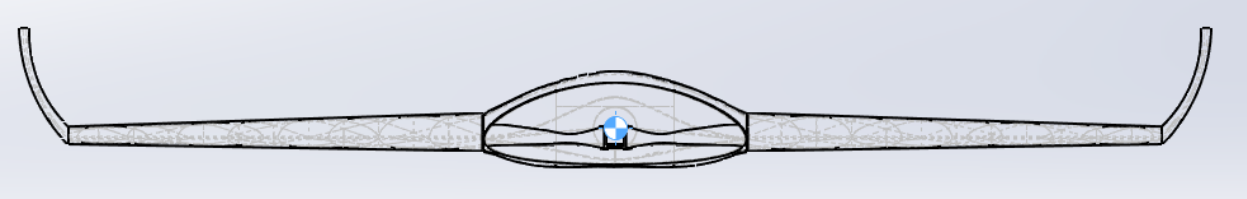

Figure 12.1 – Structure center of mass front-view

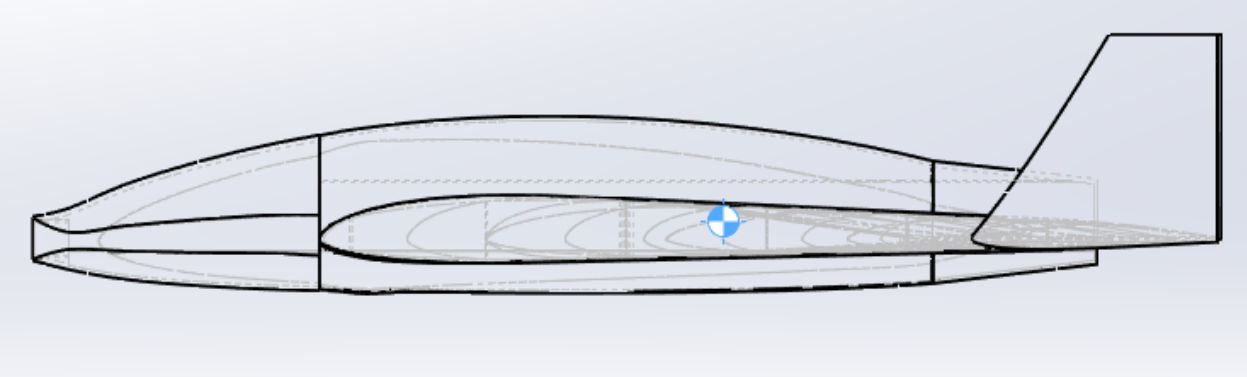

Figure 12.2 – Structure center of mass side-view

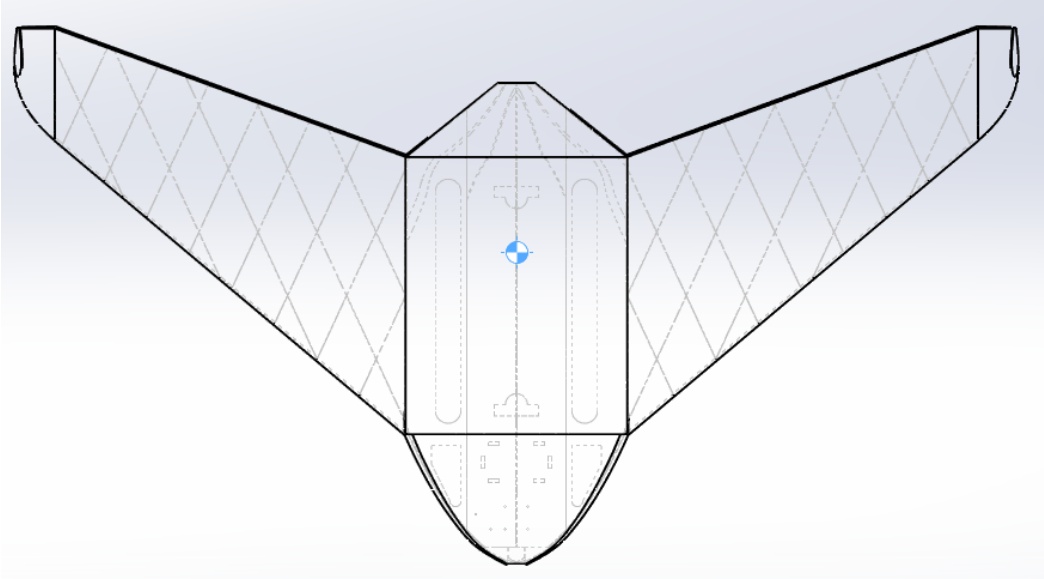

Figure 12.3 – Structure center of mass top-view

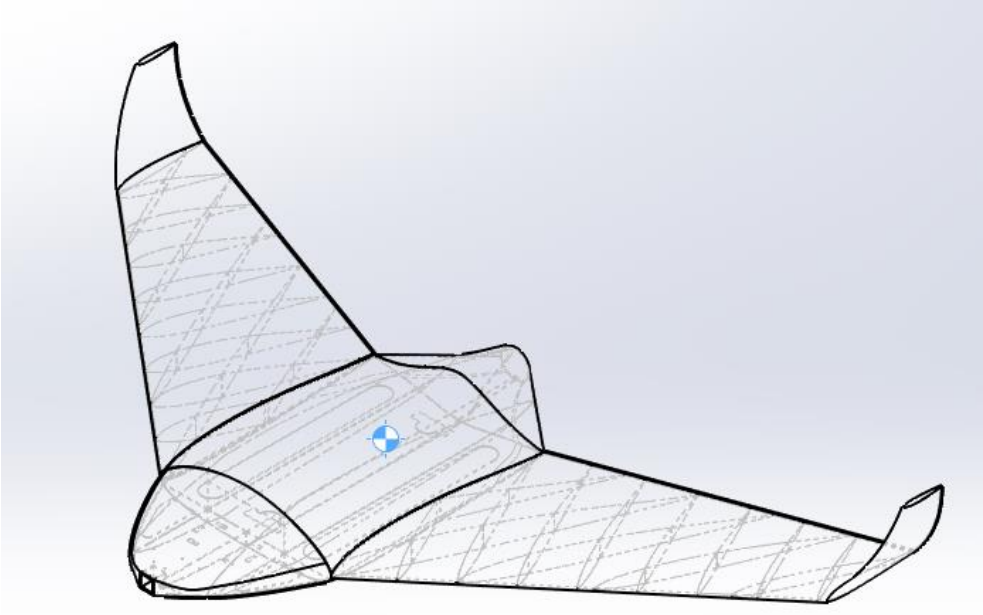

Figure 12.4 – Structure center of mass isometric-view

By using the mass properties evaluation in SolidWorks, it is possible to obtain the exact position of the center of mass. In this case, it is at x = 421.49, y = 10.47, and z =0.44. The z-axis can be ignored, due to the symmetrical design of the aircraft. The overall structural mass is 1717.68 grams.

12.3 Component Masses

The three components that need to be listed is the electric motor in the rear, the camera at the front, and battery in the nose.

Table 12.1 – Location & weight of heavy components

Component	X-axis (mm)	y-axis (mm)	Weight (g)
Camera	10	0	10
Battery	135	0	175
Motor	660	10	150
Structure	421.49	10.47	1717.68

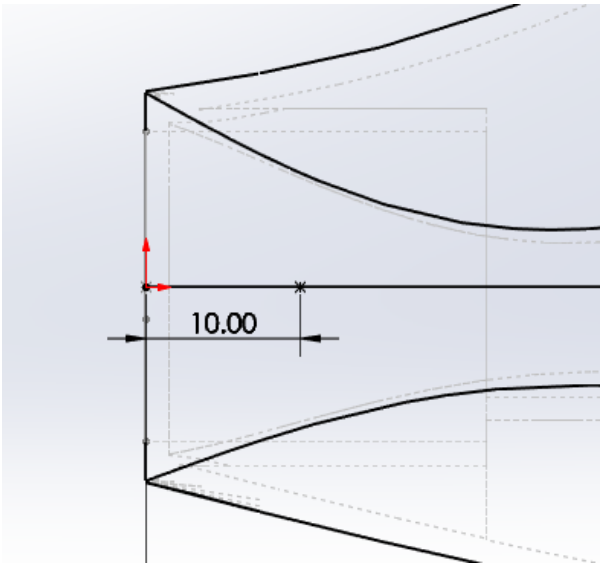

Figure 12.5 – Approximate position of camera

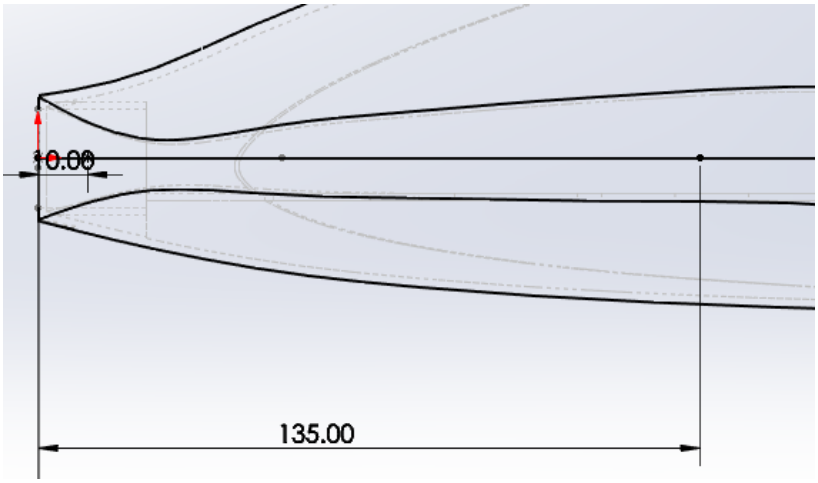

Figure 12.6 – Approximate position of battery

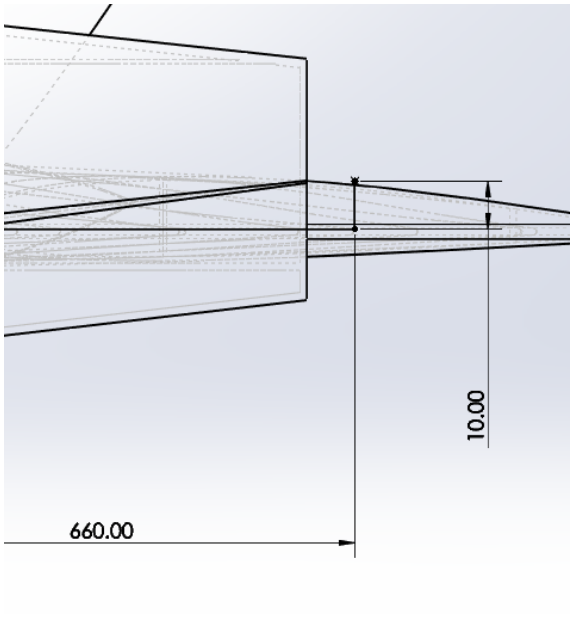

Figure 12.7 – Approximate position of motor

12.4 Total Center of Mass

To get the aircraft's center of mass, the center of mass equations is used:

$$X_{cg} = \frac{\sum m_i x_i}{m_{total}} \tag{12.1}$$

$$Y_{cg} = \frac{\sum m_i y_i}{m_{total}} \tag{12.2}$$

It is determined that the total mass is 2052.6833 grams and is located at 412.49 mm in the x-direction and 10.43 mm in the y-direction from the origin.

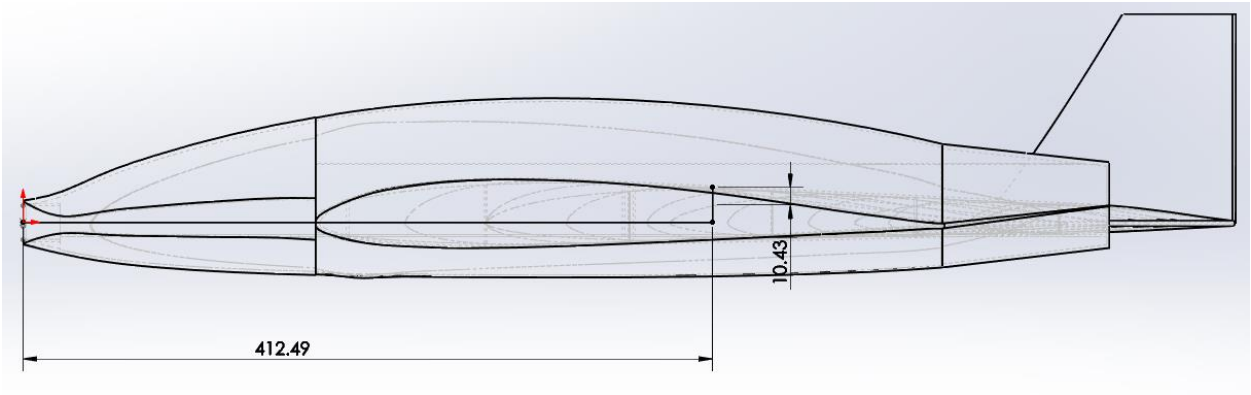

Figure 12.8 – Total center of mass side-view

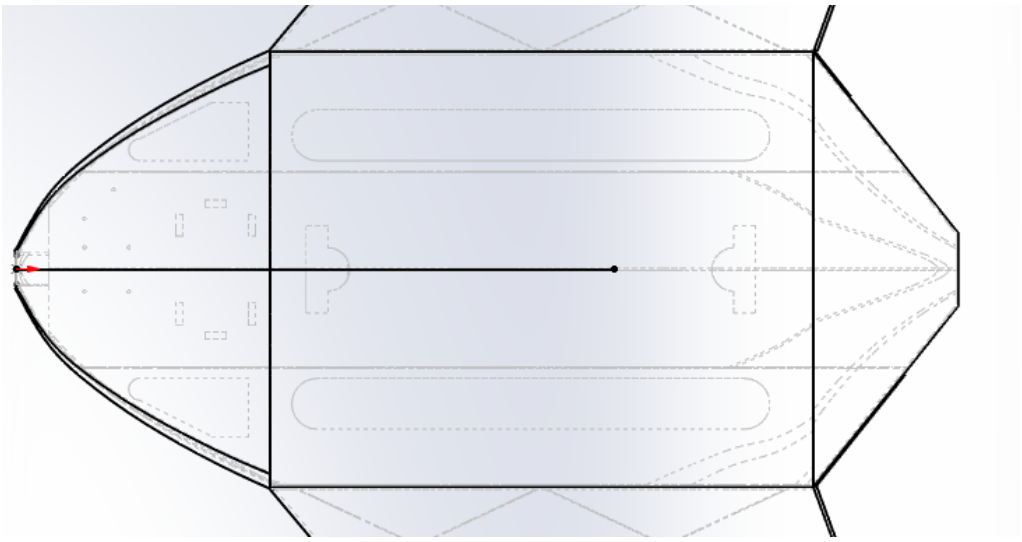

Figure 12.9 – Total center of mass top-view

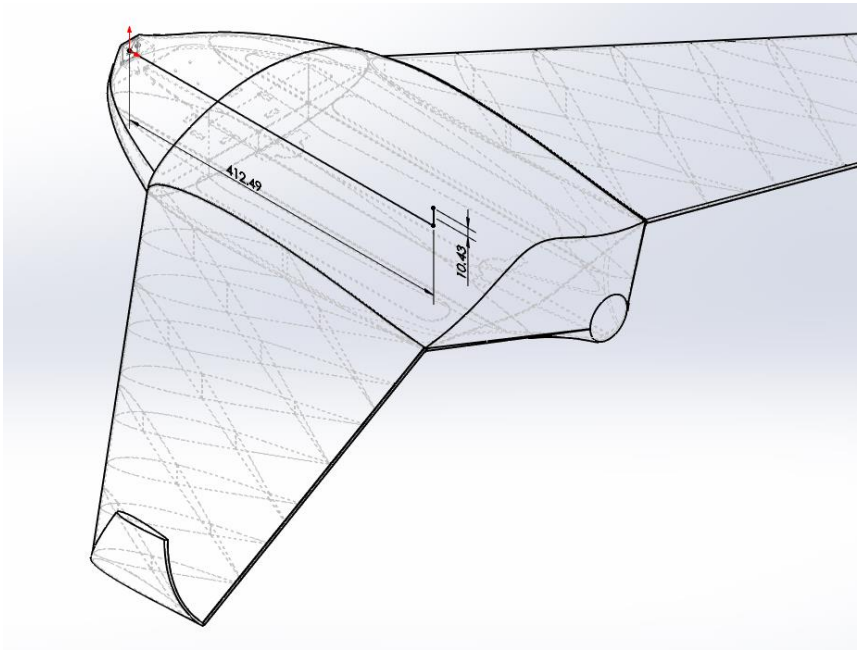

Figure 12.10 – Total center of mass isometric-view

12.5 Static Margin

The static margin is defined as the distance between the center of mass and the neutral point. It is a vital component to determine the longitudinal stability of the aircraft when pitching. Normally, a satisfactory static margin is 10%. It is assumed that the neutral point is approximate to the aerodynamic center of the flying wing, which is 348.62 mm away from the nose.

$$SM = \frac{NP-CG}{MAC} \tag{12.3}$$

The static margin is calculated to be -20%, which means that the aircraft is longitudinally unstable. To improve the SM, a ballast weight of 1000 grams is to be placed in the nose, approximately 100 mm away from the tip of the nose. This will improve the static margin to 10%, which will make it controllable.

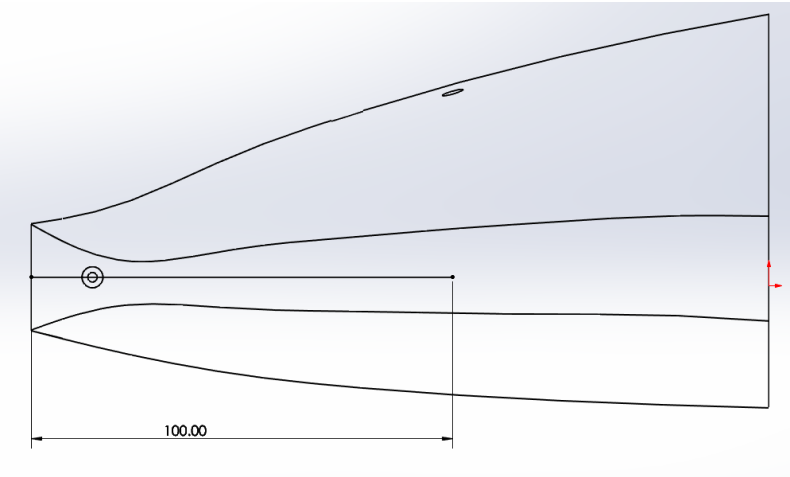

Figure 12.11 – Ballast location

12.6 Conclusion

By using SolidWorks and making assumptions of the heavier components, it is possible to calculate the center of mass of the aircraft and thus the static margin. By doing so, an issue was identified and then later fixed with the usage of a ballast. This development allows for the aircraft to gain longitudinal stability. To further improve the aircraft's controllability a PID controller can be used to insert a PID to make the aircraft stable during flight.

Chapter 13 — Flight Components

13.1 Electronics Overview

Electronics must be properly integrated into the platform to operate the aircraft. As many of these electronics are difficult to manufacture independently, they will be sourced through e-commerce.

These electronics include the flight controller (FC), electronic speed controller (ESC), one radio receiver (RX), the video transmitter (VTX), the camera, one motor, and two servos. Most of the electronics selected are based on Flightory's recommendations for their Super Stingray aircraft. However, due to my access to specific components, a few of the electronics will differ from their recommendations.

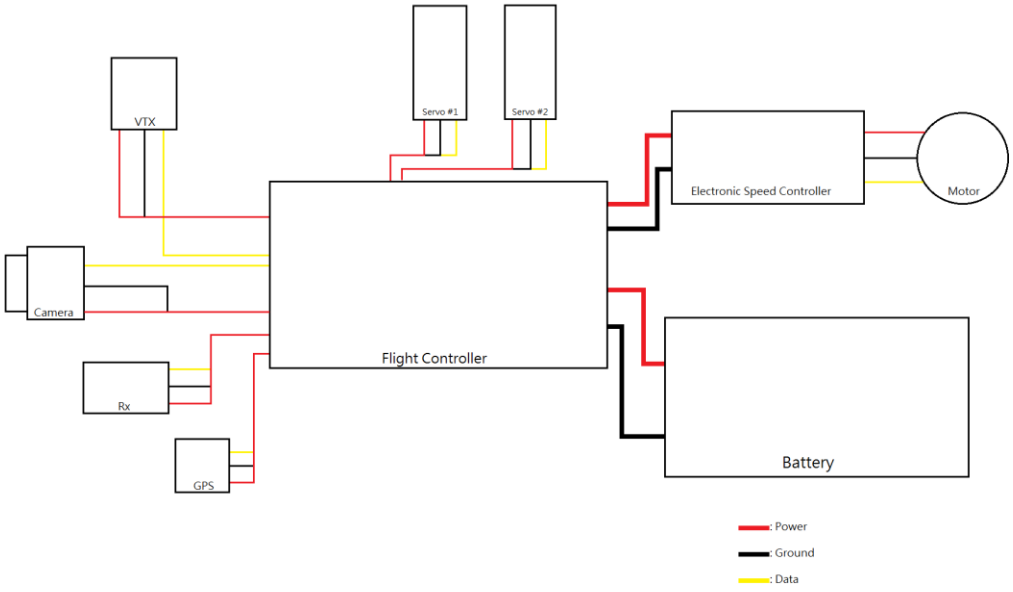

Figure 13.1 – General fixed-wing wiring diagram

Table 13.1 – Flightory Super Stingray recommended components [24]

Motor	23XX 1000-1400 KV
Propeller	10 x 5/ 10 x 6
Flight Controller	Speedybee/Matek F405 Wing or any other Mavlink FC
GPS	Matek M10Q or similar GPS
Servos	2x Emax ES08MAII Metal Gear or similar

Electronic Speed Controller	BLHeli 30-40A
Battery	4S (max 4S4P 14Ah Li-Ion) or smaller pack/Li-Po
Receiver	Matek R24-D ELRS
VTX & Camera	Walksnail Avatar

13.2 Chosen Flight Electronics

13.2.1 Motor

The Turnigy 1450KV Brushless motor was chosen to power Beansky. Although this is a more powerful than the recommended component, the 1450KV motor was selected due to the lower cost of procuring it. The specifications of the motor are as follows:

- Mass: 130 grams
- Max Thurst: 14 N of thrust
- Diameter: 24 mm
- Total Length: 42 mm

Figure 13.2 – Turnigy 1450KV brushless motor [28]

13.2.2 Flight Controller

The flight controller selected for Beansky is the MATEK F405 Wing V2, due to the recommendations from the Flightory Super Stingray. Modern FCs are extremely important, as the FC processes the pilot commands to move the individual servos responsible for the aircraft's movement (pitch, roll, and yaw). The FC is also responsible for using the built-in gyroscope and IMU to detect the aircraft's orientation and automatically make small adjustments to keep the aircraft stable. The specifications of the flight controller are as follows:

- Mass: 25 grams
- Length: 54 mm
- Width: 36 mm
- Height: 13 mm

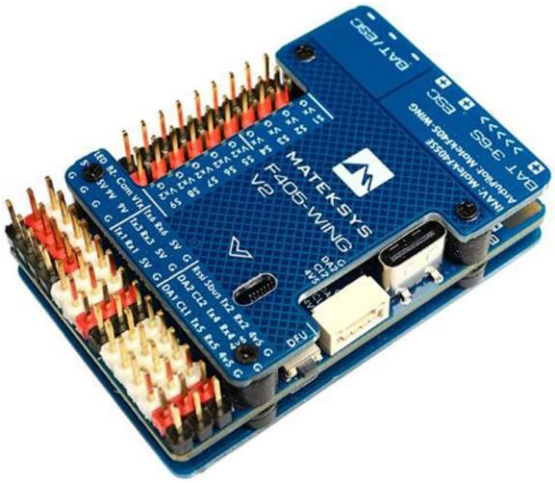

Figure 13.3 – MATEK F405 Wing V2 [29]

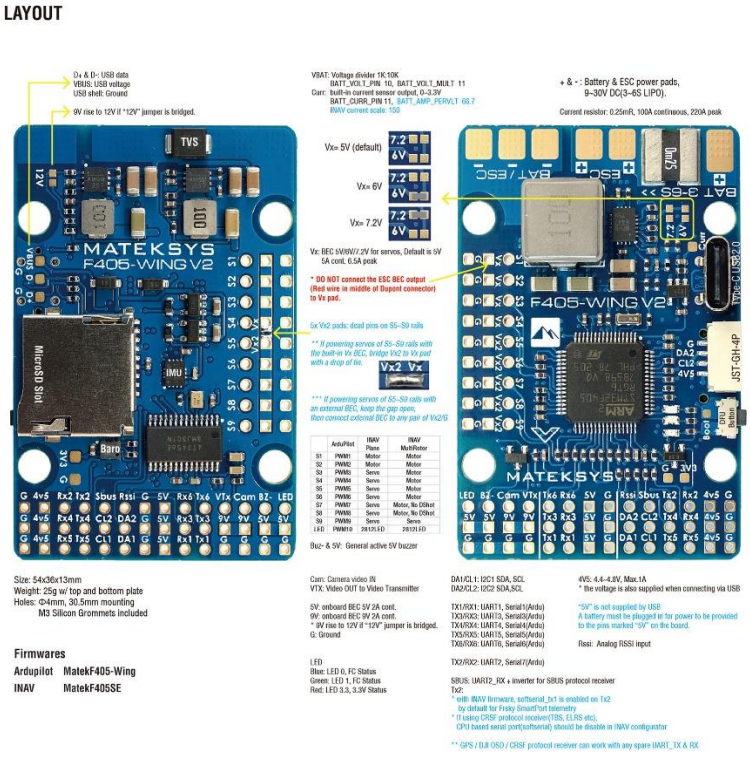

Figure 13.4 – MATEK F405 Wing V2 wiring layout [29]

13.2.3 GPS System

The HGLRC M100 GPS Compass Module is used, due to its small size and light weight. Although it isn't a recommended Matek M-10Q, the M100 GPS is similar enough that no sacrifices are made in performance. The specifications of the GPS are as follows:

- Mass: 7.73 grams
- Length: 21 mm
- Width: 21 mm
- Height: 8.02 mm

Figure 13.5 – HGLRC M100 GPS Module [30]

13.2.4 Servo

The EMAX ES08MAII Metal Gear was chosen to control the control surfaces of the aircraft, due to its low cost and small size. This is especially useful due to the minimal amount of space that's available inside the wing structure. The specifications of the servo are as follows:

- Mass: 12 grams
- Length: 23 mm
- Width: 11.5 mm
- Height: 24 mm
- Mount Height: 15 mm

Figure 13.6 – EMAX Servo [31]

Mini SERVO (ES08MAII) SERIES

SERVO ES08MA SPECIFICATIONS

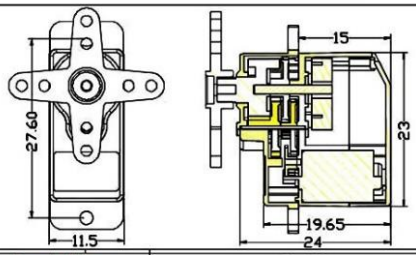

Operating Voltage:		4.8~6.0V
STD Direction:		Counter Clockwise / Pulse Traveling 1500 to 1900usec
Stall Torque:	4.8V	1.6 Kgf.cm(21.0 oz.in)
Operating Speed:	4.8V	0.12 Sec/60° at no load
Stall Torque:	6.0V	2.0 Kgf.cm(28.0 oz.in)
Operating Speed:	6.0V	0.10 Sec/60° at no load
Size:		23X11.5X24 mm
Weight:		12 g
Plug Available		FUT ;JR
Other		Analog ;Metal

Figure 13.7 – EMAX Servo Specifications [31]

13.2.5 Electronic Speed Controller

The ESC is responsible for controlling the amount of power that enters the electric motor and the electronics, ensuring that the aircraft remains safe. Furthermore, it translates the commands given by the pilot into precise motor commands, optimizing performance and stability. The ESC chosen is the Hobbywing Skywalker 50A ESC, due to ease of access. The specifications of the ESC are as follows:

- Mass: 41 grams
- Length: 60 mm
- Width: 25mm
- Height: 8 mm

Figure 13.8 – Skywalker 50A ESC [32]

13.2.6 Battery

Battery choice is vital, as it determines the flight time the aircraft has. A balance of weight and power was found in 4S batteries. Therefore, the Ovonic 4S 35C 2200 mAh LiPo battery is going to be used. The specifications of the battery are as follows:

- Mass: 176 grams
- Length: 76 mm
- Width: 35 mm
- Height: 33 mm

Figure 13.9 – Ovoinic 4S 35C LiPo [33]

13.2.7 Radio Receiver

The radio receiver is a vital component of drones, responsible for receiving signals from the pilots. The radio receiver chosen is the ELRS-R24-D from MATEK. The ELRS-R24 transmits at a frequency of 2.4 GHz and was chosen due to its small weight and small size. The specifications of the radio receiver are as follows:

- Mass: 3 grams
- Length: 21 mm
- Width: 15 mm
- Height: 3 mm

Figure 13.10 – ELRS-R24-D Radio Receiver [34]

13.2.8 Video Transmitter & Camera

The VTX and camera system is the heart of FPV drones, as without it the pilot will not be able to see where exactly the drone is traveling. In this case, the camera chosen is the RunCam Phoenix 2 SE. The Pheonix 2 SE has a 160° view and transmits at 5.8 GHz. The VTX chosen is the HGLRC Zeus Nano VTX, which was chosen due to how straightforward it is to set up.

Figure 13.11 – RunCam Pheonix 2 SE [35]

Figure 13.12 – HGLRZ Zeus Nano VTX [36]

Chapter 14 — Subsystem Arrangement

14.1 Servo Mount

The servos are located within the wing structure. To attach the commercial servos onto the aircraft, a pair of M2 screws are used. A wiring channel is installed on both wings to allow easy access to the servo wiring and will need to be covered up before flight.

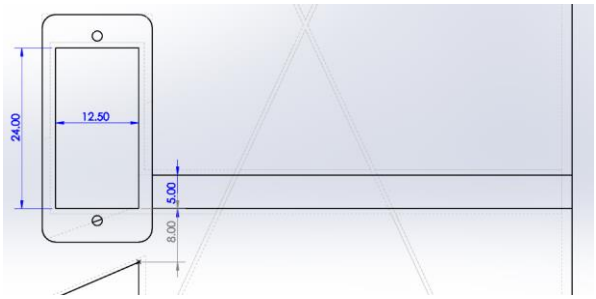

Figure 14.1 – Right wing servo mount bottom-view

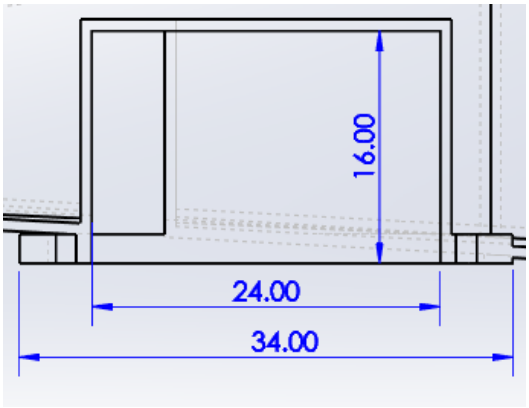

Figure 14.2 – Right wing servo mount bottom-view

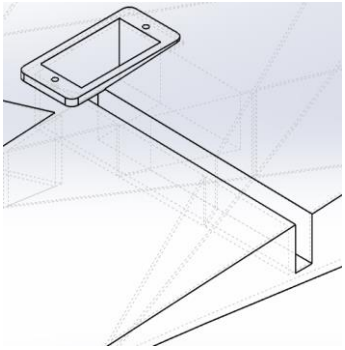

Figure 14.3 – Right wing servo mount isometric-view

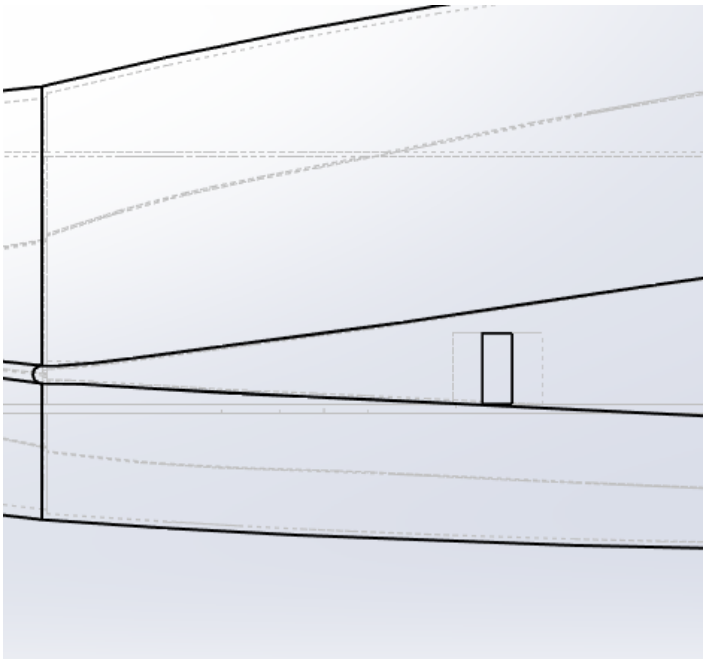

Figure 14.4 – Right fuselage servo channel side-view

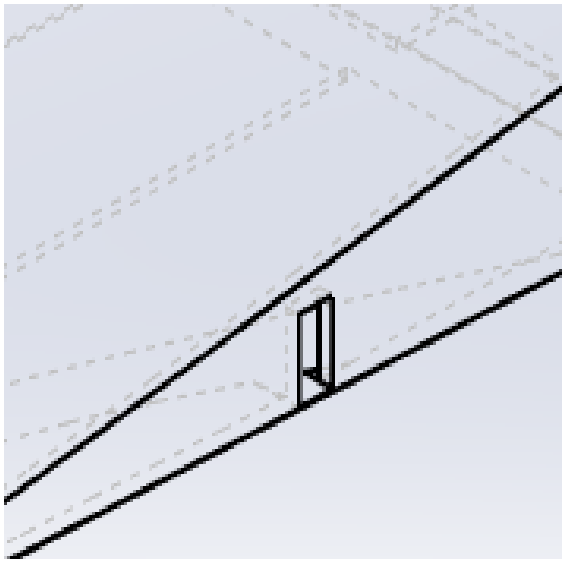

Figure 14.5 – Right wing fuselage servo channel isometric-view

14.2 Electronic Layout

The flight controller, radio receiver, VTX, camera, and battery are located in the nose to help with balancing. The radio receiver and VTX antennas will protrude through the airframe via three holes. The ESC is located inside the central fuselage in between the flight controller and the motor.

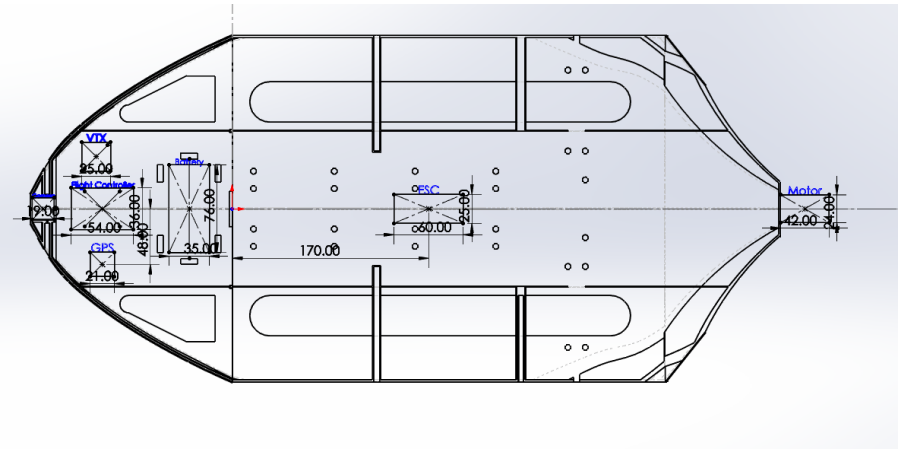

Figure 14.6 – Components location

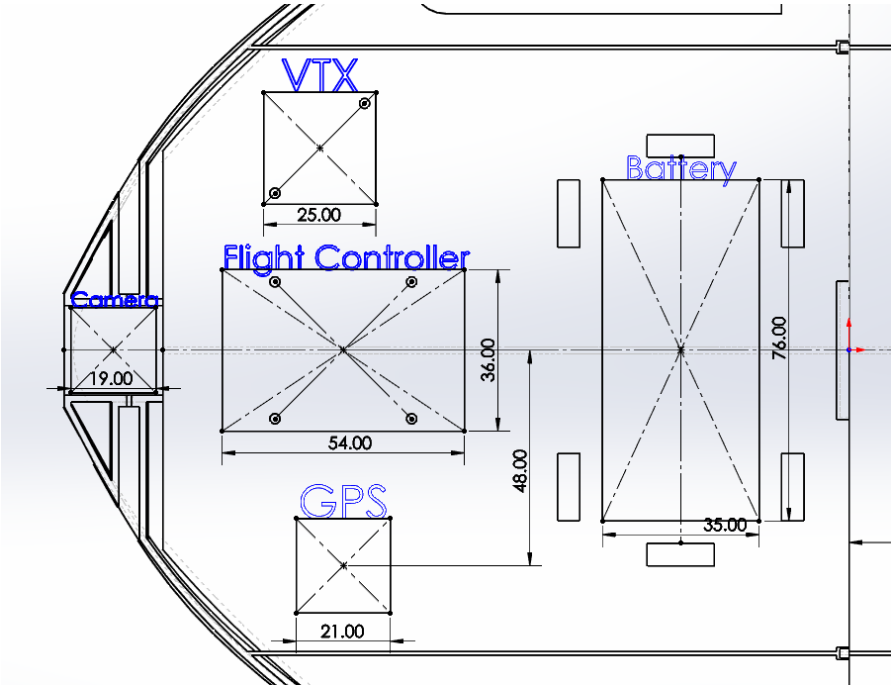

Figure 14.7 – Nose components close-up

14.3 Fuselage-Wing Support

A series of carbon fiber rods are used to not only guide the aircraft to the proper position within the fuselage but give the wings some support. In total, there are three sets of two carbon fiber rods. The dimensions of the tubes are:

- 5 mm x 200 mm
- 5 mm x 300 mm

The rods serve as guide tubes, for attaching the wings to the fuselage. To properly attach the rods into the structure, built-in tubes are used, with an outer diameter of 6.25 mm, and an inner diameter of 5.25 mm.

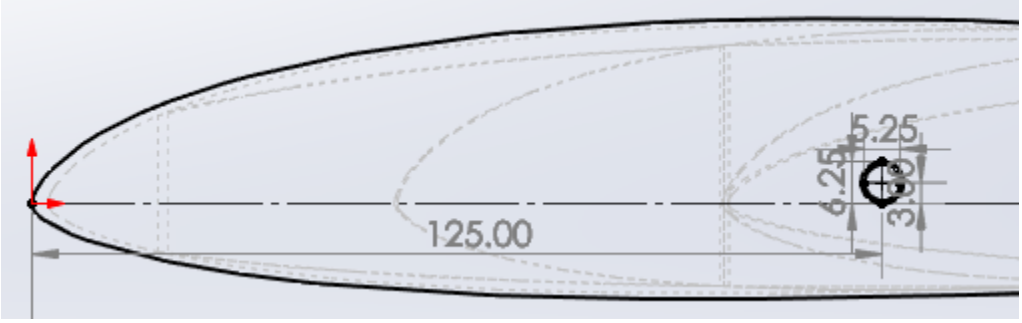

Figure 14.8 – Right wing front tube location

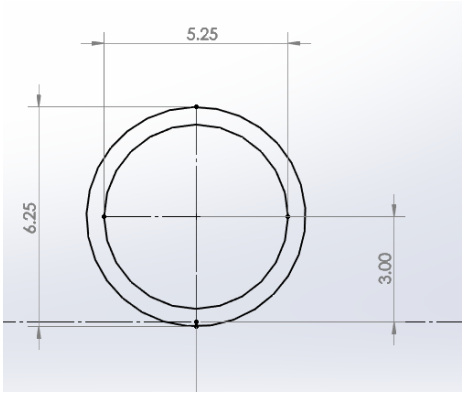

Figure 14.9 – Right wing front tube sizing

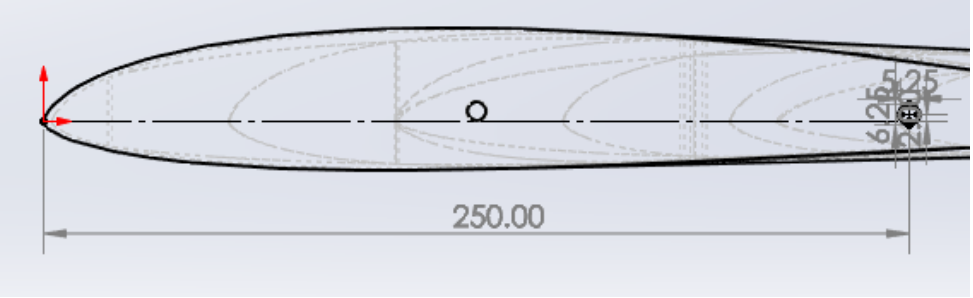

Figure 14.10 – Right wing rear tube location

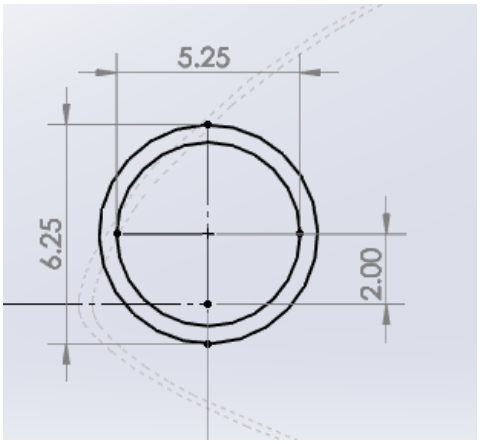

Figure 14.11 – Right wing rear tube sizing

Unlike the built-in tubes in the wings, the fuselage's built-in tubes are more reinforced, being supported with a platform. Furthermore, the outer tube is thickened by 1 mm. By combining the wing and fuselage together, the entire carbon fiber rod can be constrained.

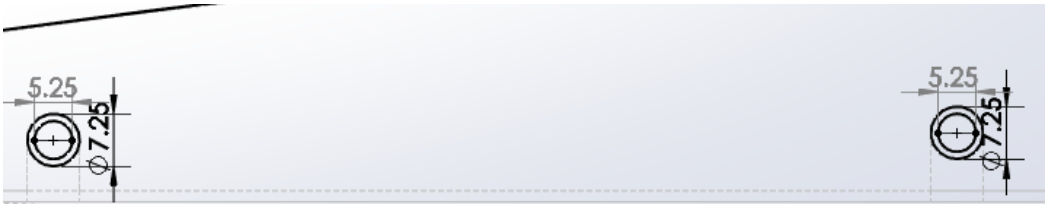

Figure 14.12 – Right wing fuselage tube supports

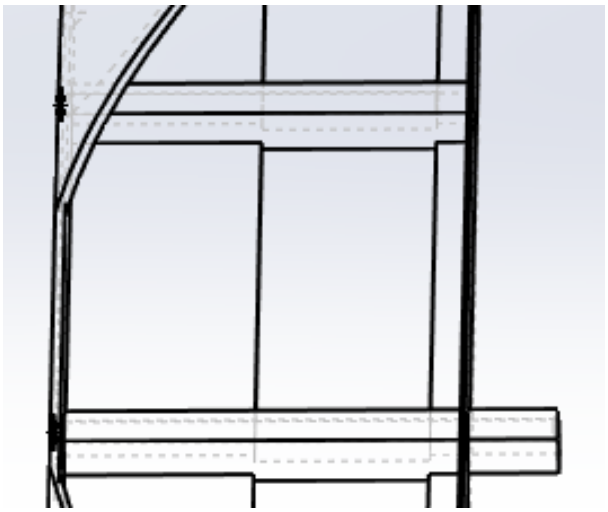

Figure 14.13 – Right wing fuselage tube supports overhead-view (note the support structure)

14.4 Elevon-Wing Attachment

To attach the elevon to the wing, a 3mm x 500 mm long carbon fiber tube is to be inserted within the wing. This will constrain the elevon from moving but still allow it to rotate. To ensure that the tube won't slip out during flight, the winglet will block the hole. The tube is going to be 15mm away, parallel to the elevon plane and centered in the y-direction.

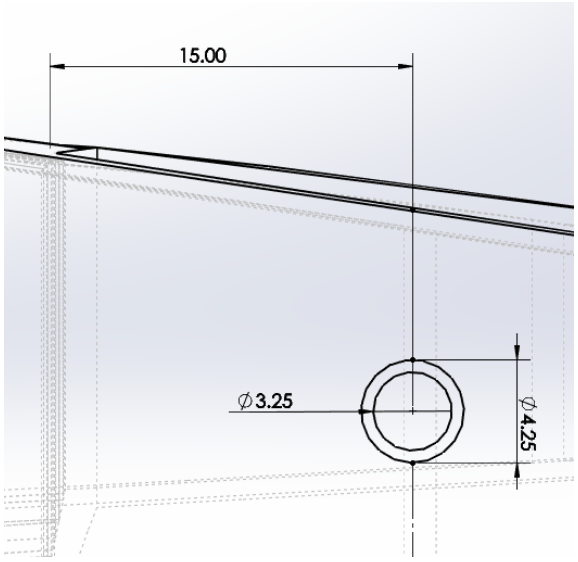

Figure 14.14 – Right elevon rotation tube

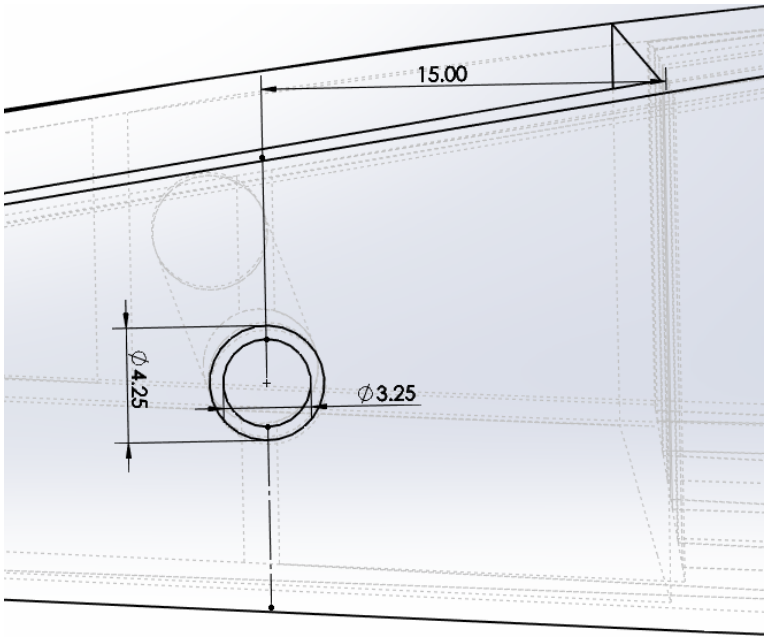

Figure 14.15 – Left elevon rotation tube

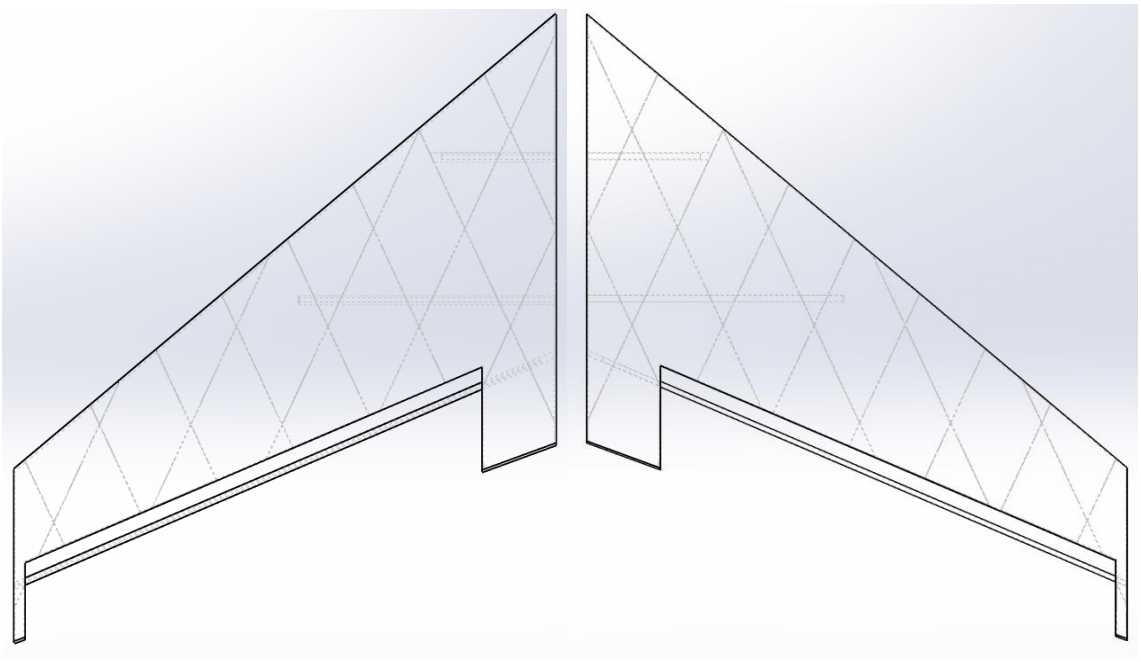

Figure 14.16 – Left & right wing w/ carbon fiber elevon tubes

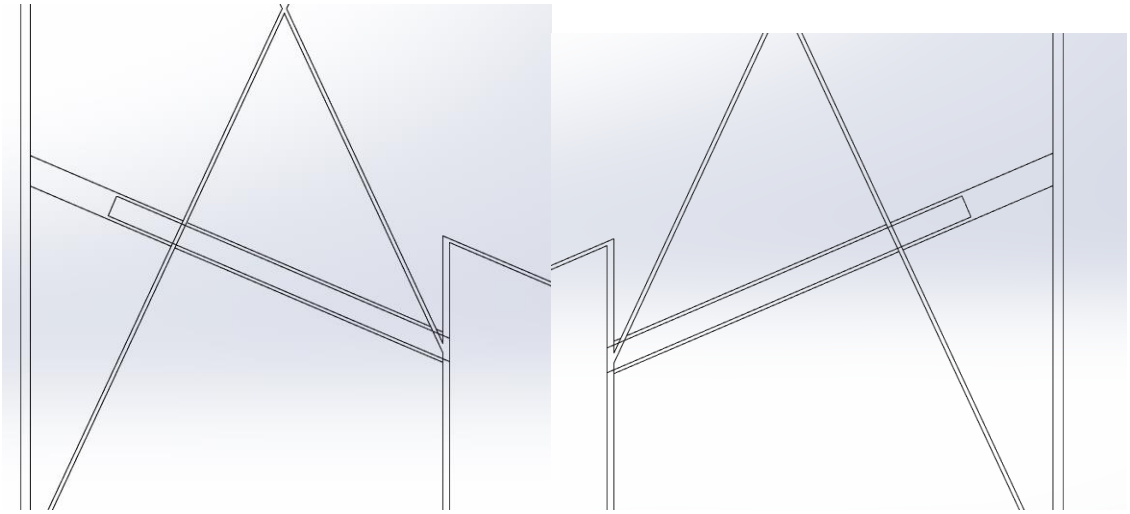

Figure 14.17 – Left & right wing elevon carbon fiber tube structure (w/o servo mount)

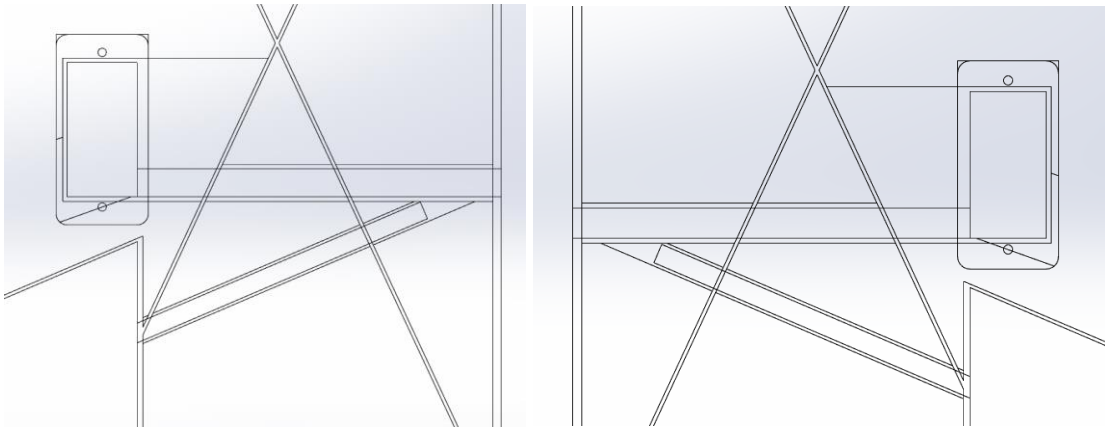

Figure 14.18 – Left & right wing elevon carbon fiber tube structure (w/ servo mount)

14.5 Motor Mount

To mount the motor, an x-mount serves as an interface between the motor and the actual fuselage. This is essential, as the motor requires space below it to run properly. To attach the motor onto the fuselage, M2 screws and nuts are going to be required. There are also wiring channels near the mount to keep them organized.

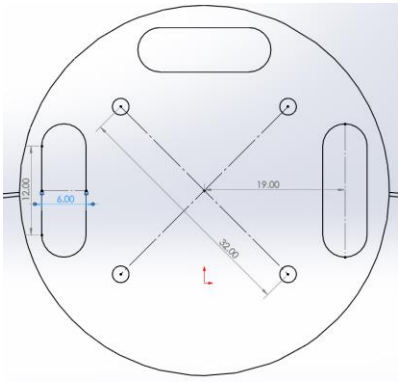

Figure 14.19 – Motor mount

14.6 Fuselage Wiring Channels

The wiring inside the fuselage will be secured by utilizing a series of holes that can be used to zip-tie the wiring in place. This will come with the advantage of also keeping them organized, making them easy to identify. Tape can also be used to identify the wires, for example the left servo wires can be marked with red tape, while the right servo wires can be marked with green tape.

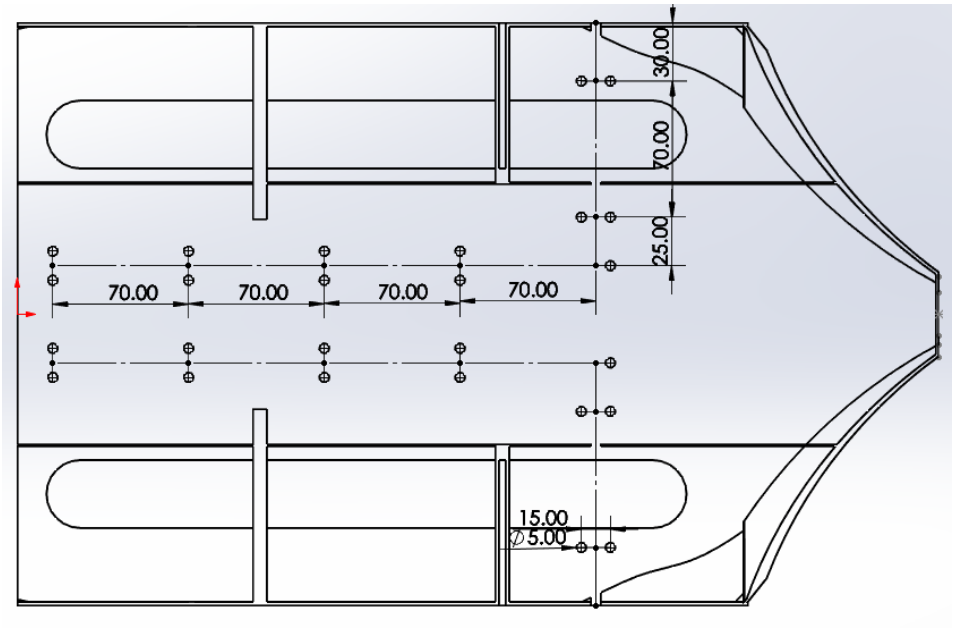

Figure 14.20 – Fuselage wiring system

14.7 Camera Mount

To mount the camera, a set of M2 screws are to be used. These M2 screws are to take advantage of the camera's mounting holes. The shaft used to gain access to the mounting holes have an outer diameter of 8 mm and an inner diameter of 5 mm. The screw is expected to pass through the hole in the center whose diameter is 2.25 mm.

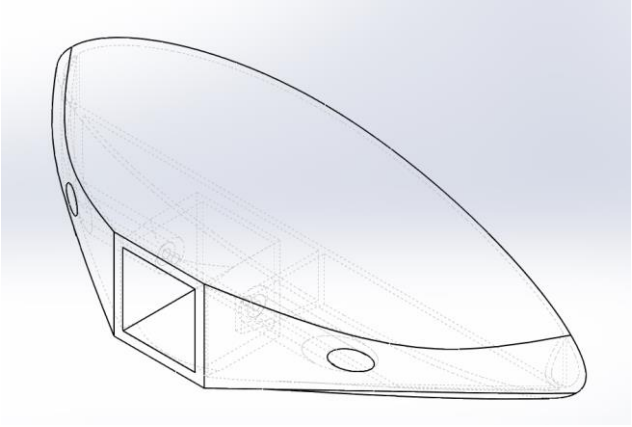

Figure 14.21 – Camera mount holes

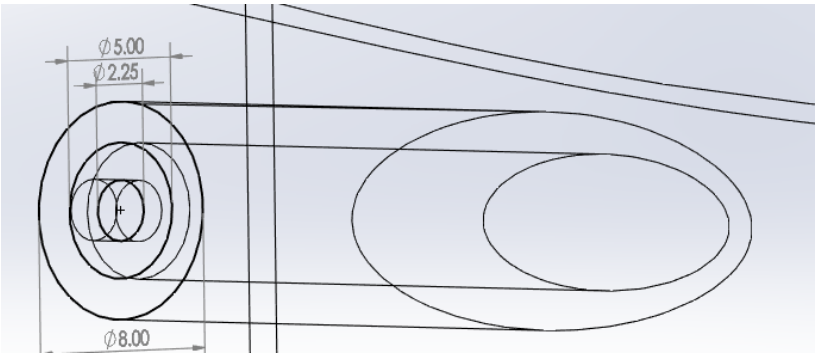

Figure 14.22 – Camera mount hole - closeup

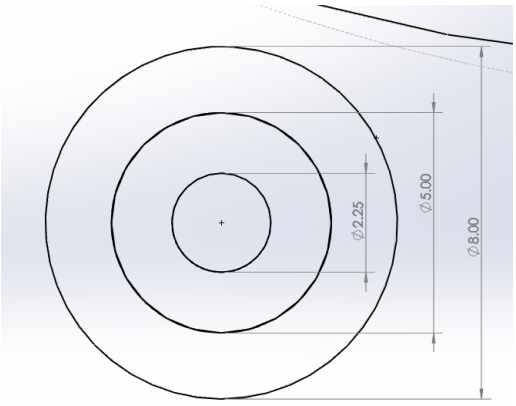

Figure 14.23 – Camera mount holes side-view

14.8 Conclusion

A major issue that showed up during the construction of the drone is the aircraft's brittleness at the wings whenever the carbon fiber support system was not present. If a chance was possible to redo the wings, longer carbon fiber rods would have been integrated within the actual structure. The 5 mm rods would also be the same size, to keep the final cost down.

Chapter 15 — 3D Printing Preparations

15.1 Aircraft Splitting

The aircraft was split into 8 subsections: the left vertical fin, the left wing, the body, the nose, the right wing, the right vertical fin, the left elevon, and the right elevon. Each subsection is further divided for one of two reasons. The first reason is to fit within the printing volume of 220 mm x 220 mm x 220 mm. The second reason a division might occur is to give the user access to the electronics stored within the airframe.

15.2 Nose and Fuselage

15.2.1 Fuselage Alignment

To ensure that each subsection properly align with each other before glue is used, each interface between sections utilizes an connection point. To properly align the subsections together, a “male” connection joins with a “female” connection. In general, the male connection is 0.2 mm smaller than the female connection, allowing for a smoother connection.

There are two main types of alignment devices that are used:

- Side-to-side alignment system
- Front-to-back alignment devices

The side-to-side use the existing vertical support located at the midline of the aircraft to create an extrusion. This extrusion would be able to fit within a hole that was made on the other split. The extrusion extends 3 mm.

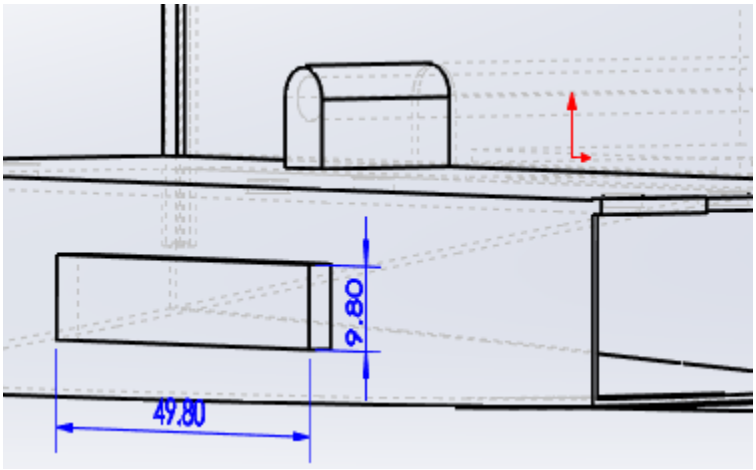

Figure 15.1 – Side-to-side male connection

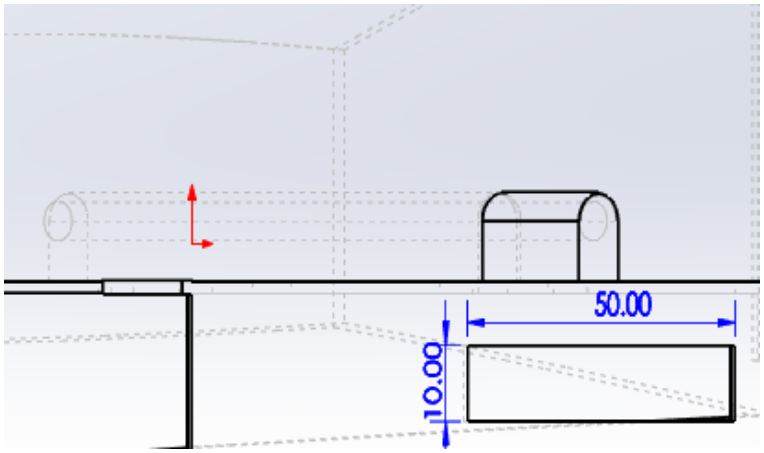

Figure 15.2 – Side-to-side female connection

The front-to-back alignment system utilize the existing central spine as well as the vertical supports on the side to form properly. These devices are much thinner when compared to the lateral alignment devices while also varying in length. Depending on which alignment device is observed. In this case, there are split by interface:

- Nose – Mid Fuselage
- Mid Fuselage – Rear Fuselage
- Rear Fuselage – Tail

The nose – mid fuselage interface utilizes a set of three attachment points, whose overall size is 30 mm x 2.0 mm. This means that the male connection is 29.80 mm x 1.80 mm.

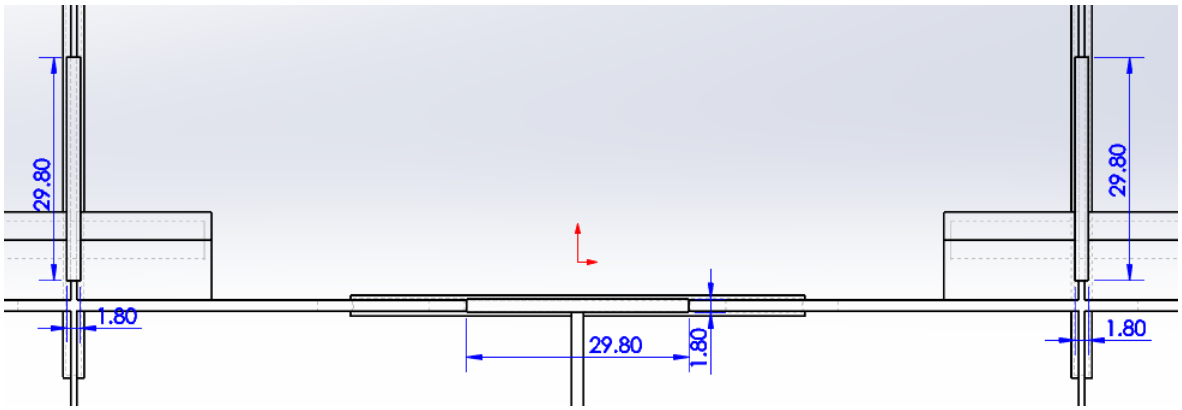

Figure 15.3 – Nose – mid fuselage male connection

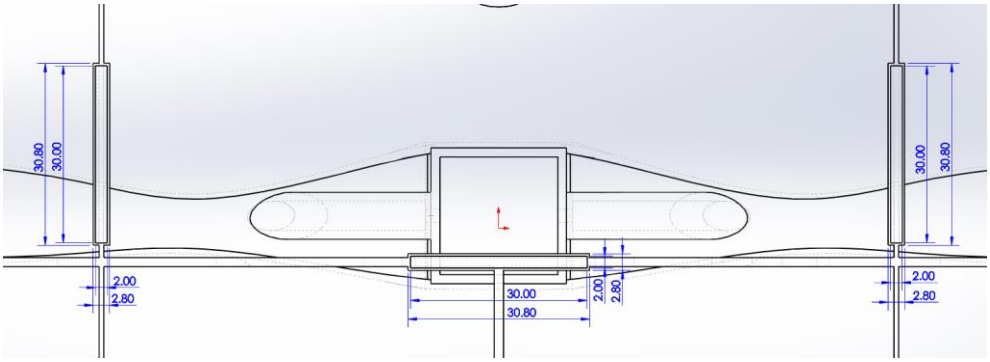

Figure 15.4 – Nose – mid fuselage female connection

The mid fuselage – rear fuselage interface utilizes connections that whose dimensions are 60 mm x 2.0 mm. This means that the male connection is 59.80 mm x 1.80 mm.

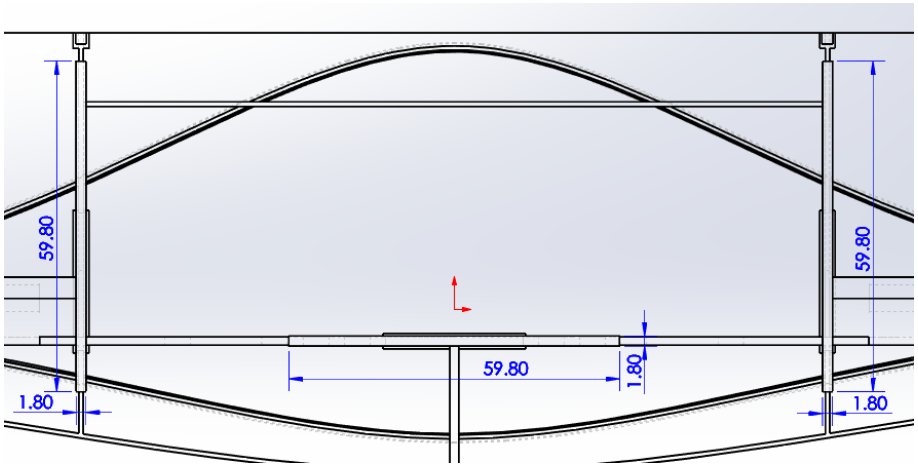

Figure 15.5 – Mid fuselage – rear fuselage male connection

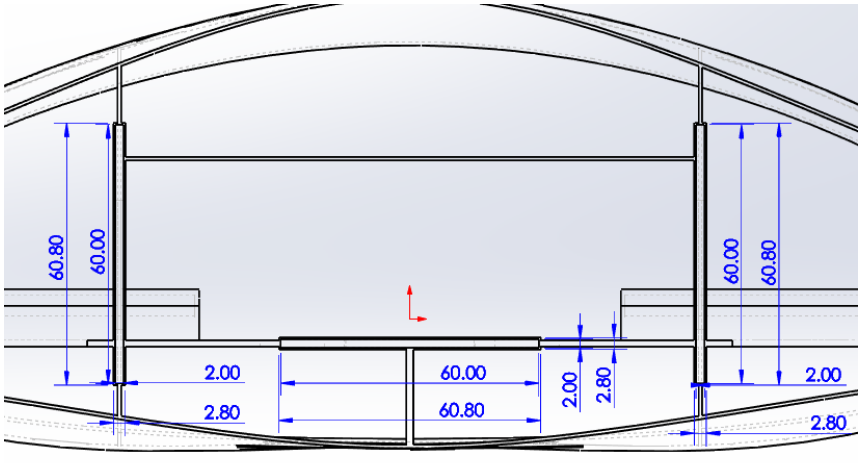

Figure 15.6 – Mid fuselage – rear fuselage female connection

The rear fuselage – tail interface utilizes connections that whose dimensions are 60 mm x 2.0 mm. This means that the male connection is 59.80 mm x 1.80 mm.

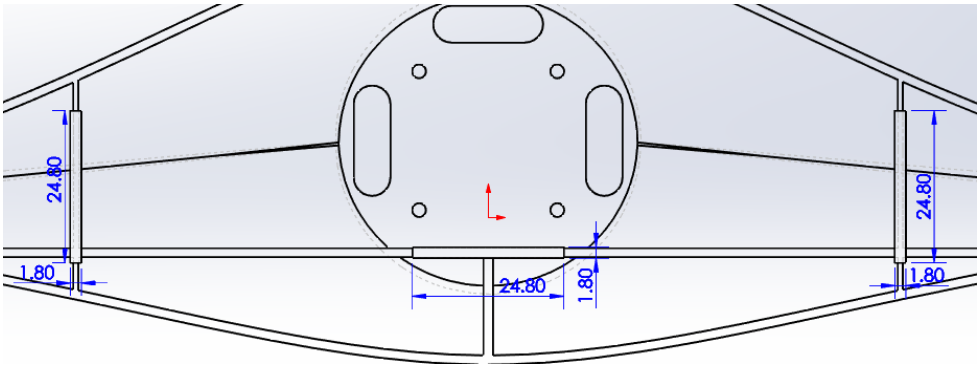

Figure 15.7 – Rear fuselage – tail male connection

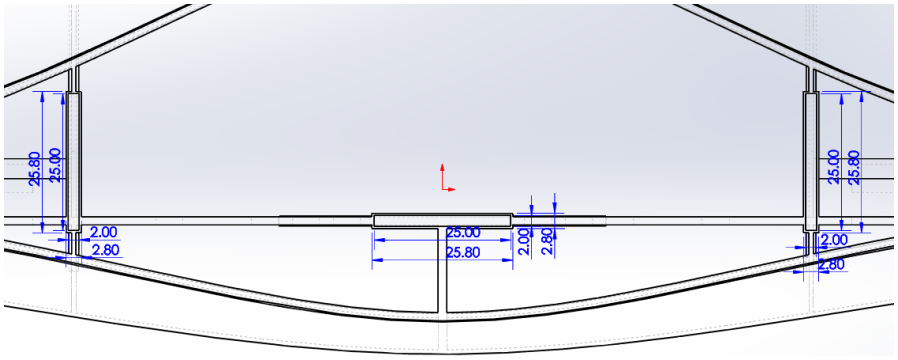

Figure 15.8 – Rear fuselage – tail female connection

The front-to-back alignment system is also used to secure the electronic hatches to the airframe.

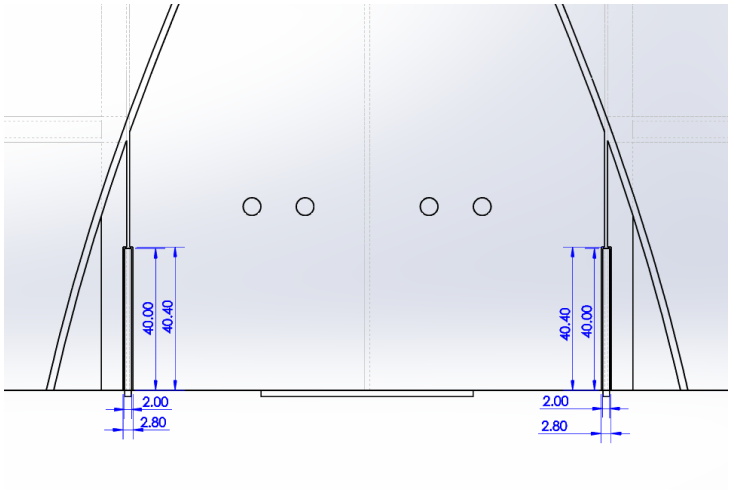

Figure 15.9 – Rear fuselage – fuselage top electronic hatch female connection

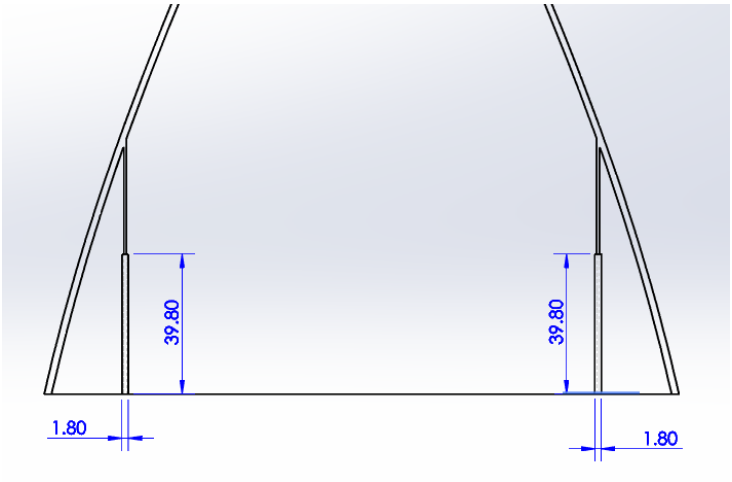

Figure 15.10 – Rear fuselage – fuselage top electronic hatch connection

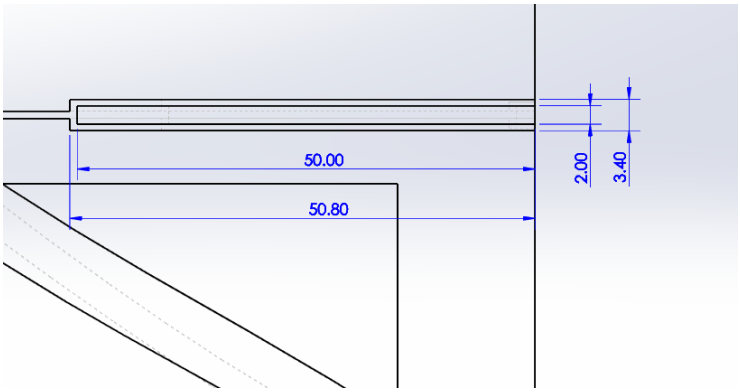

Figure 15.11 – Nose middle – nose bottom female connection

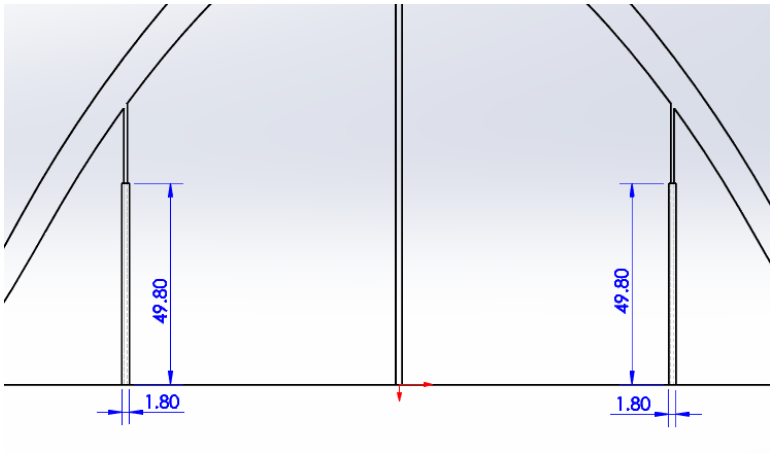

Figure 15.12 – Nose middle – nose bottom male connection

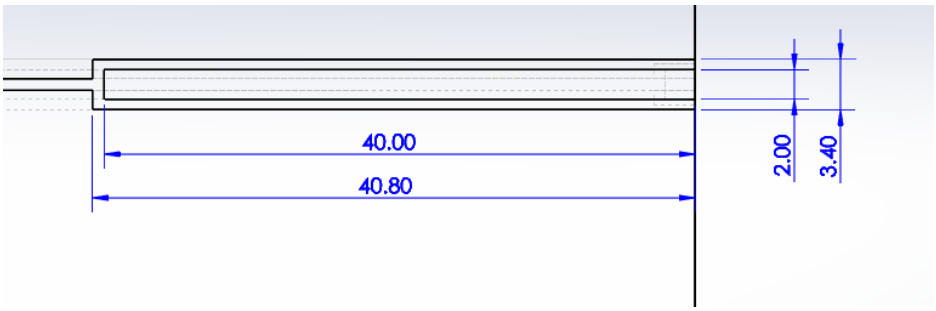

Figure 15.13 – Nose middle – nose top female connection

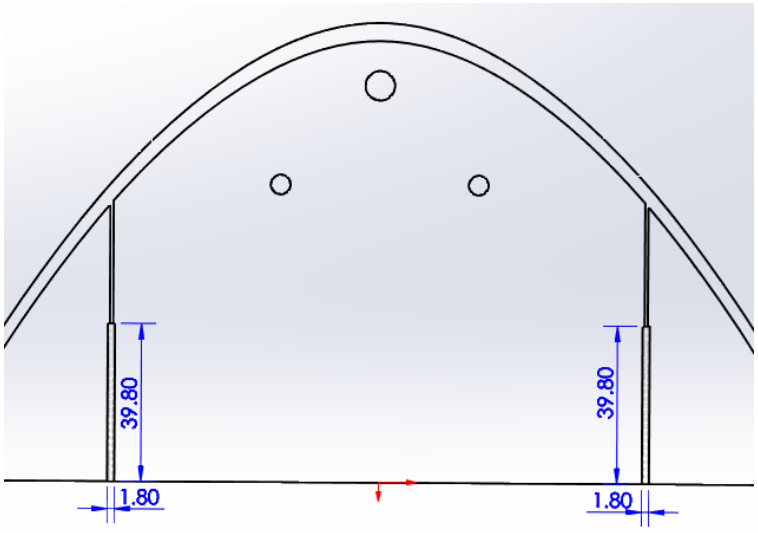

Figure 15.14 – Nose middle – nose top male connection

15.2.2 Fuselage Split

The fuselage subsection is split into 7 different sections:

- Mid fuselage left
- Mid fuselage right
- Rear fuselage left
- Rear fuselage right
- Tail left
- Tail right
- Fuselage top electronic hatch

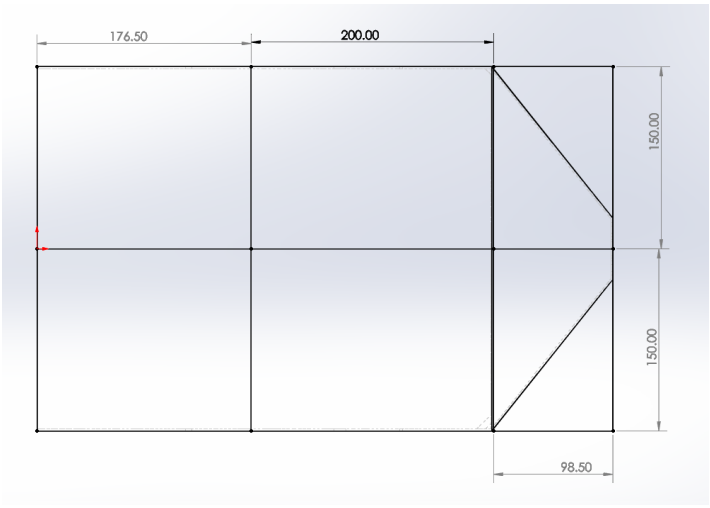

Figure 15.15 – Overall fuselage cut

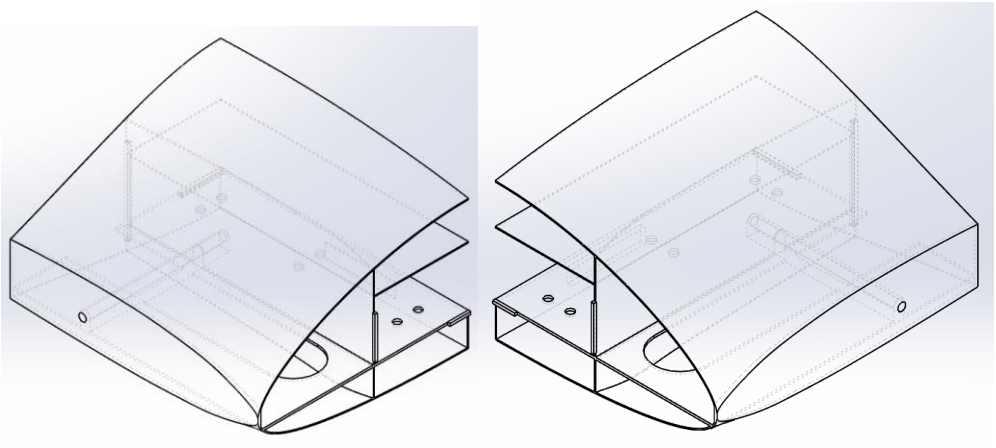

Figure 15.16 – Mid fuselage cut

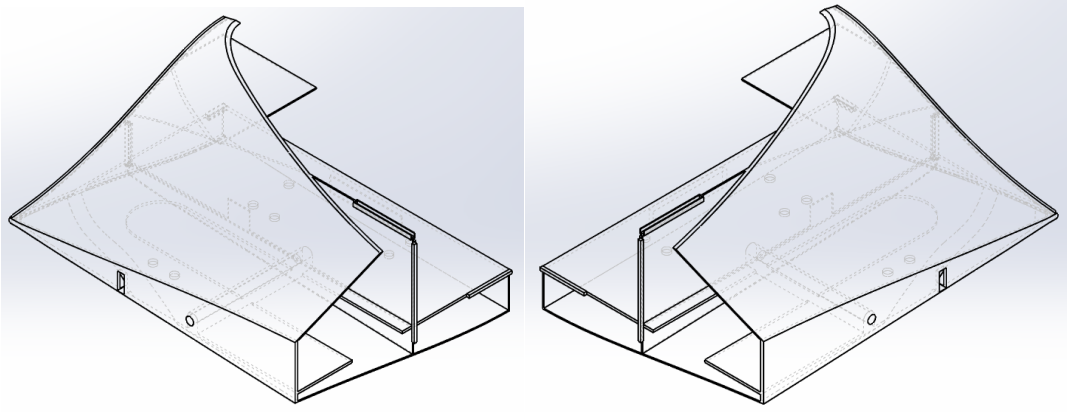

Figure 15.17 – Rear fuselage cut

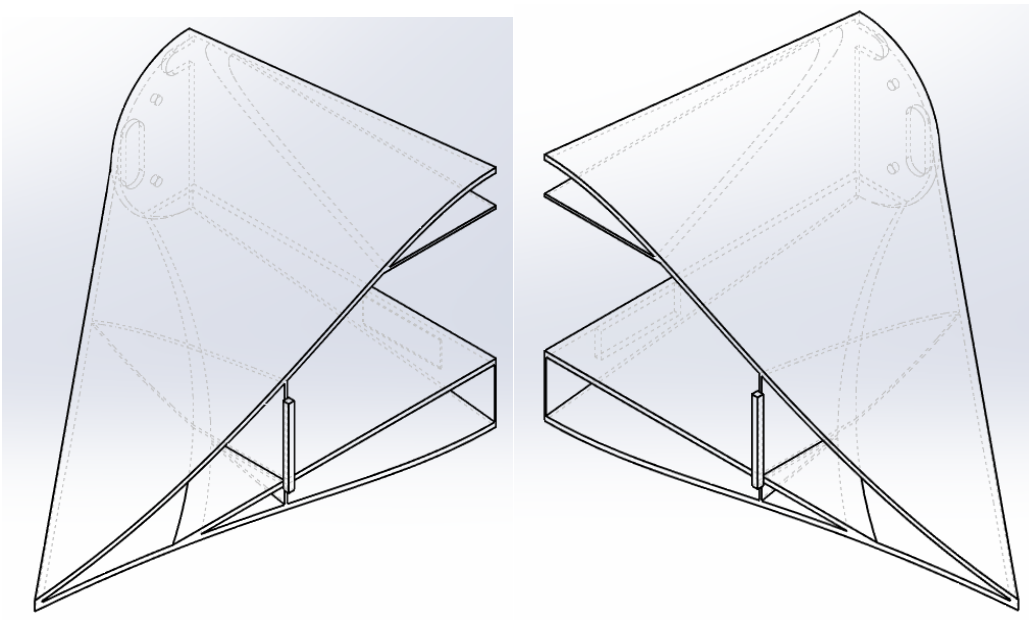

Figure 15.18 – Tail cut

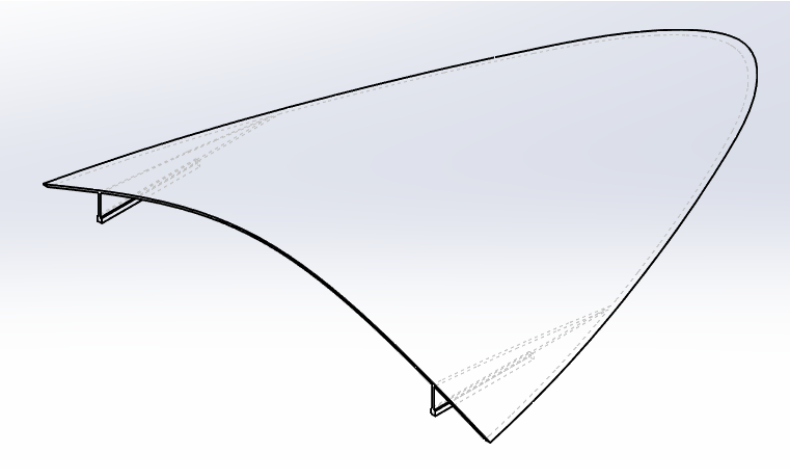

Figure 15.19 – Fuselage top electronic hatch

15.2.3 Nose Split

The nose is split into four different parts:

- Nose left
- Nose right
- Nose top electronic hatch
- Nose bottom electronic hatch

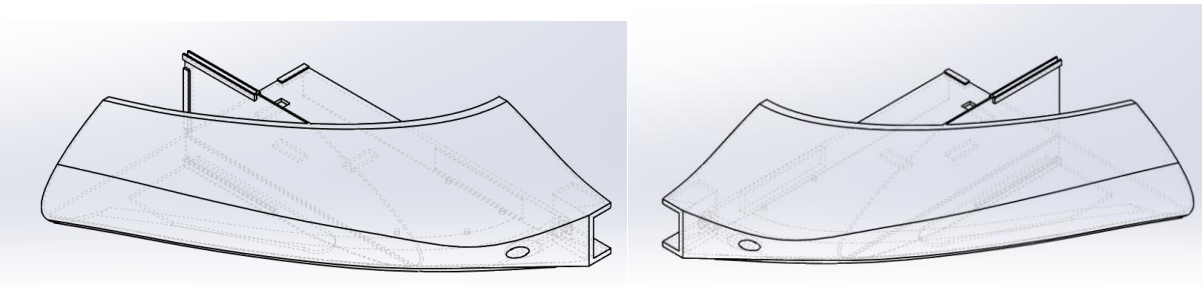

Figure 15.20 – Nose fuselage cut

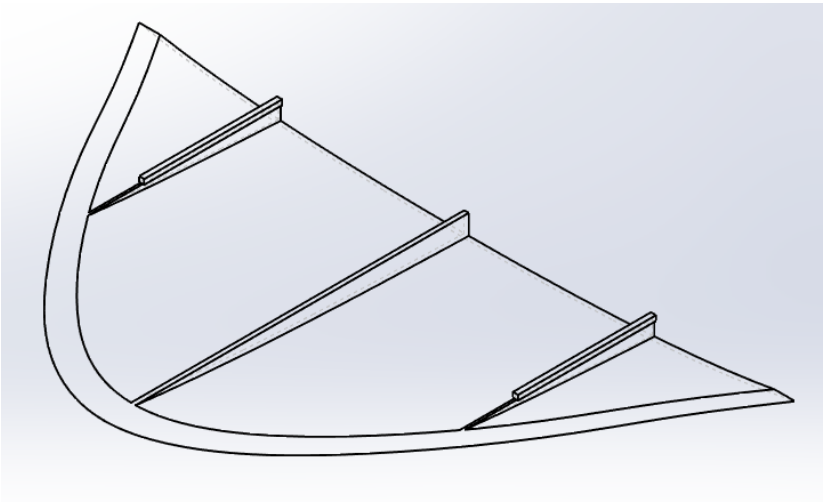

Figure 15.21 – Nose bottom electronic hatch cut

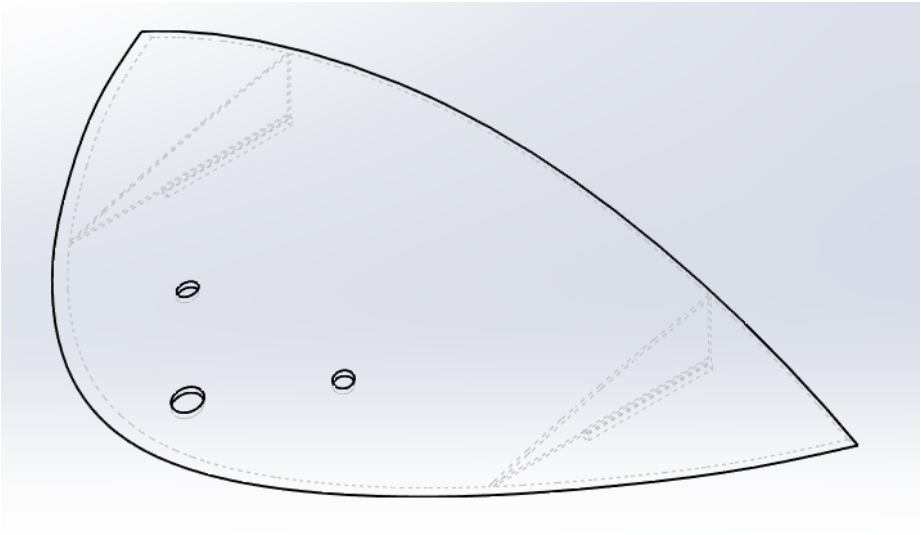

Figure 15.22 – Nose top electronic hatch cut

While printing, it was discovered that the nose side-to-side alignment system was fragile. A platform was used to strengthen the system.

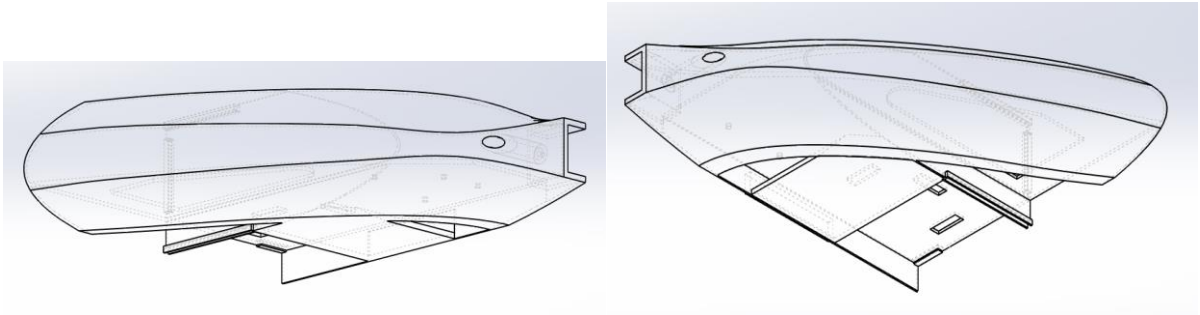

Figure 15.23 – Nose bottom

15.2 Wings

15.2.1 Winglet Alignment

To ensure the winglets are properly aligned with the winglet, an alignment system is used to interface between the two parts. The alignment system utilizes a male connector on the winglet and a female connector on the wingtip. The male connector is an extrusion that's 9mm long and makes physical contract with the interior structure of the wing. Unlike the other extensions seen in the fuselage, the male connector is much shorter than the female connector, allowing it to be "clicked" into place

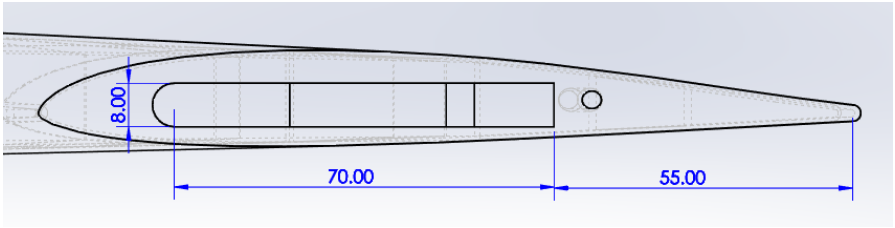

Figure 15.24 – Left wingtip female connection

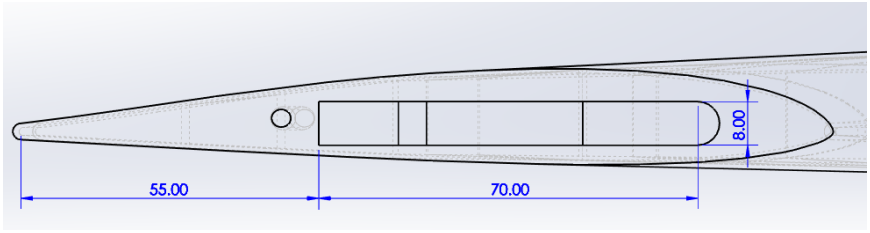

Figure 15.25 – Right wingtip female connection

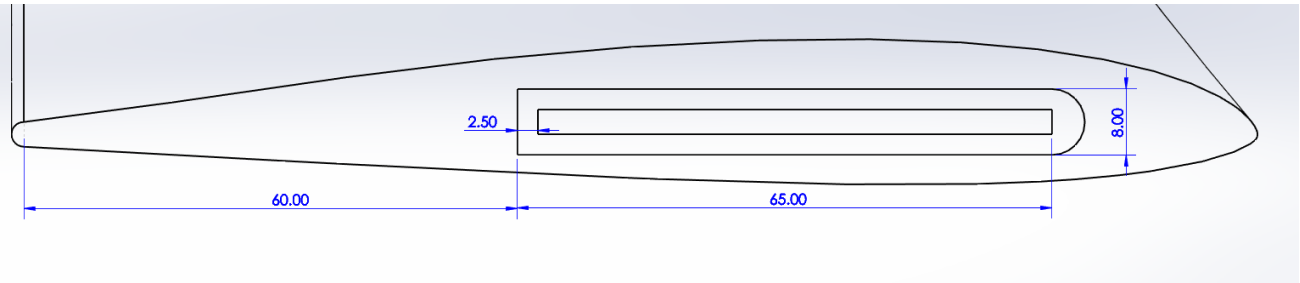

Figure 15.26 – Left wingtip male connector

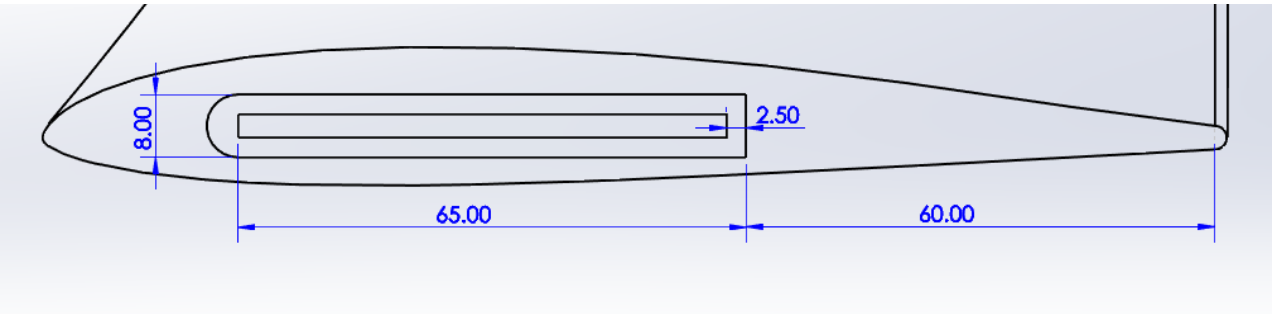

Figure 15.27 – Right wingtip male connector

15.2.2 Wing Alignment

To ensure that the wings are properly installed, a series of channels are built into the wing structure. These channels will hold 3D printed “pins” which will in turn be connected to another channel. By doing this, every single wing part will be connected to another, giving rigidity to a structure. Glue will be used to reinforce the structure.

There are two main diameter pins that will be used, a pin measuring 10 mm and another pin measuring 5 mm. The 10 mm pins will be used on parts located close to the wing root, while the 5 mm pins will be used on parts near the wingtip. Special care has to be taken to ensure that the channel is capable of being printed. To ensure rigidity, each interface has 2 pins.

The dimensions of the 3D-printed channels for each wing interface are as follows:

- TE-LE @ Wing Root: 2x 10 mm x 50 mm
- Wing Root to Mid-wing: 10 mm x 50 mm
- TE-LE @ Mid-wing: 2x 10 mm x 50 mm
- Mid-wing to Wingtip: 2x 5mm x 50 mm
- TE-LE @ Wingtip: 2x 5mm x 30 mm

To allow for some tolerance, the pins are made 2 mm shorter in height. Note that the wing root to mid-wing interface only has 1 pin. This is due to a carbon fiber guide beam that can act as a pin.

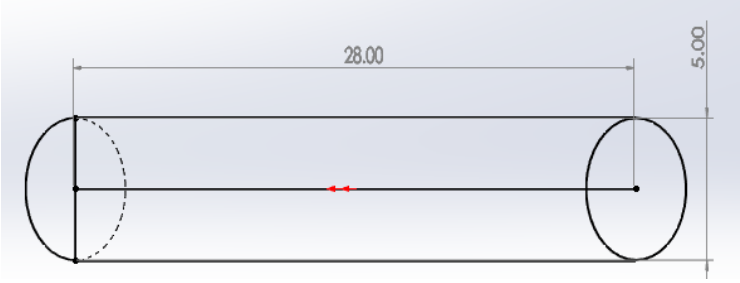

Figure 15.28 – 5 mm x 28mm pin

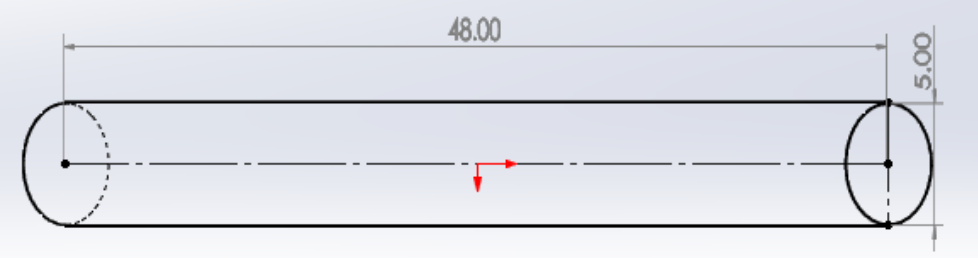

Figure 15.29 – 5 mm x 48 mm pin

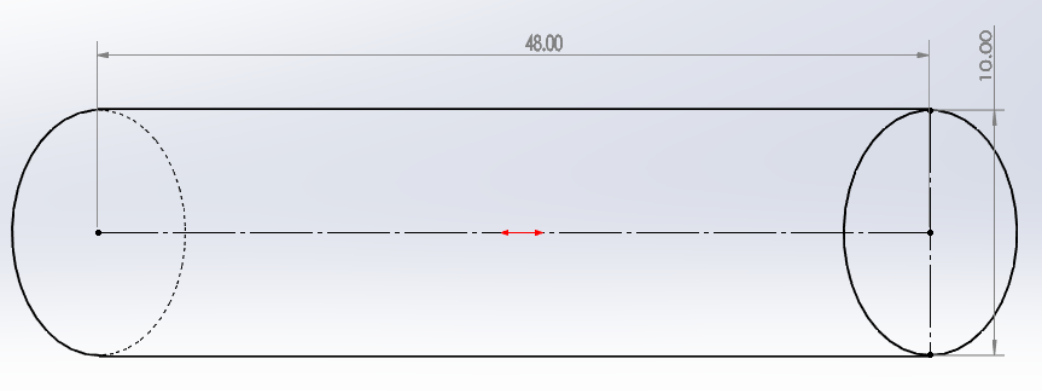

Figure 15.30 – 10 mm x 548 mm pin

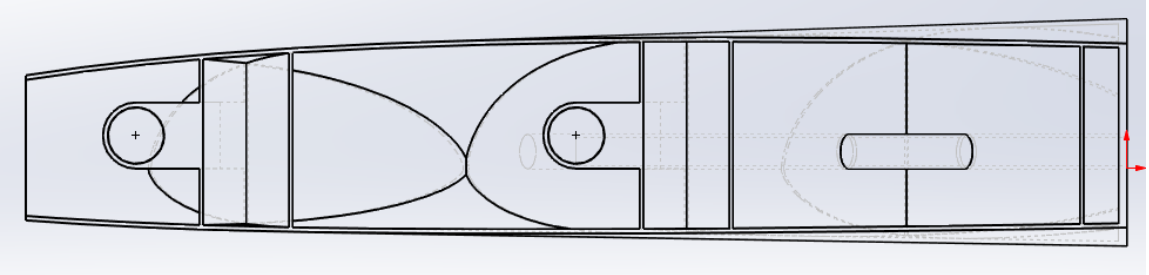

Figure 15.31 – Example wing alignment system (left wing – wing root)

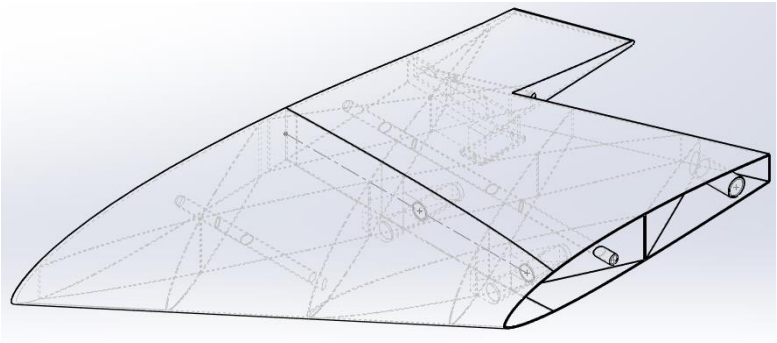

Figure 15.32 – Left wing – wing root

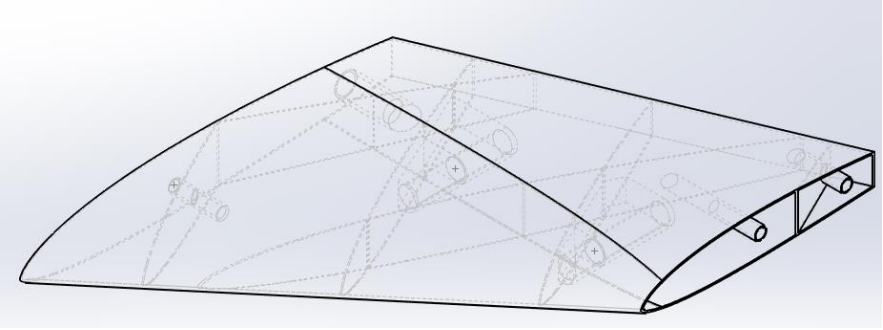

Figure 15.33 – Left wing – mid-wing

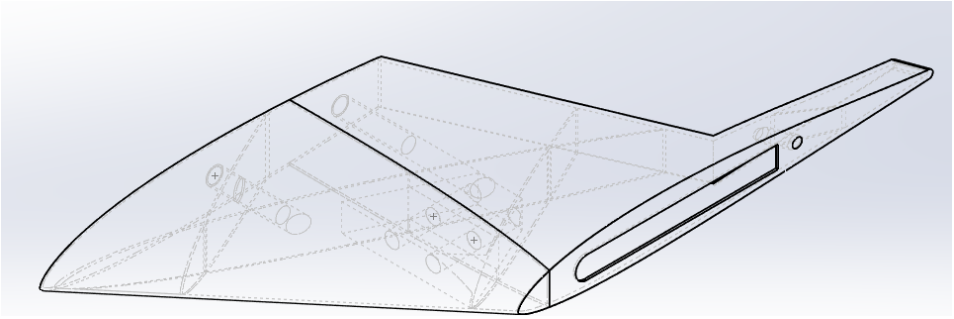

Figure 15.34 – Left wing – wingtip

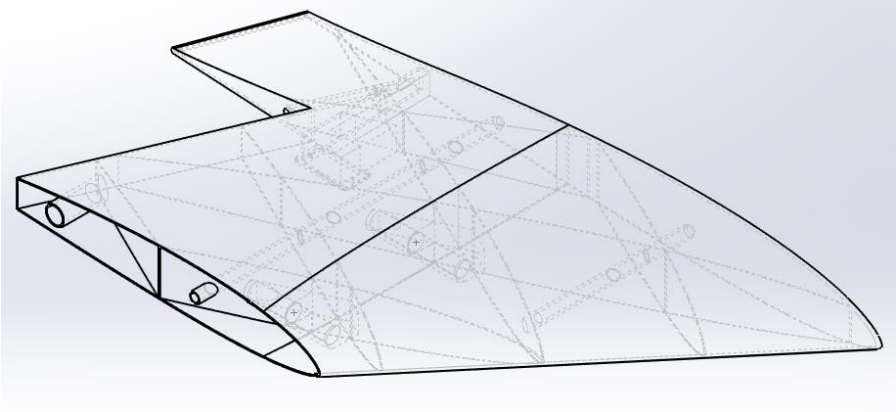

Figure 15.35 – Right wing – wing root

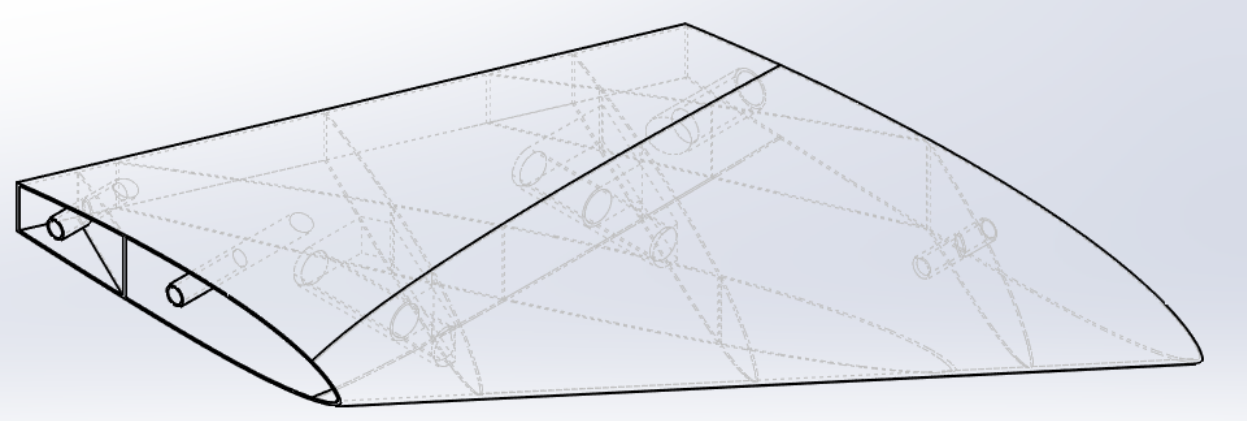

Figure 15.36 – Right wing – mid-wing

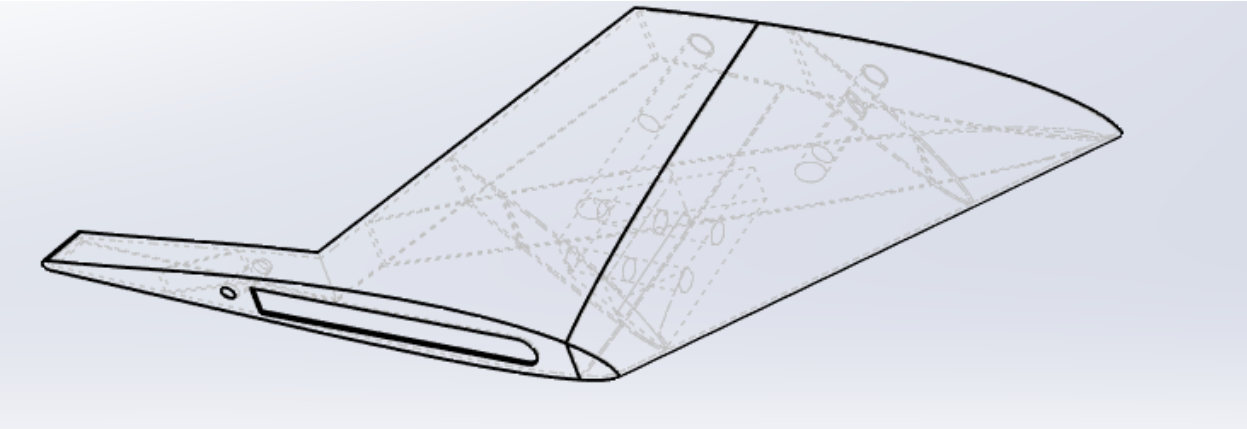

Figure 15.37 – Right wing – wing tip

15.2.3 Wing Split

The left and right wings are divided into 6 different sections each. To identify each part, the wing is segregated based on whether they have the trailing edge or leading edge, as well as their position along the wing, being wing-root, mid-wing, and wingtip.

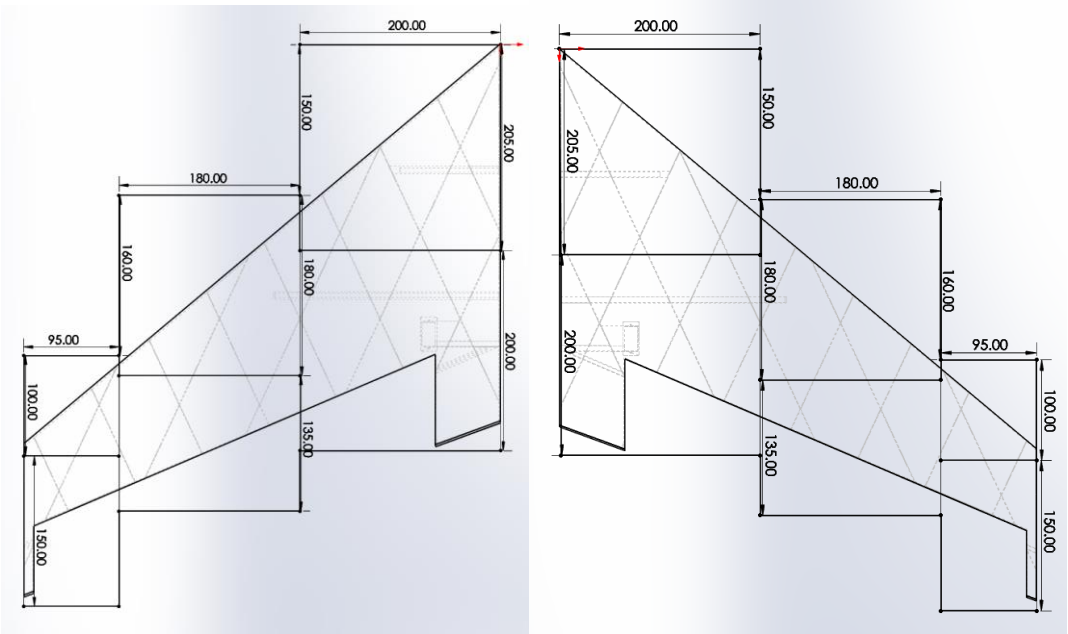

Figure 15.38 – Left & right wing sections

15.2.4 Left Wing

The left-wing sections are divided as:

- Left Leading Edge, Wing-root
- Left Trailing Edge, Wing-root
- Left Leading Edge, Mid-wing
- Left Trailing Edge, Mid-wing
- Left Leading Edge, Wingtip
- Left Trailing Edge, Wingtip

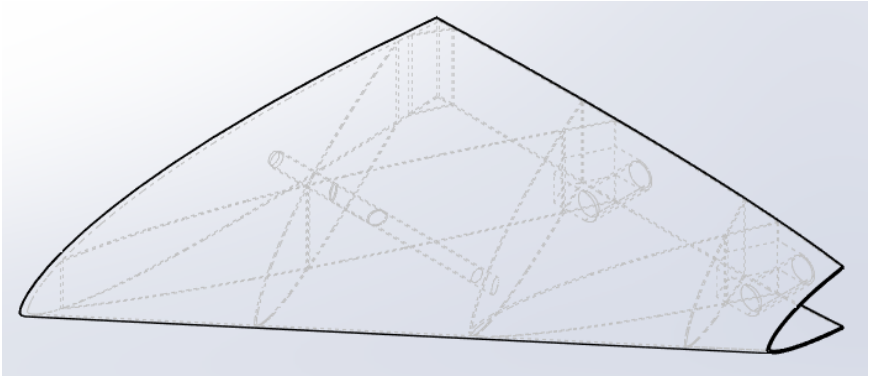

Figure 15.39 – Left leading edge, wing-root

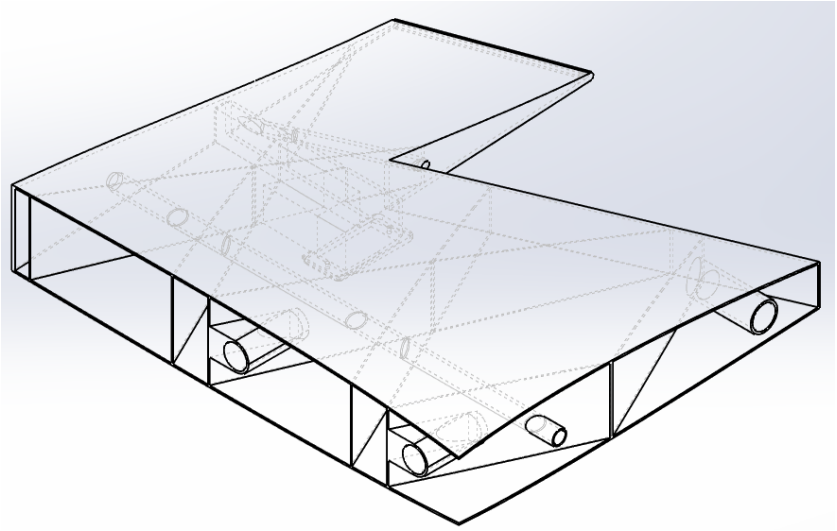

Figure 15.40 – Left trailing edge, wing-root

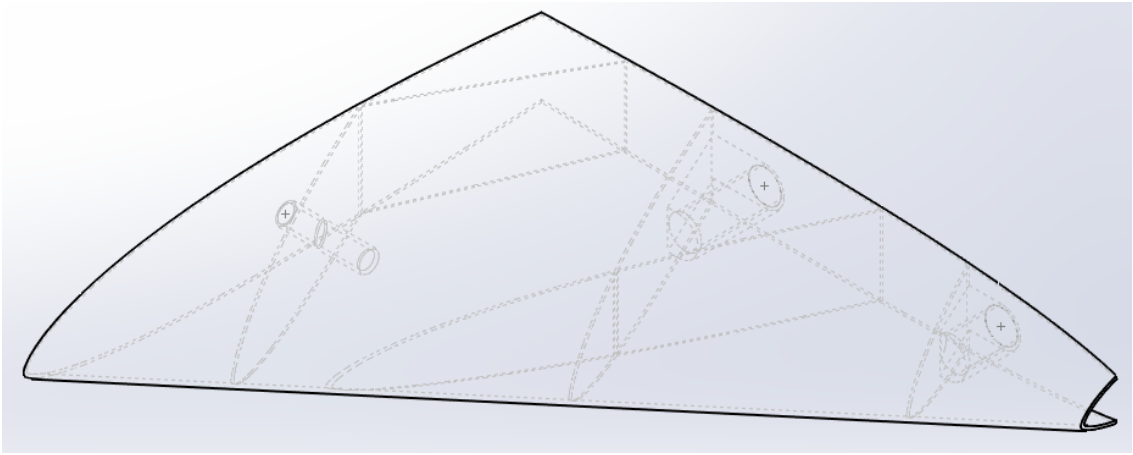

Figure 15.41 – Left leading edge, mid-wing

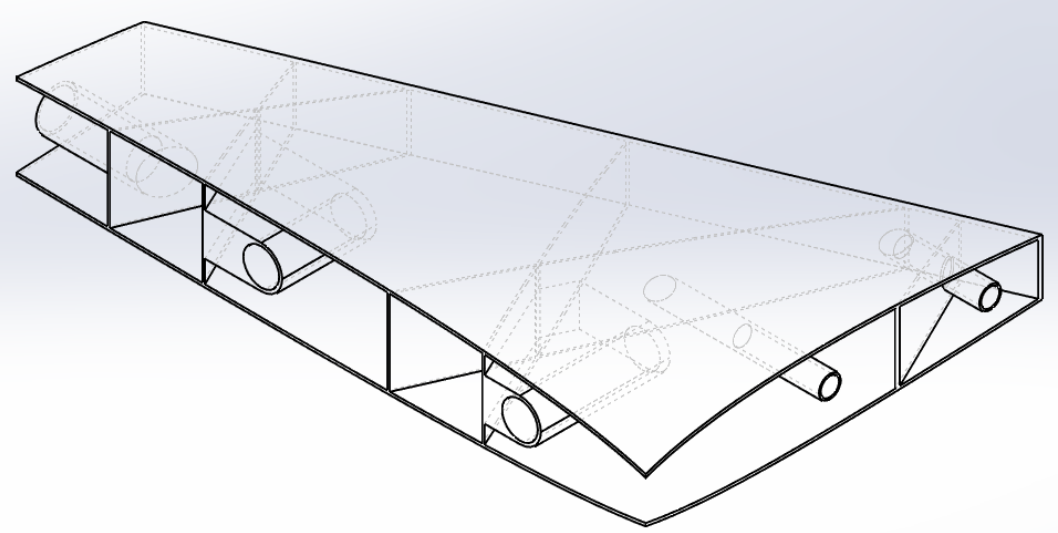

Figure 15.42 – Left trailing edge, mid-wing

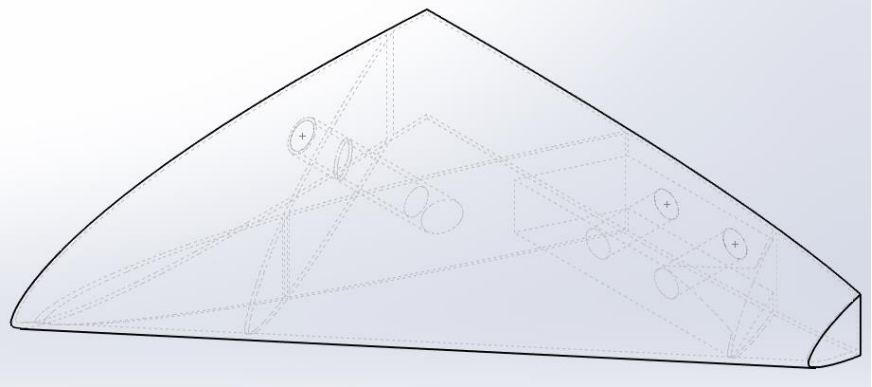

Figure 15.43 – Left leading edge, wingtip

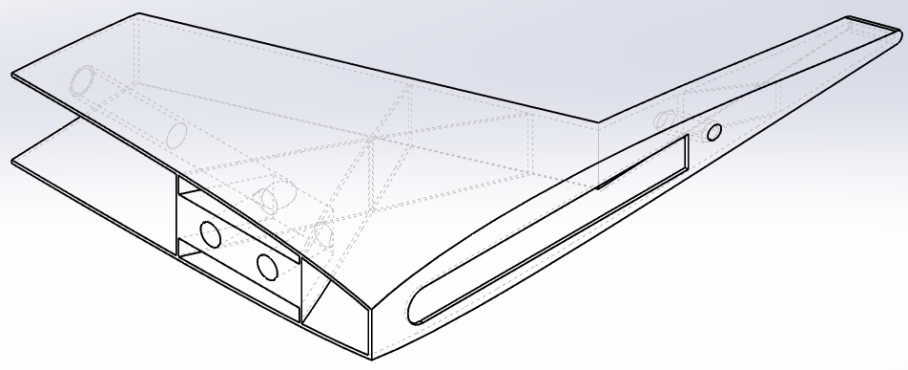

Figure 15.44 – Left trailing edge, wingtip

15.2.5 Right Wing

The right-wing sections are divided as:

- Right Leading Edge, Wing-root
- Right Trailing Edge, Wing-root
- Right Leading Edge, Mid-wing
- Right Trailing Edge, Mid-wing
- Right Leading Edge, Wingtip
- Right Trailing Edge, Wingtip

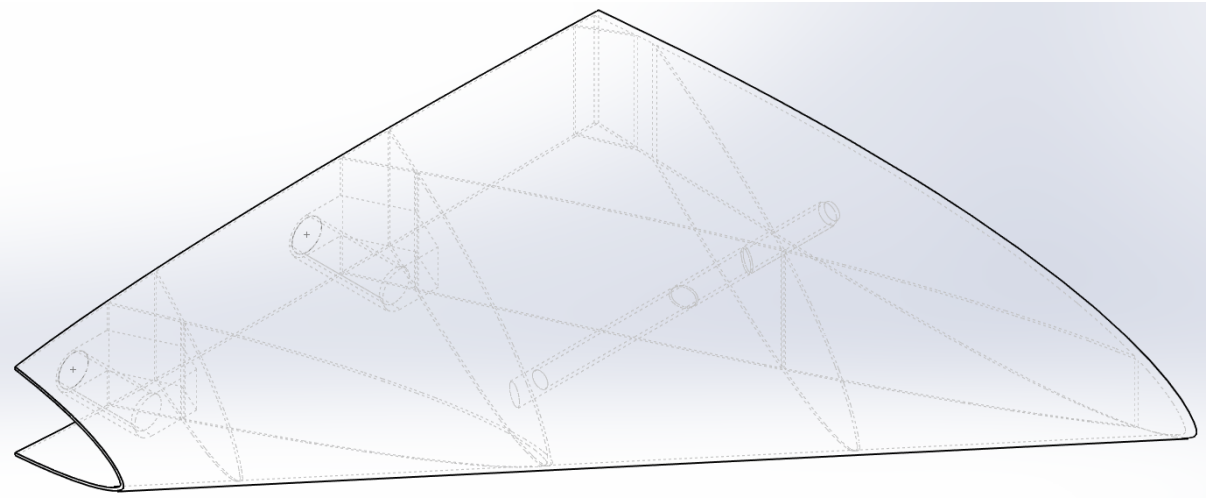

Figure 15.45 – Right leading edge, wing-root

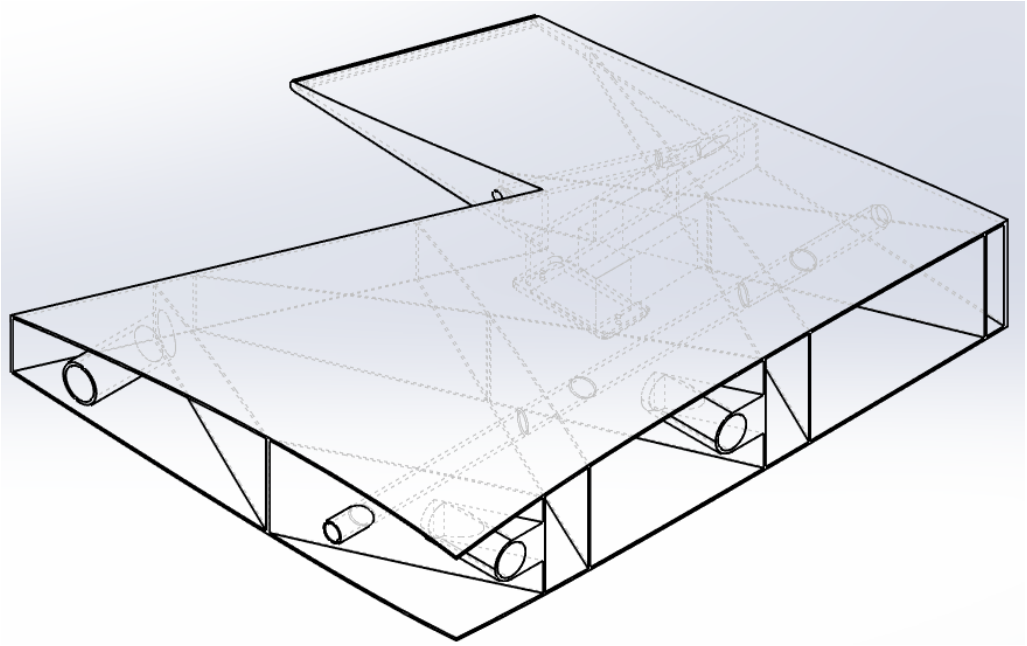

Figure 15.46 – Right trailing edge, wing-root

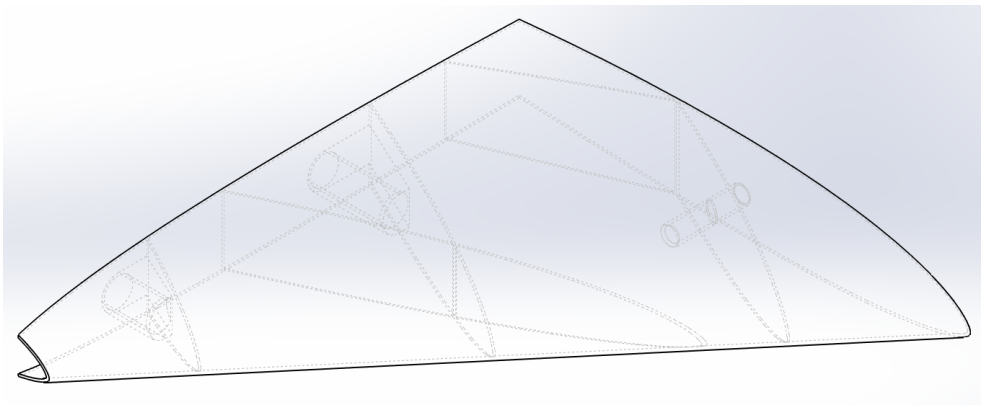

Figure 15.47 – Right leading edge, mid-wing

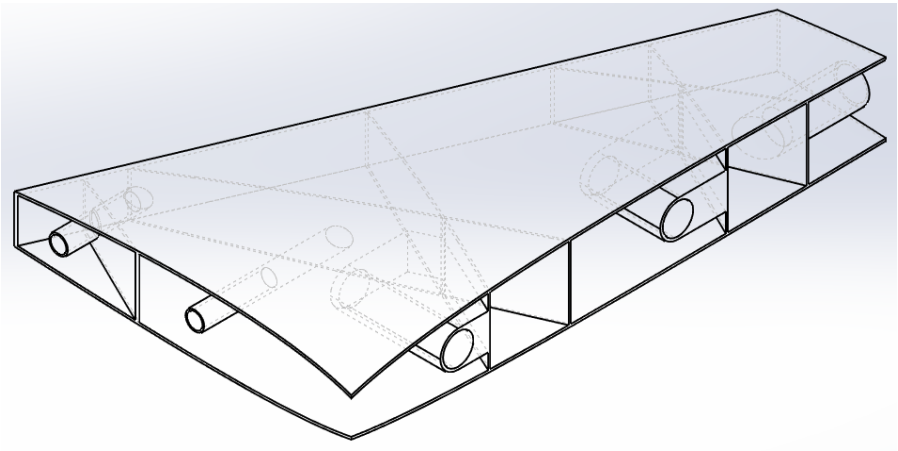

Figure 15.48 – Right trailing edge, mid-wing

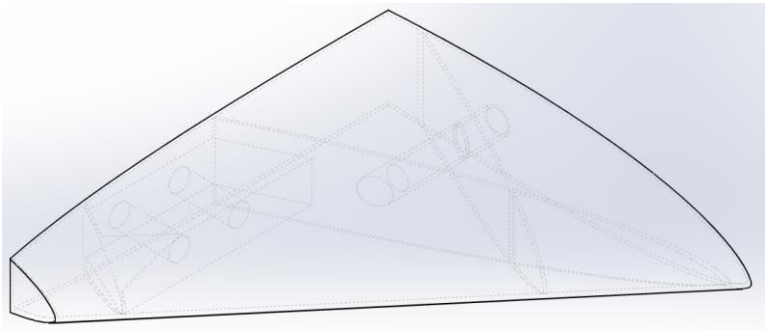

Figure 15.49 – Right leading edge, wingtip

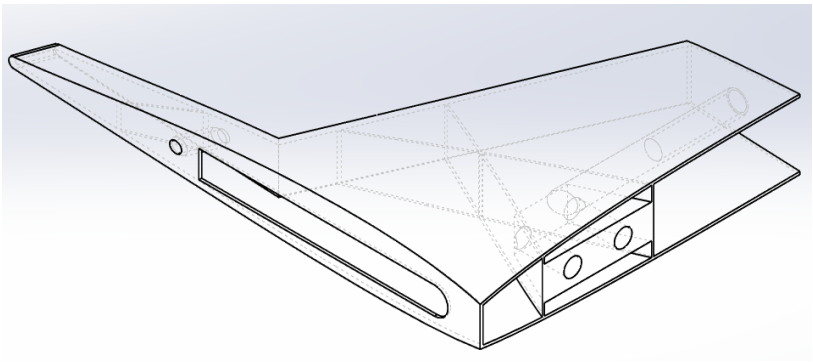

Figure 15.50 – Right trailing edge, wingtip

15.3 Elevon

15.3.1 Elevon Controls

To control the elevons, a pushrod is connected to the servo, which is in turn linked to the elevon, via micro control horns. The micro control horns have a “shaft” that is 5 mm long, 2 mm wide, and 12 mm tall. A hole is incorporated into the elevon to fit the shaft. It can be secured in place using glue.

Figure 15.51 – Micro control horns [37]

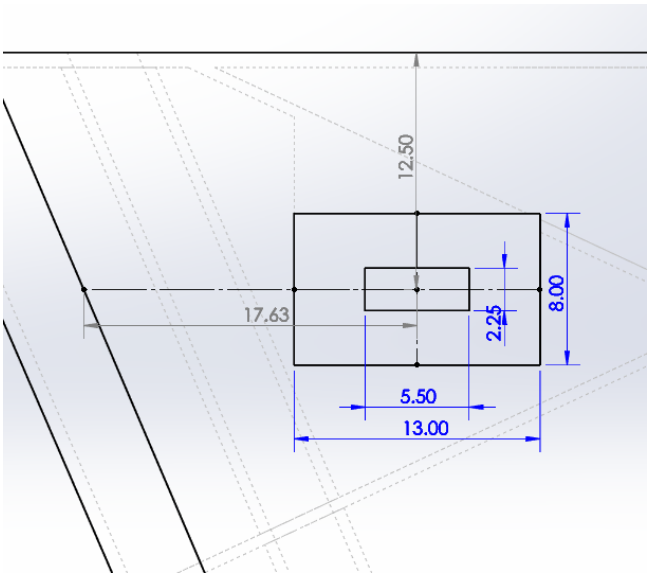

Figure 15.52 – Elevon attachment point

15.3.2 Elevon Split

To ensure the elevons can rotate freely, the ends of each elevon are shaved down by 1 mm. The left elevon is split into 2 sections:

- Left Elevon Root
- Left Elevon Tip

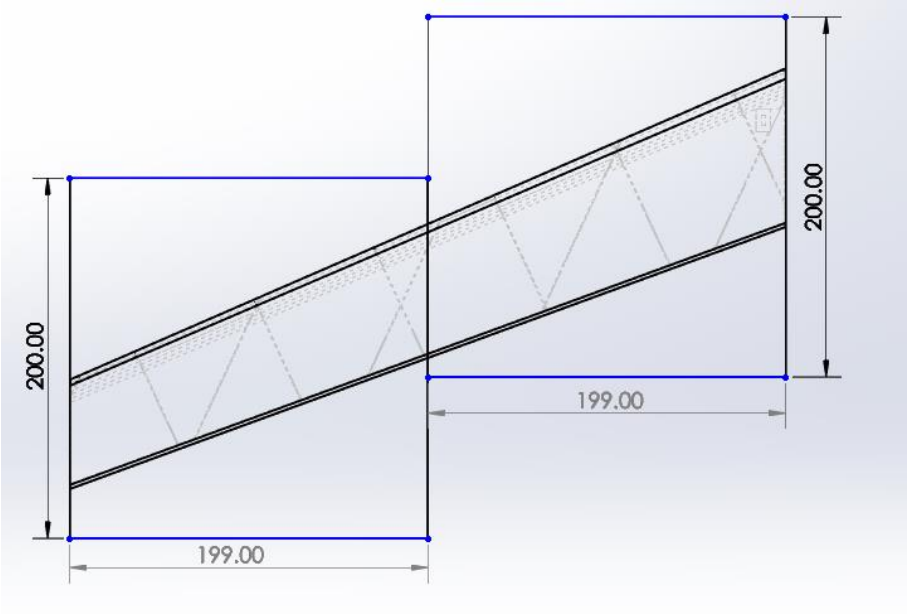

Figure 15.53 – Left elevon split

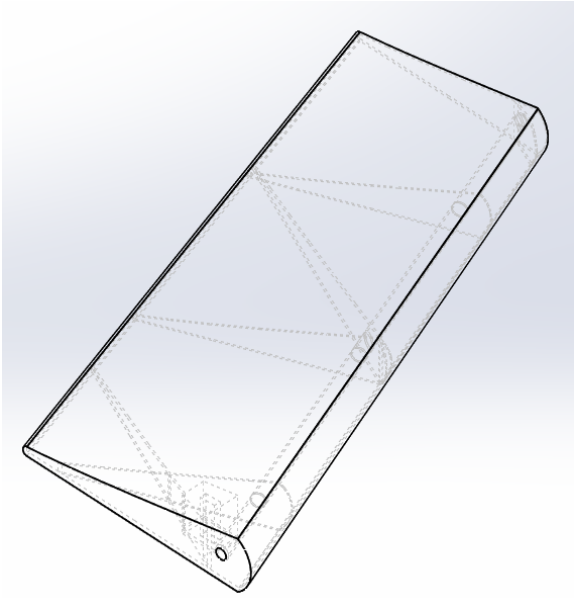

Figure 15.54 – Left elevon root

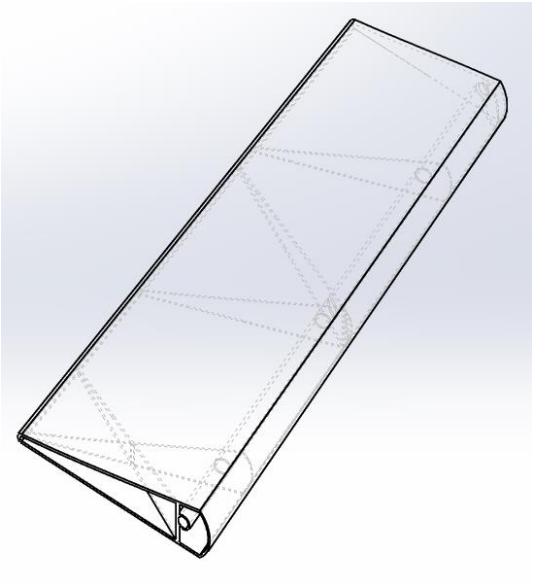

Figure 15.55 – Left elevon tip

The right elevon is split as:

- Right Elevon Root
- Right Elevon Tip

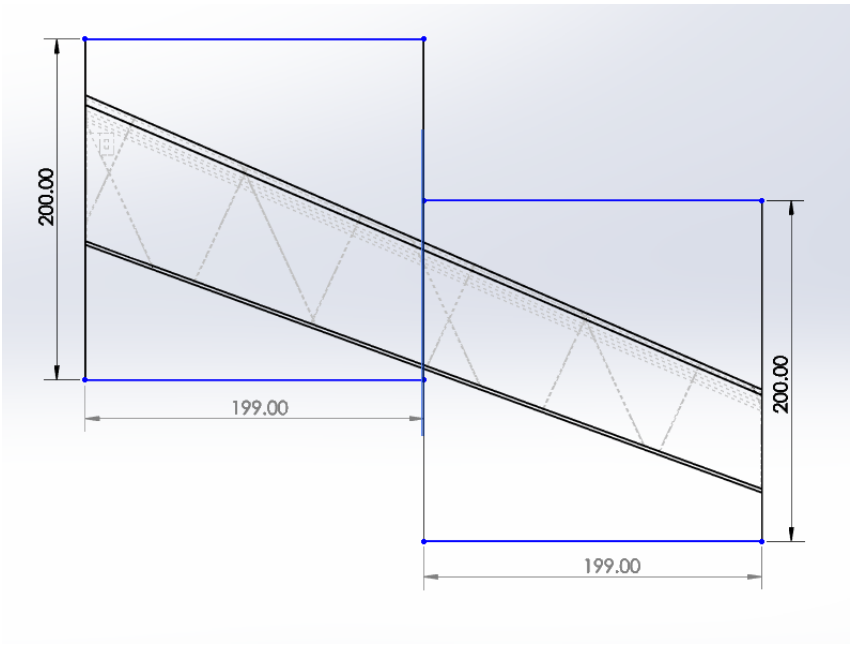

Figure 15.56 – Right elevon split

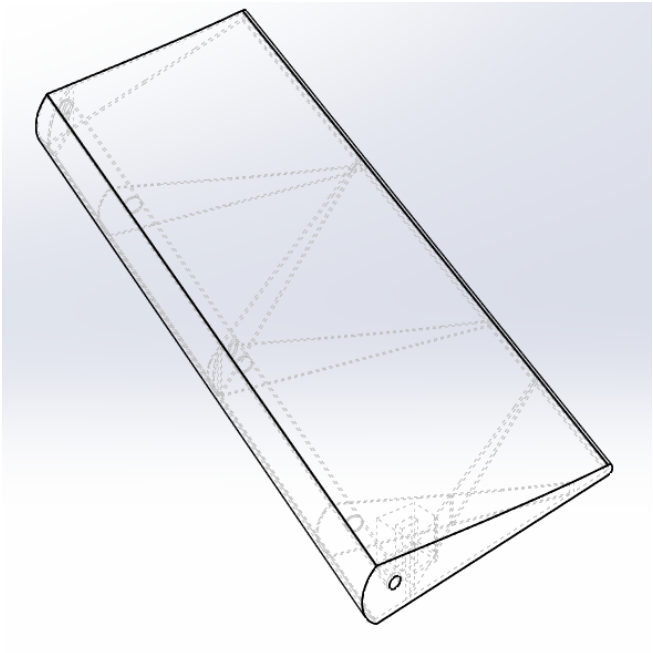

Figure 15.57 – Right elevon root

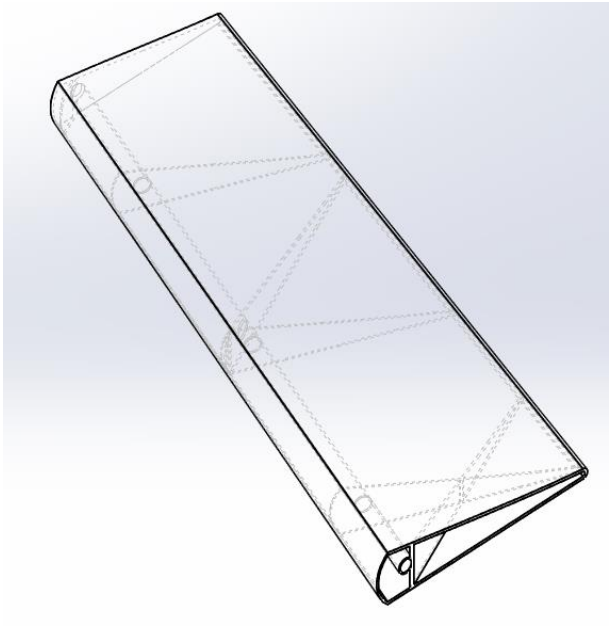

Figure 15.58 – Right elevon tip

15.4 Winglet

Each winglet can be printed individually and are divided accordingly:

- Left Winglet
- Right Winglet

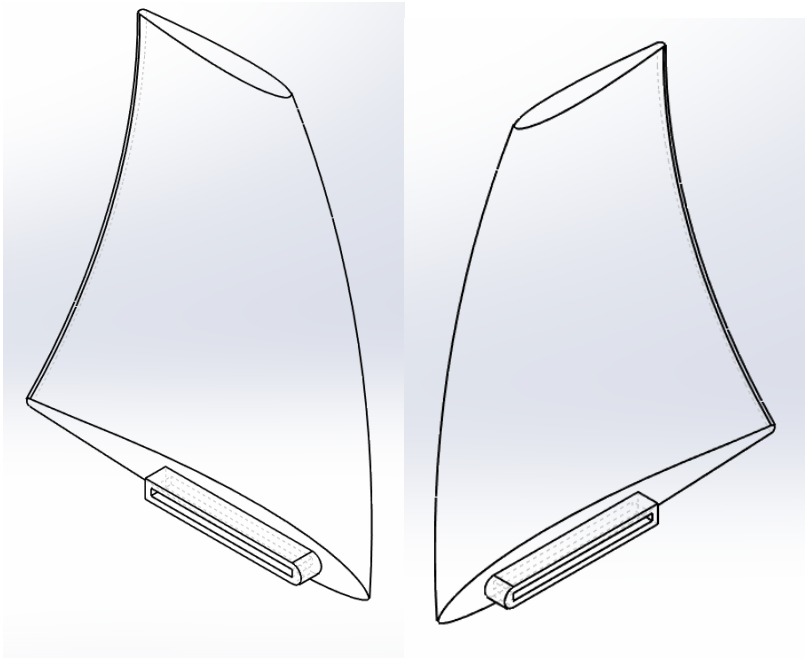

Figure 15.59 – Left & right winglet

15.5 Conclusion

Initially, there wasn't a need for the connection point system as it was believed that it would just create extra weight for a piece that would just be attached together using a epoxy resin or something similar. However, it was quickly discovered that alignment between subsections was a necessity. A quick prototype was created to determine if a small system was feasible. The system was and the new connection point idea took shape. This was able to be done in a few hours thanks to rapid-prototyping.

Chapter 16 — 3D Printing Settings and Process

16.1 Introduction

The first prototype was built using the Flashforge Adventurer 5M. The accompanying software used to slice the 3D model is Flashprint 5. A useful feature Flashprint 5 has is the ability to send the slicing file over through LAN, making the project easy to manage. The project utilized a 0.4 mm nozzle and PLA.

16.2 Global Settings

To print the extruder temperature is set to 225°C, while the platform is set to 60°C. The abase print speed is 300 mm/s, travel speed 500 mm/s, and minimum speed 20 mm/s.

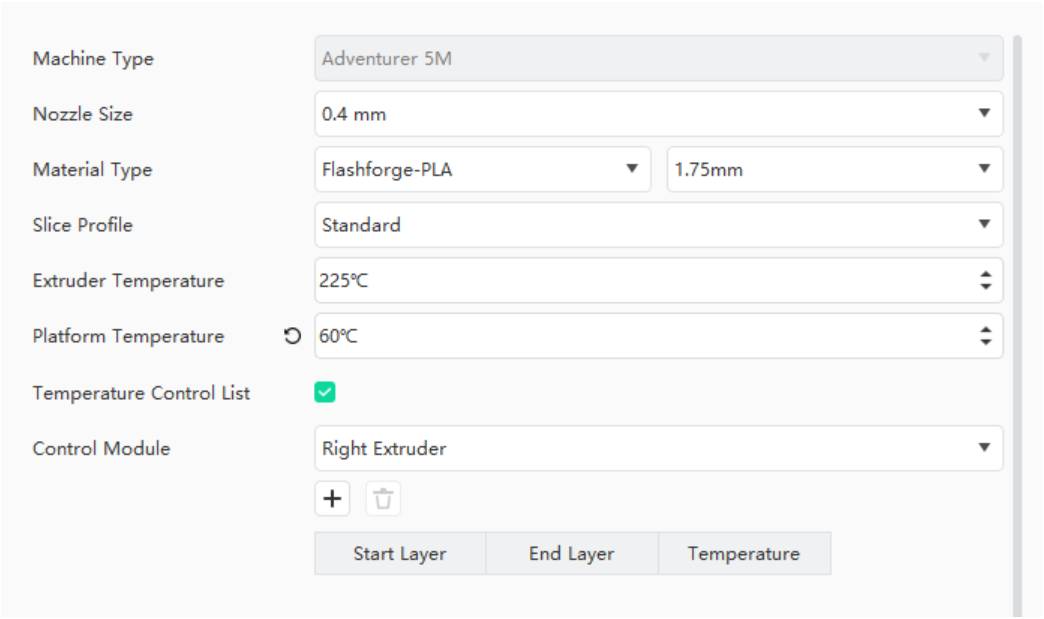

Figure 16.1 – Nozzle settings

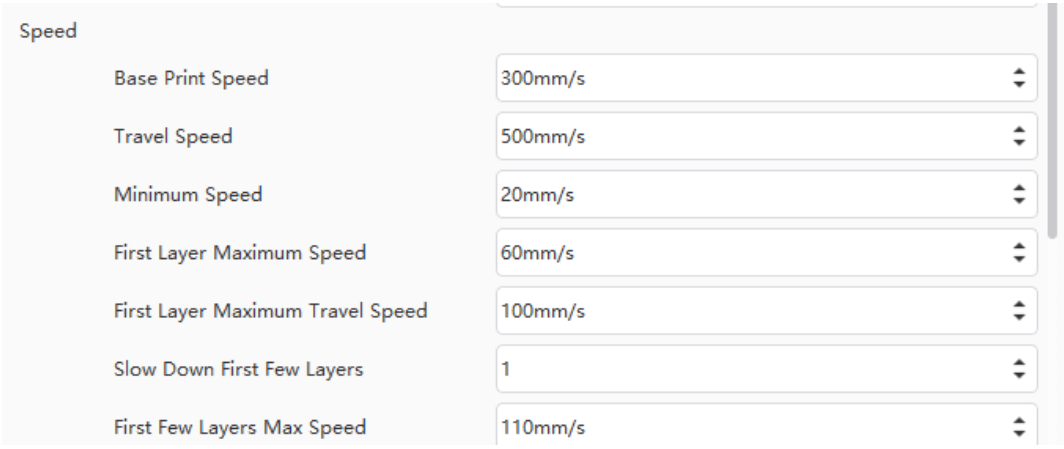

Figure 16.2 – Nozzle speed

16.3 Supports

The supports are structures added to a model to prevent overhangs and bridges while printing, ensuring that there is no sagging. Supports are meant to be temporary and can be later removed after the print is complete. Support structures are generated using the slicer software, making them easy to set up. The support settings are listed below:

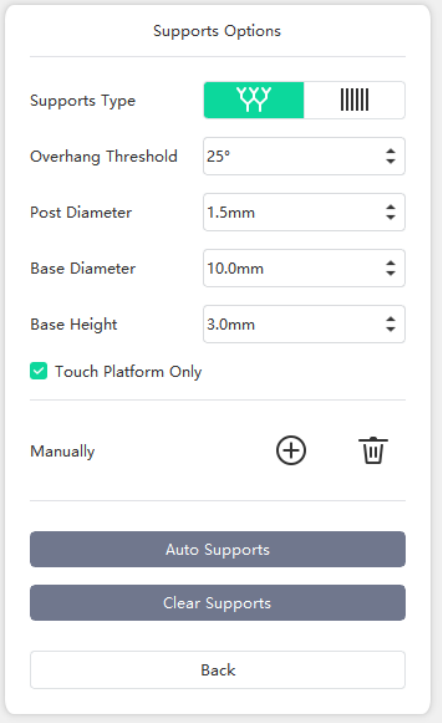

Figure 16.3 – Support settings

There are two types of supports that are used, tree supports and linear supports. Linear supports use vertical pillars to hold overhangs, while tree supports utilize a system of branches. Tree support has the advantage of being extremely efficient when it comes to material use, ease of removal and time to print. However, they aren't as stable as a linear support. For this project, a tree support was used.

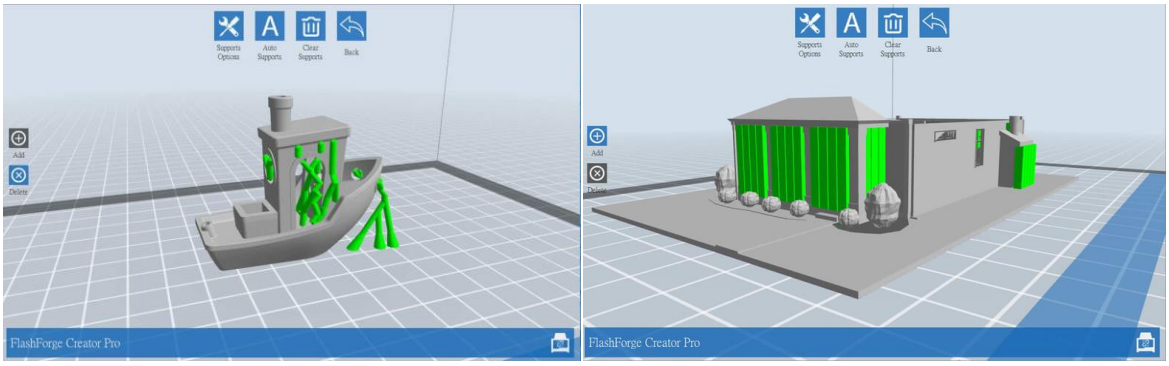

Figure 16.4 – Support comparison (tree-left, linear-right) [38]

16.4 Brim

A brim is a temporary structural component of the print that is generated using slicer software to further improve the bed adhesion and reduce warping. There are especially useful when the print has a small base, or has limited contact with the bed. The brim is used throughout the entire aircraft to ensure a stable print.

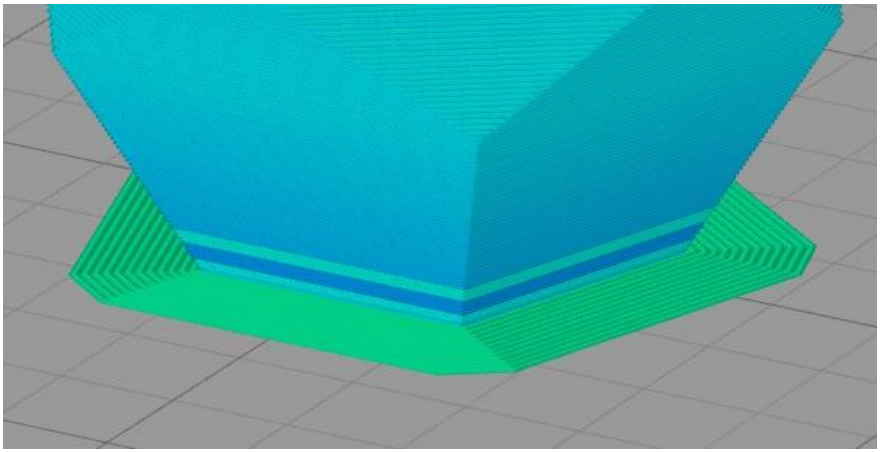

Figure 16.5 – Brim example [39]

16.5 Prints

16.5.1 Nose

Both the left and right sides of the nose use both a brim and a support structure. The top and bottom uses only a brim.

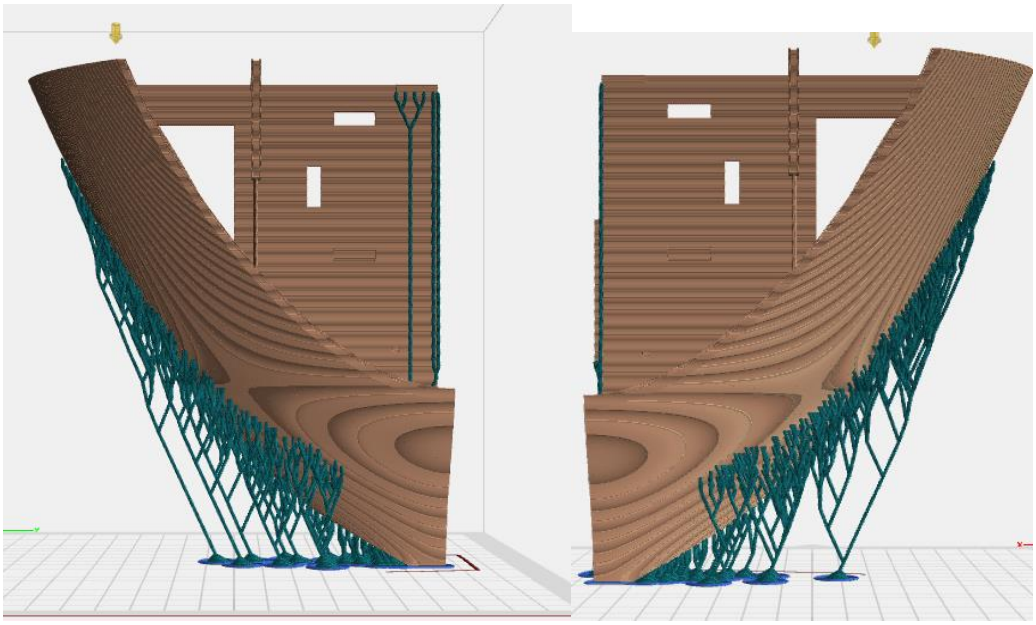

Figure 16.6 – Nose – top view

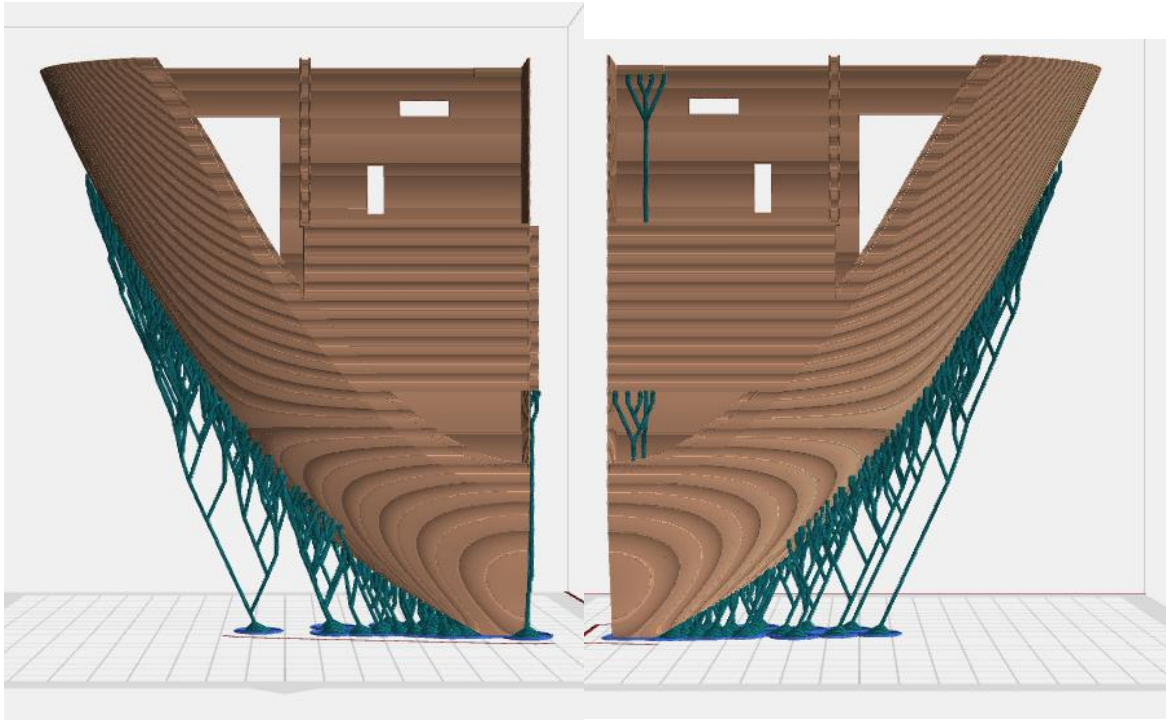

Figure 16.7 – Nose – bottom view

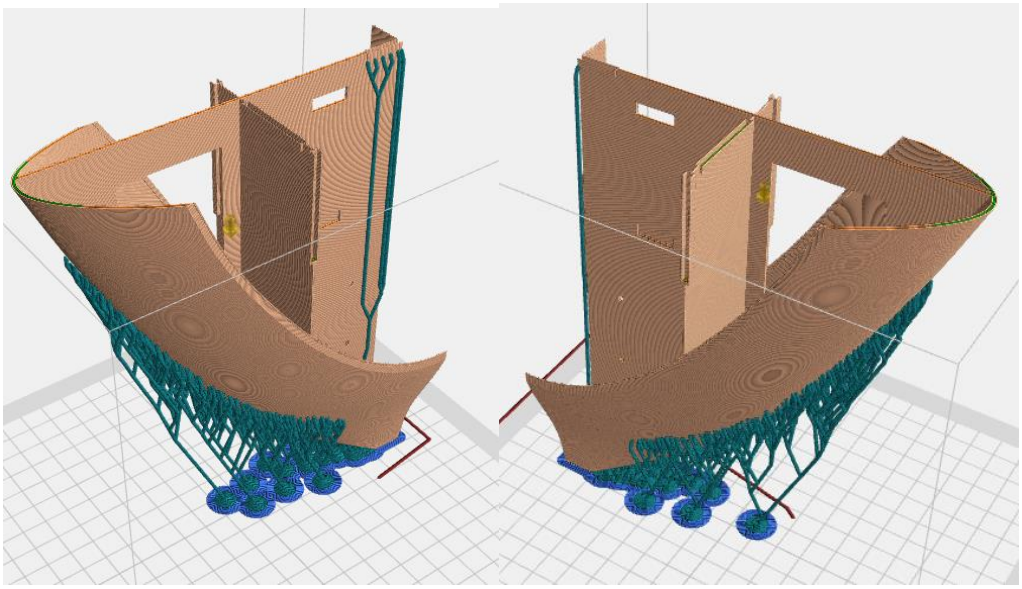

Figure 16.8 – Nose left – isometric view

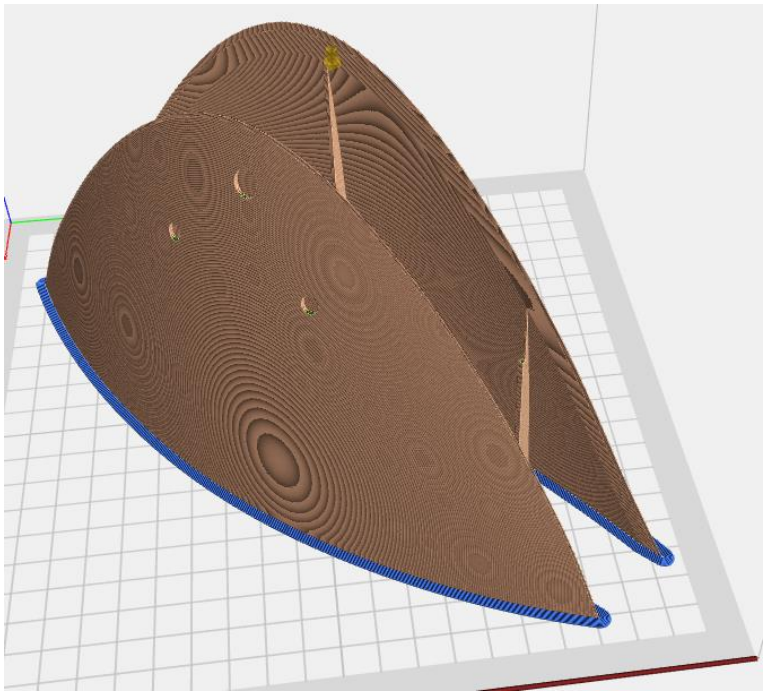

Figure 16.9 – Nose top – isometric view

16.5.2 Fuselage

Most of the fuselage uses both a brim and support structure except for the top, which uses only a brim.

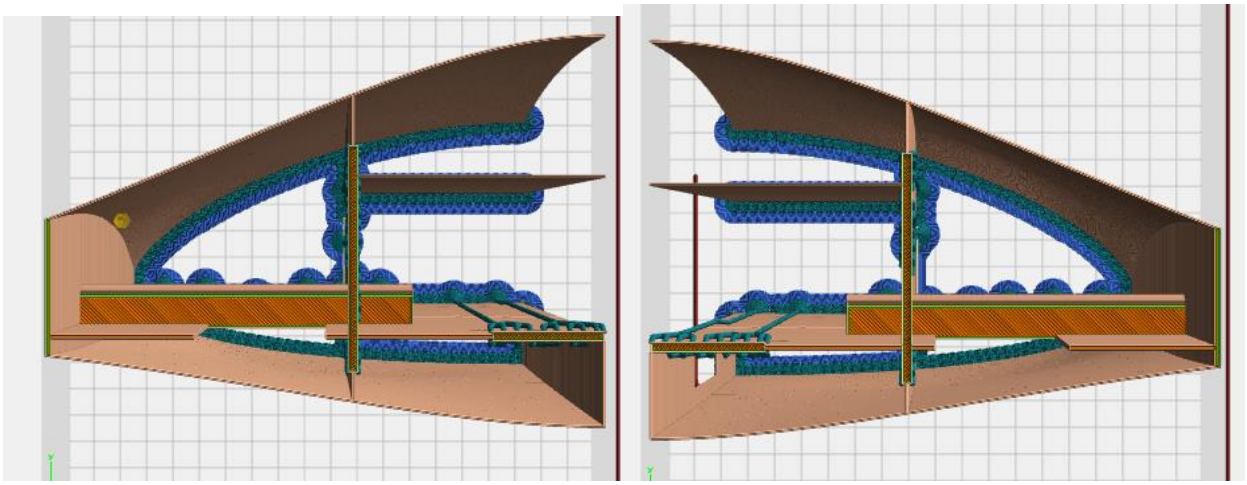

Figure 16.10 – Mid fuselage – top view

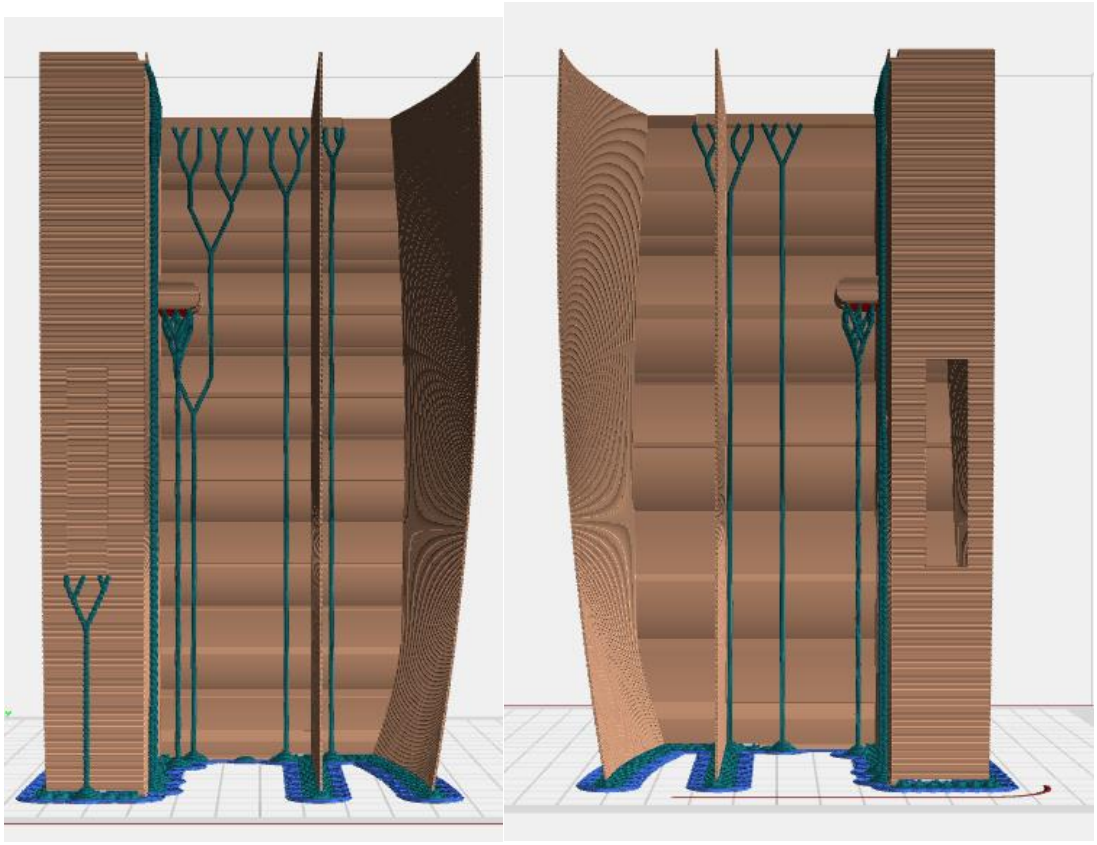

Figure 16.11 – Mid fuselage– interior view

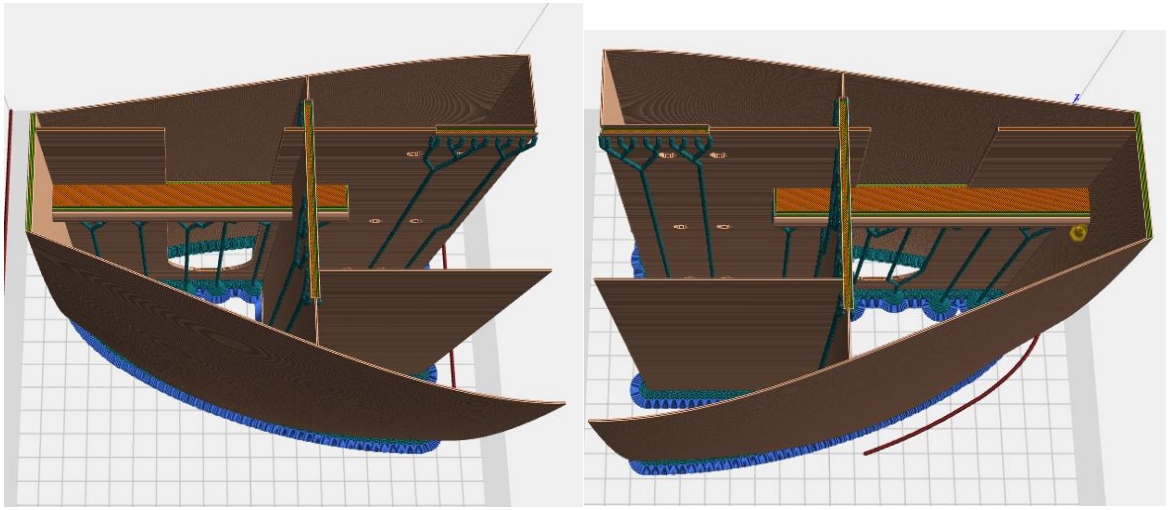

Figure 16.12 – Mid fuselage – isometric-view

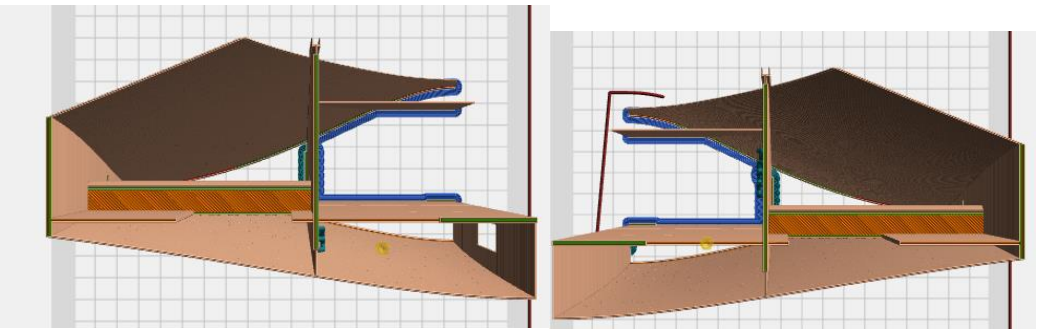

Figure 16.13 – Rear fuselage – top view

Figure 16.14 – Rear fuselage – interior view

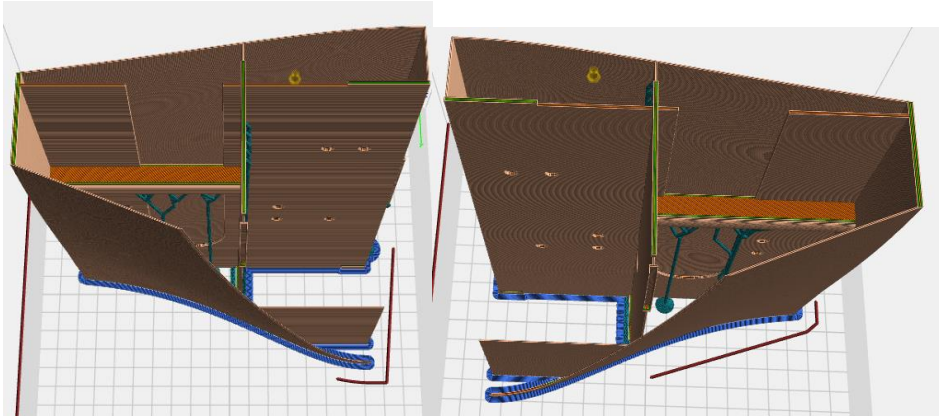

Figure 16.15 – Rear fuselage – isometric view

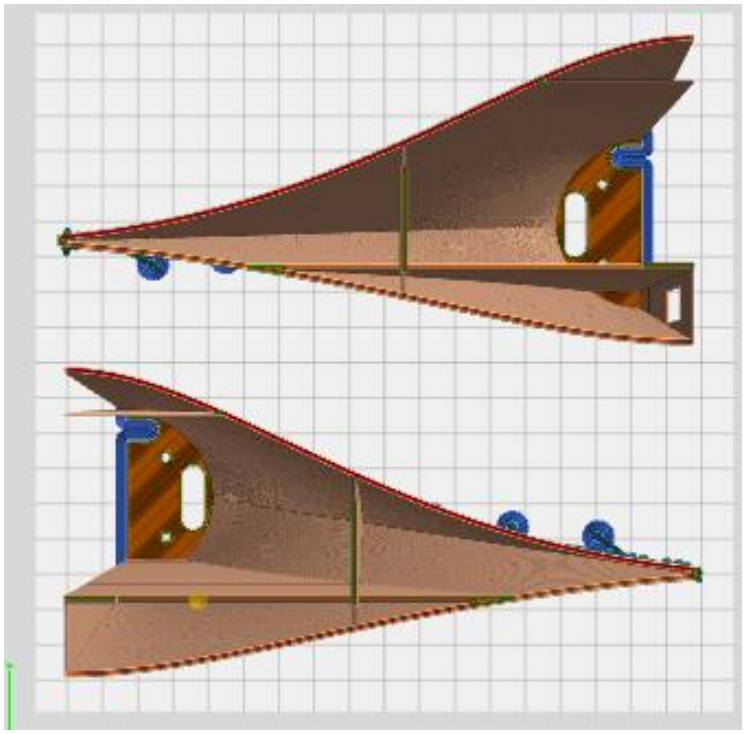

Figure 16.16 – Tail – top view

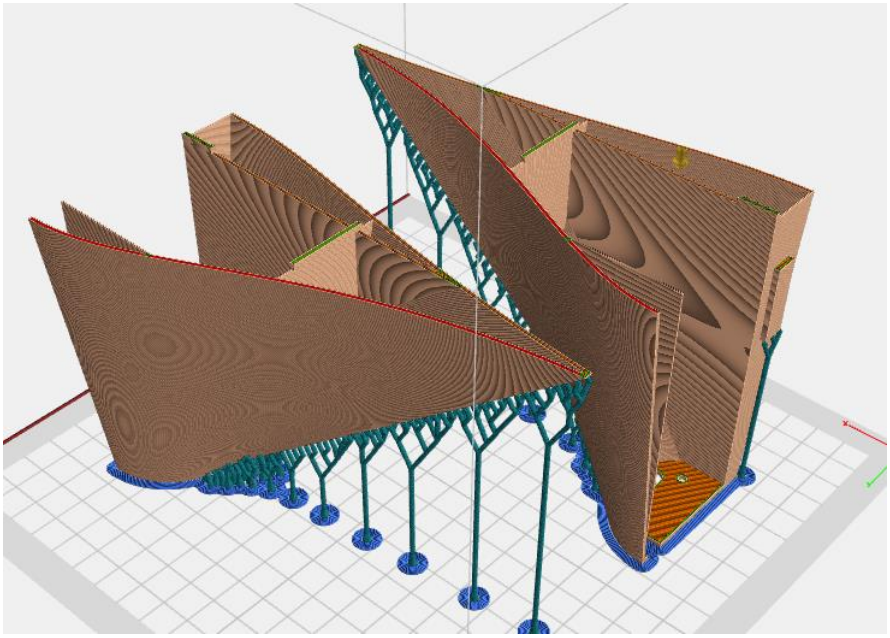

Figure 16.17 – Tail – isometric view

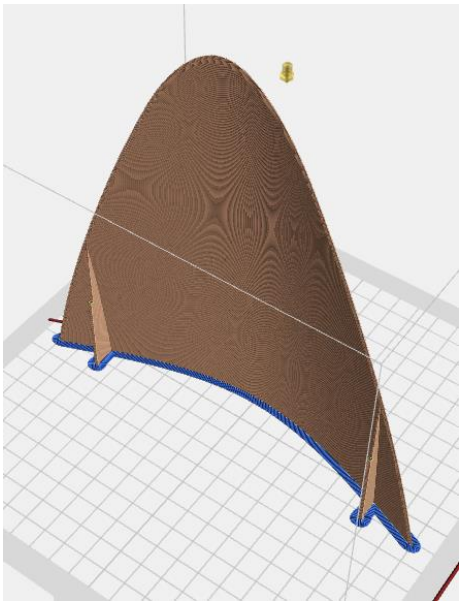

Figure 16.18 – Fuselage top – isometric view

16.5.3 Left Wing

The entire left wing is printed using a brim to improve the bed adhesion. Supports were only used at the trailing edge at the wing root to remove any bridging issues that might come as a result of the servo mount.

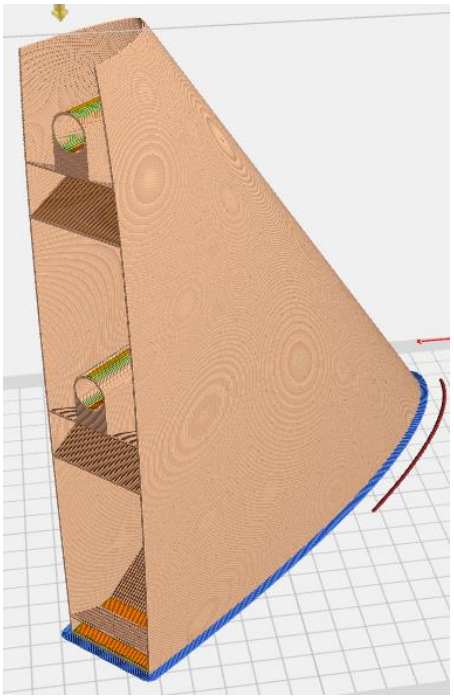

Figure 16.19 – Left leading edge, wing-root

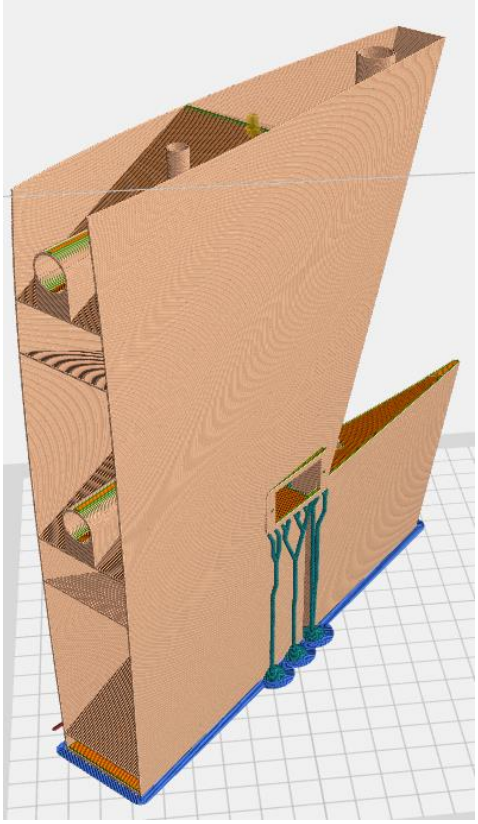

Figure 16.20 – Left trailing edge, wing-root

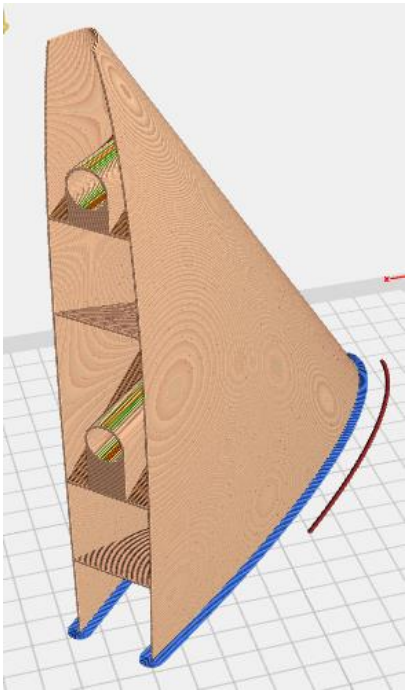

Figure 16.21 – Left leading edge, mid-wing

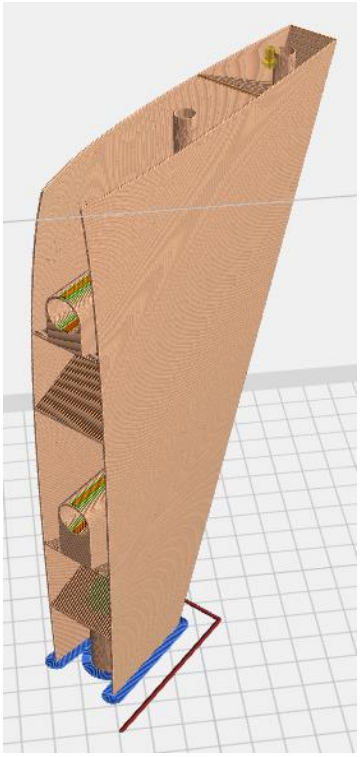

Figure 16.22 – Left trailing edge, mid-wing

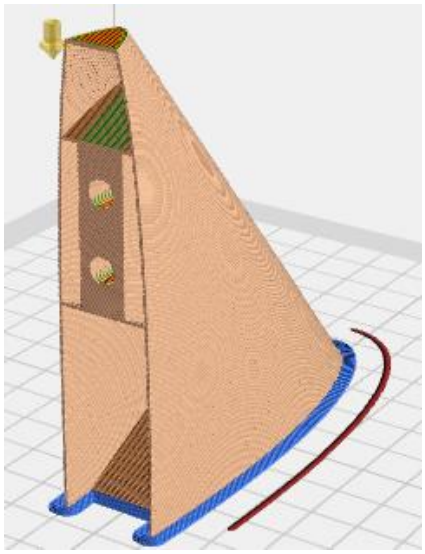

Figure 16.23 – Left leading edge, wingtip

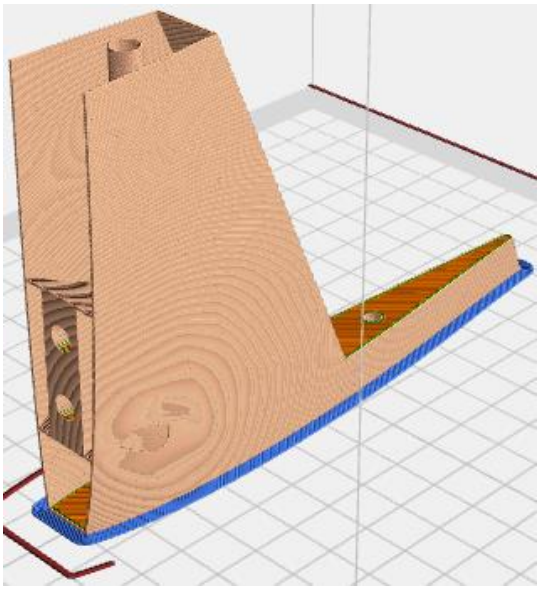

Figure 16.24 – Left trailing edge, wingtip

16.5.4 Right Wing

The same conditions used in the left wing are utilized on the right wing as well.

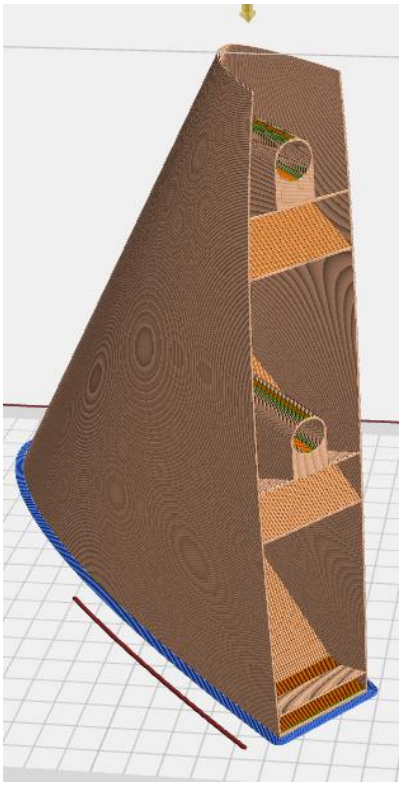

Figure 16.25 – Right leading edge, wing-root

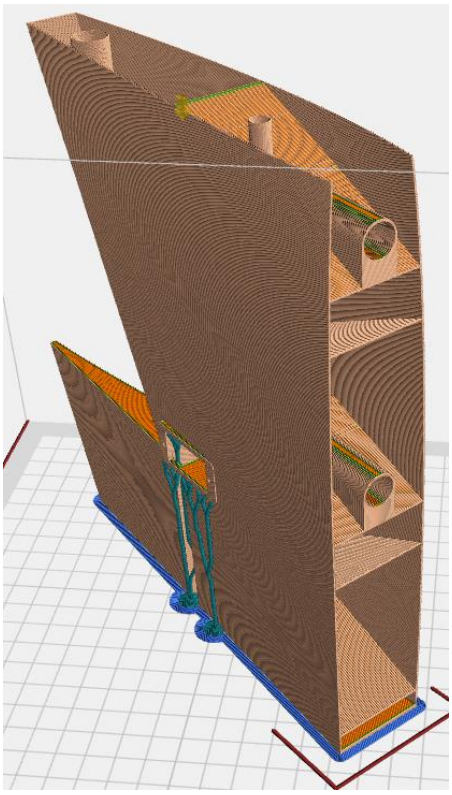

Figure 16.26 – Right trailing edge, wing-root

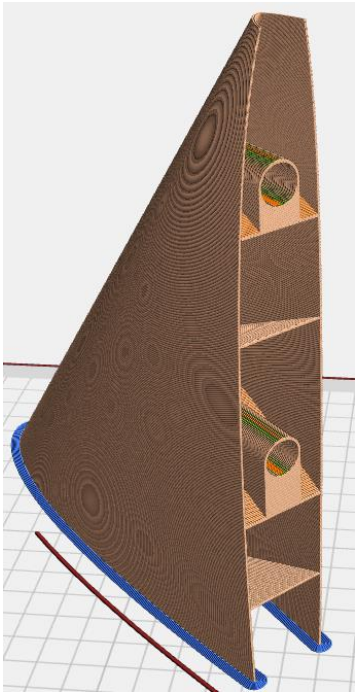

Figure 16.27 – Right leading edge, mid-wing

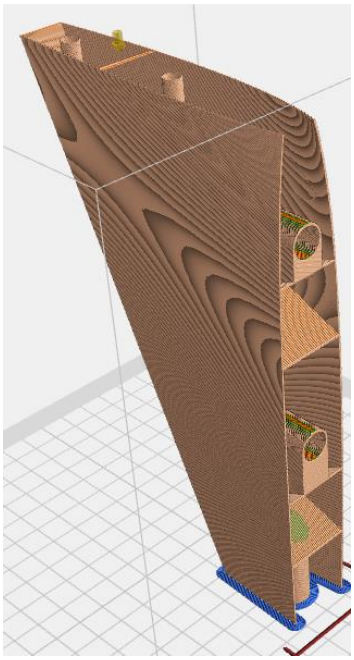

Figure 16.28 – Right trailing edge, mid-wing

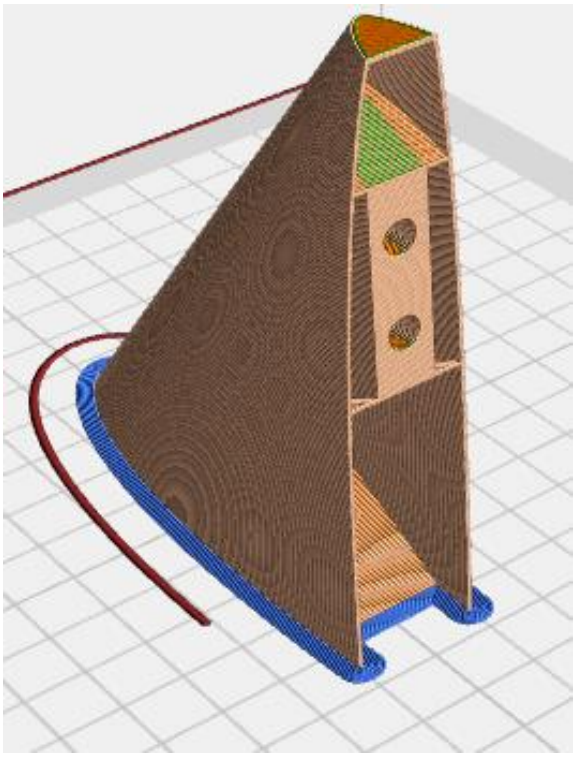

Figure 16.29 – Right leading edge, wingtip

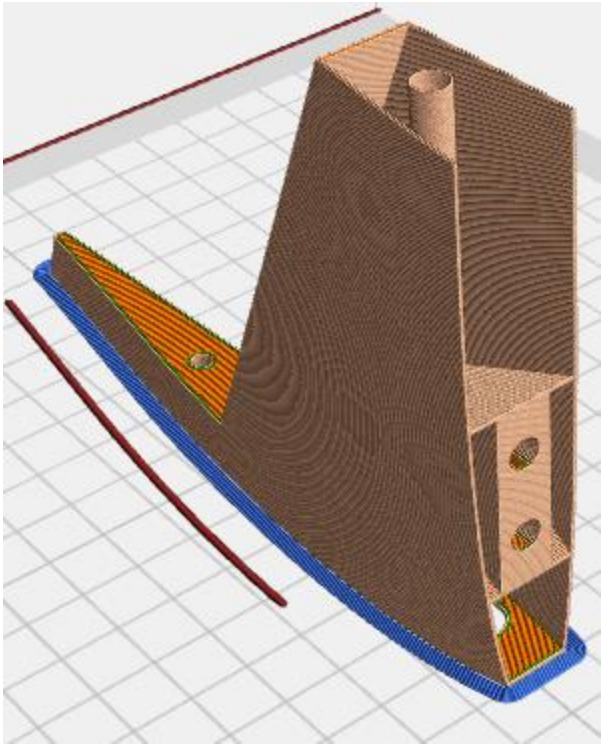

Figure 16.30 – Right trailing edge, wingtip

16.5.5 Elevons

Although the left and right elevons are split, they are printed in a single pass. The printed parts all use a brim.

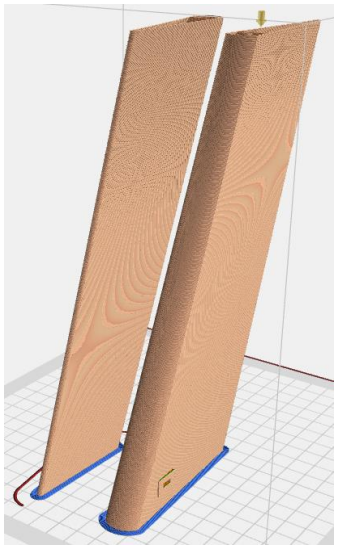

Figure 16.31 – Left elevon

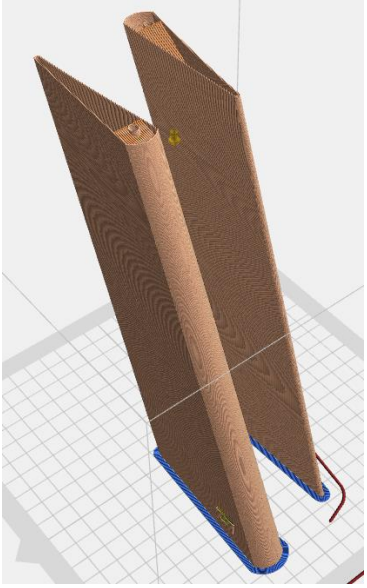

Figure 16.32 – Right elevon

16.5.6 Winglets

The winglets are printed together. They use both a brim, and a support structure to stabilize the winglet alignment node.

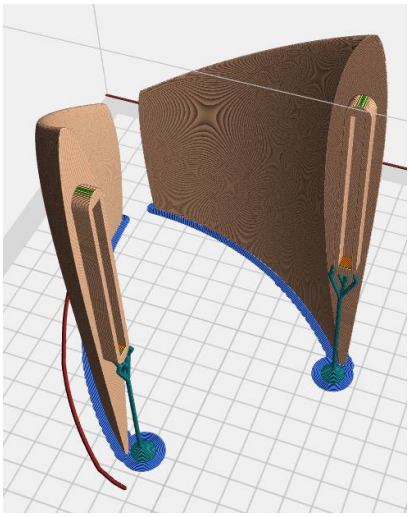

Figure 16.33 – Winglet

16.6 Conclusion

After printing, the support for a few components was failing. However, due to the overall print being successful, these errors were negligible and could be fixed by increasing the post diameter. However, this would have come at the cost of the ease of removal.

Chapter 17 — Production Costs

The production costs cover the financial costs it takes to construct the aircraft. The following lists does not cover the cost of miscellaneous items, such as scissors, disposable glovers, solder, etc.

17.1 Tools

Table 17.1 – Tools used and cost

Component	**Cost (USD)**
3D Printer	$380
Glue	$18
Total	$398

17.2 Airframe 3D Printing

The estimated weight is influenced by not only the structure of the aircraft, but the supports and brim used to stabilize the component as the 3D printer works. The cost of each component is based on $15 / kg of PLA. The estimated weight is calculated using FlashPrint 5.

Table 17.2 – Nose characteristics

Nose	**Weight (gram)**	**Print time**
Left	83.1	3 hrs, 46 min
Right	89.37	4 hrs, 4 min
Top & Bottom Electronic Hatch	77.88	3 hrs, 42 min
Total	**250.35**	**12 hrs, 32 min**

Table 17.3 – Nose characteristics

Fuselage	**Weight (gram)**	**Print time**
Front Left	151.83	5 hrs, 2 min
Front Right	152.65	4 hrs, 55 min
Mid Left	125.6	3 hrs, 32 min
Mid Right	125.49	3 hrs, 49 min
Rear	106.14	4 hrs, 37 min
Top Electronic Hatch	24.69	49 min
Total	**686.4**	**22 hrs, 44 min**

Table 17.4 – Left wing characteristics

Left Wing	**Weight (gram)**	**Print time**
Leading Edge 1	79.18	2 hrs, 21 min
Leading Edge 2	40.47	1 hr, 17 min

Leading Edge 3	12.89	26 min
Trailing Edge 1	90.54	2 hrs, 39 min
Trailing Edge 2	36.43	1 hr, 3 min
Trailing Edge 3	17.68	26 min
Total	**277.19**	**8 hrs, 12 min**

Table 17.5 – Right wing characteristics

Right Wing	**Weight (gram)**	**Print time**
Leading Edge 1	79.18	2 hrs, 23 min
Leading Edge 2	40.46	1 hr, 16 min
Leading Edge 3	12.89	24 min
Trailing Edge 1	90.73	2 hrs, 39 min
Trailing Edge 2	36.49	1 hr, 2 min
Trailing Edge 3	17.71	29 min
Total	**277.46**	**8 hrs, 13 min**

Table 17.6 – Elevon characteristics

Elevon	Weight (gram)	**Print time**
Left elevon	71.67	2 hrs, 10 min
Right elevon	71.66	2 hrs, 10 min
Total	**143.44**	**4 hrs, 20 min**

Table 17.7 – Winglet characteristics

Winglet	**Weight (gram)**	**Print time**
Left & Right	89.93	2 hrs, 27 min
Total	**89.93**	**2 hrs, 27 min**

Table 17.8 – Total airframe production cost

Component	Weight (grams)	Cost (USD)	Print Time
Nose	250.35	$3.76	12 hrs, 32 min
Fuselage	686.4	$10.30	22 hrs, 44 min
Left Wing	277.19	$4.16	8 hrs, 12 min
Right Wing	277.46	$4.16	8 hrs, 13 min
Elevon	143.44	$2.15	4 hrs, 20 min
Winglet	89.93	$1.35	2 hrs, 27 min
Total	**1724.77**	**$25.87**	**60 hrs, 28 min**

17.3 Electronics Costs

Table 17.9 – Electronic cost

Number	Component	Cost (USD)
1x	Flight Controller	$64
1x	Electronic Speed Controller	$20
2x	Servo	$10 each
1x	Radio Receiver	$27
1x	Video Transmitter	$25
1x	Antenna	$20
1x	Battery	$21
1x	GPS	$20
1x	Motor	$20
	Total	**$237**

17.4 Structural Costs

Table 17.10 – Carbon fiber tubes

Number	Component	Cost (USD)
2x	300 mm x 5 mm carbon fiber tubes	$3 each
2x	200 mm x 5 mm carbon fiber tubes	$2 each
2x	500 mm x 3 mm carbon fiber tubes	$5 each
3x	Antenna Covers	$2 each
	Servo Pushrods & Micro Control Horns	$8
	Total	**$34**

17.5 Final Price

Table 17.11 – Total costs

Component Category	Price
3D-Printed Airframe	$25.87
Electronics Components	$237
Structural Components	$34
Total	**$296.87**

Chapter 18 — Assembly

18.1 Introduction

The assembly process is split into two main portions. The first portion is the component assembly. This is the part where all the components that were previously split are glued together. This means that by the end of the process, the individual left wing, right wing and fuselage are all in one piece. The electronics used in the aircraft are installed at this time as well. The next portion is in-field assembly. During in-field assembly, the left and right wings will be attached to the fuselage, the servos connected to the flight controller, the battery enabled, propeller installed, and the electronic hatches closed. The in-field assembly is designed to be simple, and quick to do.

18.2 Wing Assembly

The elevons are the first to be glued together. The wings are attached together based on their position along the wing, so the wing-root, mid-wing, and wingtips parts are attached together. These parts are then connected, with the help of the wing alignment system discussed in 15.2.2. The control tabs are also attached to the elevons with the usage of glue. To secure the elevons to the wings, the 3mm x 500 mm carbon fiber rod that was discussed in 14.4 is used. The winglets are the last wing component to be installed. As for the servo, it can be slid and then secured in place with the usage of M2 screws. The servo would manipulate the elevon with the usage of a pushrod. Tape is used to cover the servo wiring channel.

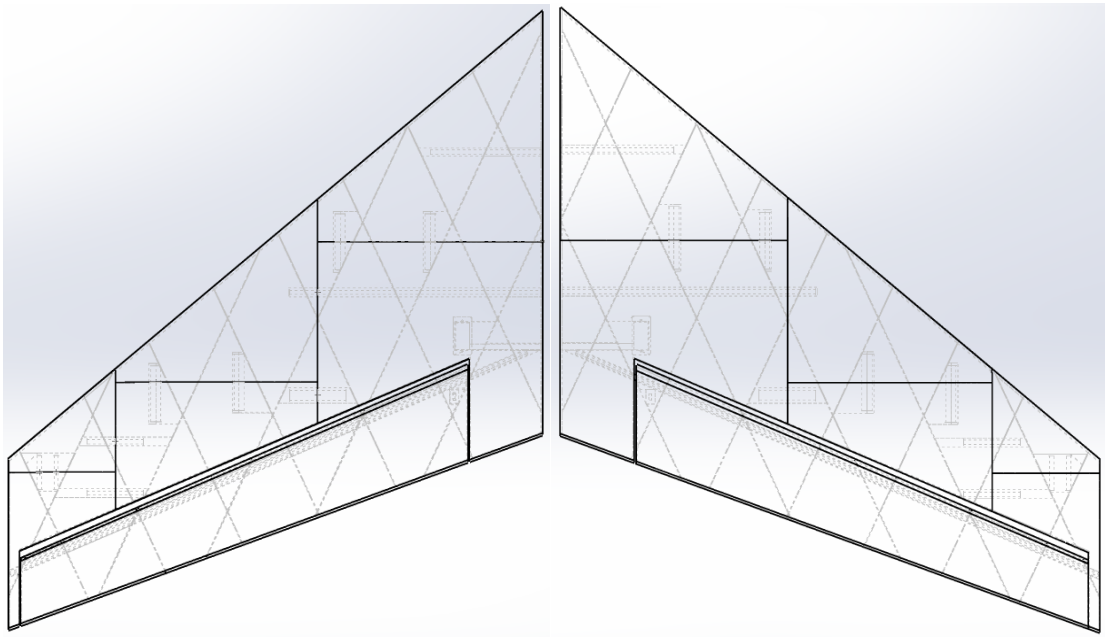

Figure 18.1 – Full wing assembly simulation

Figure 18.2 – Left & right wing assembly

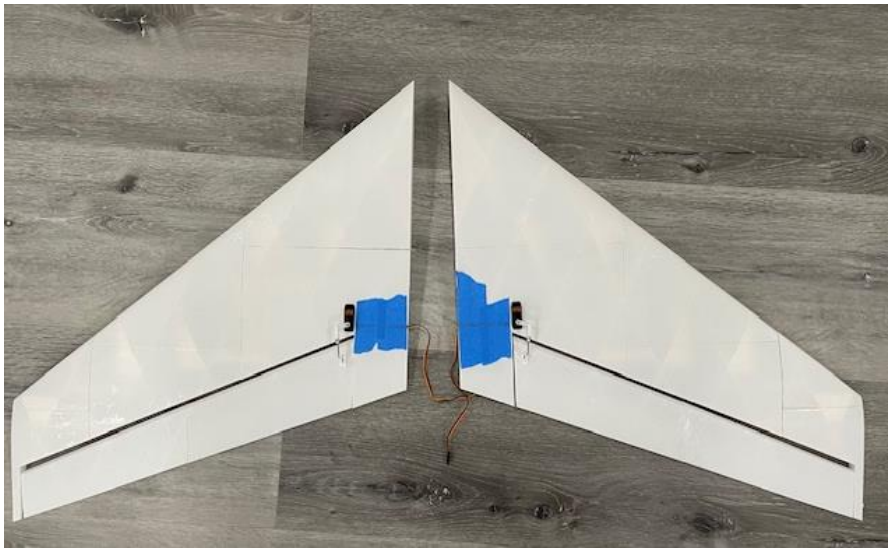

Figure 18.3 – Left & right wing assembly (underside)

Figure 18.4 – Left & right wing assembly (w/ winglets)

Figure 18.5 – Servo close-up

18.3 Fuselage Assembly

The side-to-side alignment system is used to assemble the 4 portions that make up the fuselage, the nose, the mid fuselage, the rear fuselage, and the tail. To prevent issues with installation, the motor would also be installed at the rear fuselage while the camera would be installed in the nose, early on. The mid fuselage, rear fuselage, and tail would be glued together first, while the nose would be put on last. Once the airframe is complete, the electronics can be secured. In this case, tape is used due to difficulties securing the components with fasteners.

Figure 18.6 – Nose assembly

Figure 18.7 – Mid fuselage

Figure 18.8 – Rear fuselage

Figure 18. 9 – Tail Assembly

Figure 18.10 – Motor mount

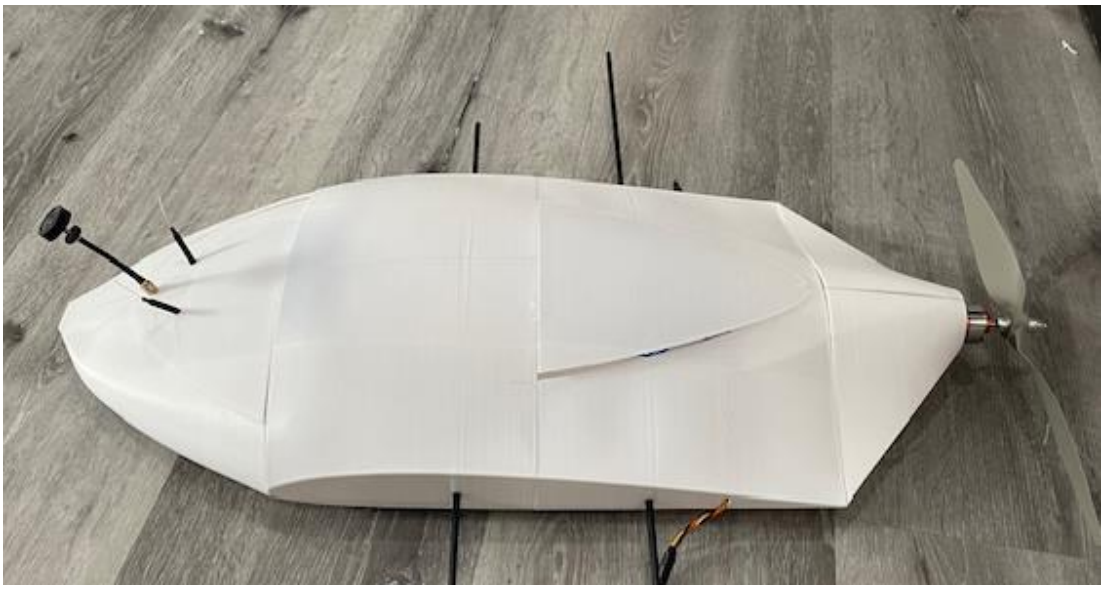

Figure 18.11 – Fuselage assembly

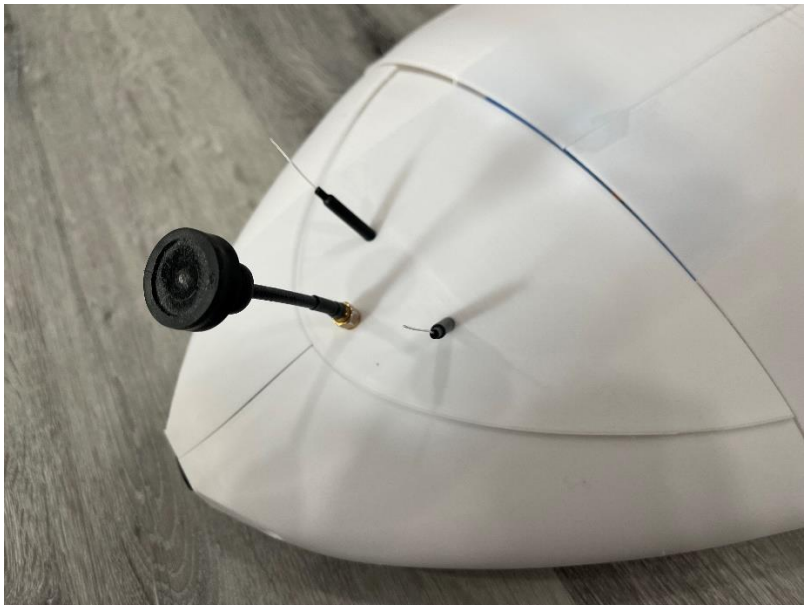

Figure 18.12 – Nose

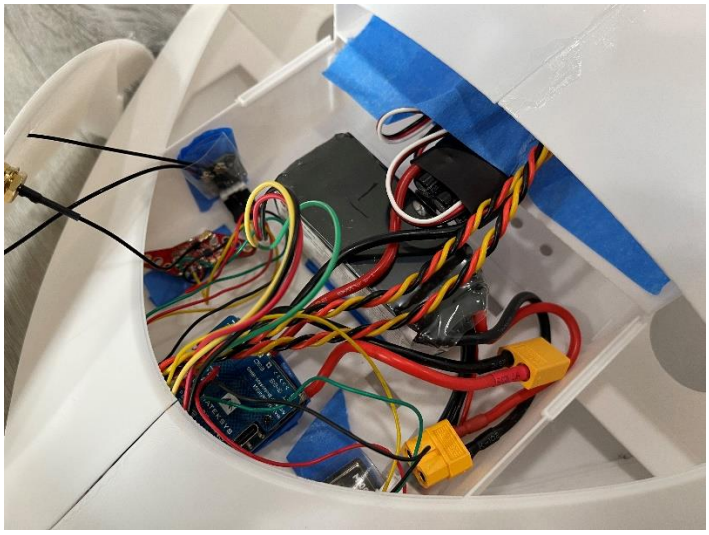

Figure 18.13 – Nose electronics

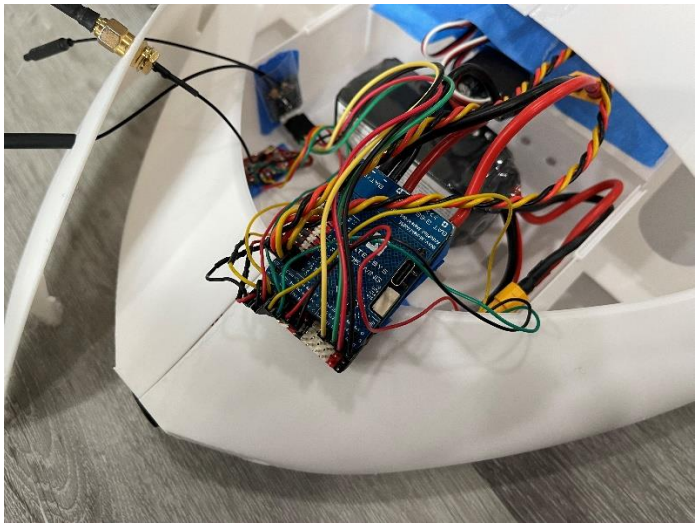

Figure 18.14 – Nose electronics (exposed FC)

18.4 In-Field Assembly

The left and right wings would be installed in the field to make the aircraft more storable. They would slide into place with the usage of the fuselage-wing support discussed in 14.3. The servos would be connected to a pair of extension wires that would connect them to the flight controller. To access the drone electronics, the top and bottom of the nose are detachable, and can be secured before flight with tape. Both the battery and the propeller are the last components to be installed for safety. After setup and a control test, the aircraft would be able to fly.

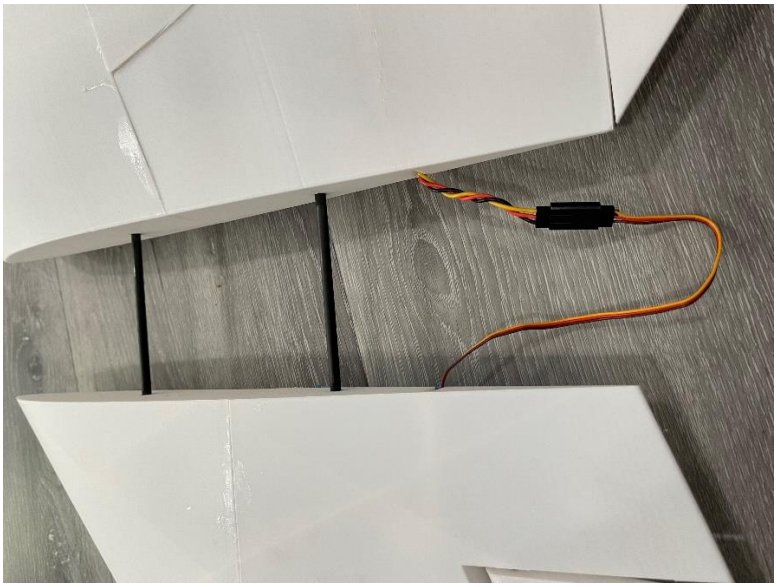

Figure 18.15 – Wing mount (w/ servo connections)

Figure 18.16 – Beansky side-view

Figure 18.17 – Beansky top-view

Figure 18.18 – Beansky isometric-view

Chapter 19 — Closing Remarks

19.1 Fuselage Design Changes

After construction of the mock-up, it was revealed that Beansky's build quality is inconsistent. To improve the build quality of the fuselage, the team recommends redesigning the fuselage to be narrower to reduce weight and reduce the number of prints needed. Larger electronic hatches are required to access the electronics stored within the aircraft. Furthermore, it is noted that the fasteners were difficult to attach to the airframe, which is why tape was used, and that more access to the underside of the electronics platform should be utilized. To reduce weight, the material used could also be changed, from PLA to Lightweight PLA. The size of the carbon fiber tubes used to connect the wings and fuselage together can be standardized to reduce complexity.

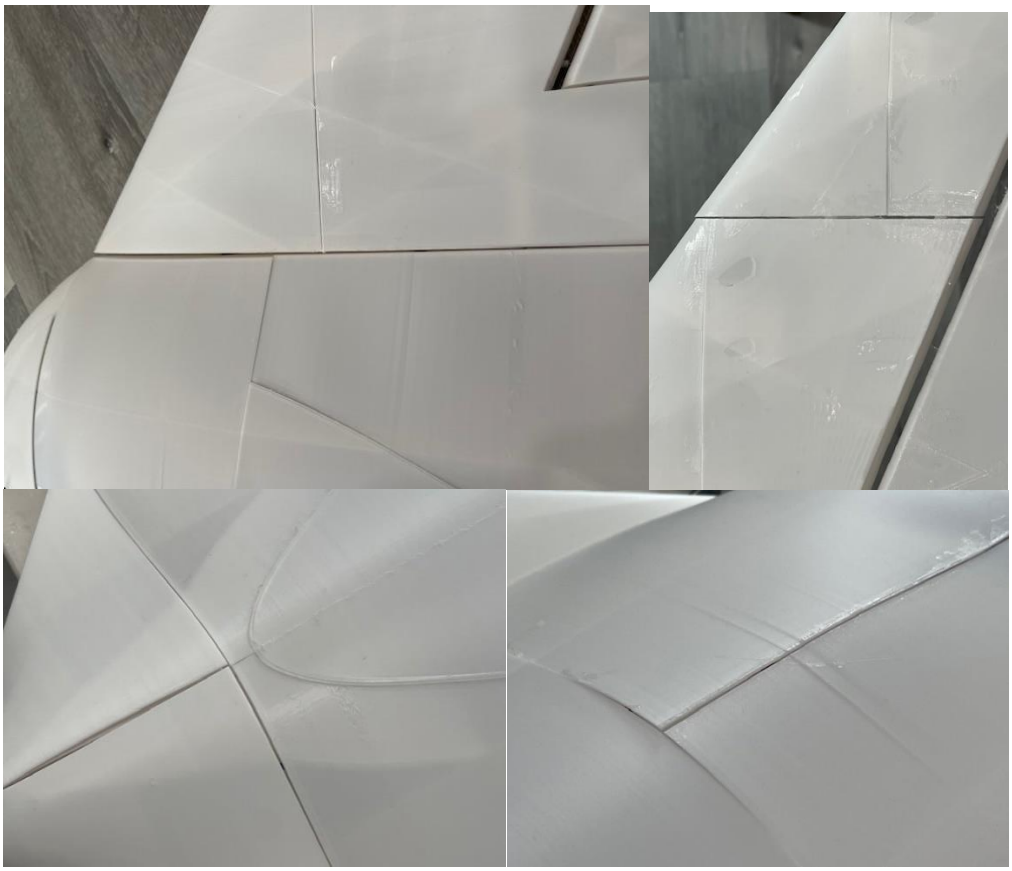

Figure 19.1 – Inconsistent airframe examples

19.2 Electronics

The main barrier to entry for the drone would be the cost. The total cost of the electronics is estimated to be $237. For context, that is roughly 9 times more expensive than the airframe itself. To combat this, an Arduino-based flight controller could be used to lessen the cost, combining the GPS and FC to one component would reduce wiring complexity. However, the video transmitter, RC receiver, battery, and servos would have to remain sourced from the market, making them expensive to acquire.

19.3 Final Thoughts

The entire point of the project was not only to design an aircraft, but to learn and discover both the positive and negatives 3D printing has. By the end of the project, 3D printing has shown to be a valuable tool for manufacturing, with the team making use of rapid prototyping to quickly modify the design when problems arise. For example, early versions of the wing were reliant on the glue to connect each other. When prints were made and it was time to attach each part together, the prints were unstable, with some parts of the wing deforming due to the glue. To fix this issue the wing-alignment system seen in 15.2.2 was created and used. There was a total of roughly 26 prints that were rejected due to a myriad of issues, including poor conductivity between components, sizing issues between the carbon fiber tubes and the airframe, etc. Beansky itself is not perfect as seen in the design changes recommended, it has proven itself to be a valuable proof-of-concept.

References

[1] Fu, X., Lin, Y., Yue, X.-J., Hur, B., and Yue, X.-Z., "A Review of Additive Manufacturing (3D Printing) in Aerospace: Technology, Materials, Applications, and Challenges," *Mobile Wireless Middleware, Operating Systems and Applications,* No. 1, 2022, pp.73-98.

[2] Kennedy R., "Outside the Box: How GE Aviation Entered the Brave New World of Additive Manufacturing," GE Aerospace, 2019. Retrieved from https://www.geaerospace.com/news/articles/100-year-anniversary-manufacturing-technology/outside-box-how-ge-aviation-entered-brave

[3] "How Greg Morris created the 3D printed nozzle for GE's LEAP engine," VoxelMatters, 2017. Retrieved from https://www.voxelmatters.com/ge-reveals-greg-morris-created-3d-printed-nozzle-leap-jet-engine/

[4] Jasiuk, I., Abueidda, D. W., Kozuch, C., Pang, S., Su, F. Y., and McKittrick, J., "An Overview on Additive Manufacturing of Polymers," *The Journal of the Minerals, Metals & Materials Society (TMS)*, Vol. 70, No. 3, 2018, pp. 275–283. https://doi.org/10.1007/s11837-017-2730-y

[5] Kalender, M., Kilic, S. E., Ersoy, S., Bozkurt, Y., and Salman, S., "Additive Manufacturing and 3D Printer Technology in Aerospace Industry," *2019 9th International Conference on Recent Advances in Space Technologies (RAST),* Istanbul, Turkey, 2019. https://doi.org/10.1109/rast.2019.8767881

[6] Prashar, G., Vasudev, H., and Bhuddhi, D., "Additive Manufacturing: Expanding 3D Printing Horizon in Industry 4.0," *International Journal on Interactive Design and Manufacturing (IJIDeM)*, Vol. 17, No. 5, 2023, pp. 2221–2235. https://doi.org/10.1007/s12008-022-00956-4

[7] Moon, S. K., Tan, Y. E., Hwang, J., and Yoon, Y.-J., "Application of 3D Printing Technology for Designing Light-Weight Unmanned Aerial Vehicle Wing Structures," *International Journal of Precision Engineering and Manufacturing-Green Technology*, Vol. 1, No. 3, 2014, pp. 223–228. https://doi.org/10.1007/s40684-014-0028-x

[8] Wood, A., "Wing Loads and Structural Layout," AeroToolbox, 2022. Retrieved from https://aerotoolbox.com/wing-structure/

[9] Dobrenez, T. L., Spadoni, A., and Jorgensen M., "Aviation Archeology of the Horten 229 v3 Aircraft," *10th AIAA Aviation Technology, Integration, and Operations (ATIO) Conference, Fort Worth Texas*, 2012. https://doi.org/10.2514/6.2010-9214

[10] Correll, J. T., "Jack Northrop and the flying wing," *Air Force magazine*, Vol. 100, No. 2, 2017. Retrieved from https://www.airandspaceforces.com/article/jack-northrop-and-the-flying-wing/

[11] Liddle, S. C., "Pearcy, Newby, and the Vulcan," *Journal of Aeronautical History,* 2021, pp 117-159. Retrieved from https://www.aerosociety.com/publications/jah-pearcey-newby-and-the-vulcan/

[12] Wood, R. M., and Bauer. S. X. S., "Flying wings/flying fuselage." *39th AIAA Aerospace Sciences Meeting & Exhibit,* Reno, Nevada, 2001. https://doi.org/10.2514/6.2001-311

[13] "Northrop N-1M," *Smithsonian National Air and Space Museum.* Retrieved from https://airandspace.si.edu/collection-objects/northrop-n-1m/nasm_A19600302000

[14] Torenbeek, E., "Aerodynamic Performance of Wing-Body Configurations and the Flying Wing," *SAE Transactions,* Vol. 100, 1991, pp. 158-163. https://www.jstor.org/stable/44547589

[15] Martínez-Val, R., Martinez Cabenza, J. A., and Perez, E., "Flying Wings and Emerging Technologies: An Efficient Matching," *International Council of Aeronautical Sciences,* 2004. *https://www.icas.org/ICAS_ARCHIVE/ICAS2004/PAPERS/044.PDF*

[16] Stenfelt, G., and Ringertz, U., "Yaw Control of a Tailless Aircraft Configuration," *Journal of Aircraft*, Vol. 47, No. 5, 2010. https://doi.org/10.2514/1.C031017

[17] Harris, T., "How Stealth Bombers Work," HowStuffWorks. Retrieved from https://science.howstuffworks.com/stealth-bomber2.htm

[18] El Adawy, M., Abdelhalim E. H., Mahmoud M., Ahmed Abo zeid, M., Mohamed I. H., Othman M. M., ElGamal, G, S., and ElShabasy, Y. H., "Design and fabrication of a fixed-wing Unmanned Aerial Vehicle (UAV)," *Ain Shams Engineering Journal*, Vol. 14, No. 9, 2023. https://doi.org/10.1016/j.asej.2022.102094

[19] Millard, J., Booth, S., Rawther, C., Hayashibara, S., "Xflr5 as a design tool in remotely controlled design-build-fly applications," *AIAA SCITECH 2022 Forum*, San Diego, California, 2022. https://doi.org/10.2514/6.2022-0003

[20] Panagiotopoulos, I., Sakellariou, L., and Hatziefremidis, A., "Design, Construction, and Flight Performance of an Electrically Operated Fixed-Wing UAV," *Drones*, Vol. 8, No. 6, 2024, p. 217. https://doi.org/10.3390/drones8060217

[21] Sharma, S., Sharieff, U., Singh, A., and Tarnacha, R. S.,"Design and Fabrication of Fixed-Wing UAV for Commercial Monitoring," *International Research Journal of Engineering and Technology,* Vol. 8, No. 8, 2021, pp. 1153-1177. https://www.irjet.net/archives/V8/i8/IRJET-V8I8162.pdf

[22] Chung, P.-H., Ma, D.-M., and Shiau, J.-K., "Design, Manufacturing, and Flight Testing of an Experimental Flying Wing UAV," *Applied Sciences*, Vol. 9, No. 15, 2019, p. 3043. https://doi.org/10.3390/app9153043

[23] "Skywalker X8 Strong Composite 23122 mm UAV Fixed Wing," *UAV Model Co., Limited.* Retrieved from https://www.uavmodel.com/products/skywalker-x8-strong-composite-2122mm-uav-fixed-wing?variant=39912047640730

[24] "Super Stingray – Flightory," Flightory. Retrieved from https://flightory.com/product/superstingray/

[25] "Eclipson EGW-80 Fast FPV Plane," Eclipson Airplanes. Retrieved from https://www.eclipson-airplanes.com/egw-80

[26] Raymer, Daniel P., "Electric Aircraft," *Aircraft Design: A Conceptual Approach,* 6th ed., American Institute of Aeronautics and Astronautics, Virginia, 2018, pp.735-762.

[27] Hall N., "Navier-Stokes Equations," *NASA,* 2021. Retrieved from https://www.grc.nasa.gov/www/k-12/airplane/nseqs.html

[28] "Turnigy D3536/5 1450KV Brushless Outrunner Motor v2," RapidRCModels. Retrieved from https://www.rapidrcmodels.com/turnigy-d35365-1450kv-brushless-outrunner-motor-v2-306-p.asp

[29] "Flight Controller F405-Wing V2," MATEKSYS. Retrieved from https://www.mateksys.com/?portfolio=f405-wing-v2#tab-id-3

[30] "HGLRC M100-5883 GPS Compass Module, upgraded 10th Generation Chip Compatible with FPV Fixed-Wing UAV," Amazon. Retrieved from https://www.amazon.com/dp/B0CB5N8RQ8?psc=1&ref=ppx_pop_dt_b_product_details

[31] "EMAX ES08MA II 12g Mini Metal Gear Analog Servo for RC Model," Amazon. Retrieved from https://www.amazon.com/dp/B07KYK9N1G?psc=1&ref=ppx_pop_dt_b_product_details

[32] "HOBBYWING Skywalker 50A V2," Amazon. Retrieved from https://www.amazon.com/HOBBYWING-Skywalker-50A-V2-UBEC/dp/B0BZWZJXWN/142-8866212-7693657?pd_rd_w=XRpUe&content-id=amzn1.sym.00d8f370-c2ec-4432-aa57-10d669af24cb&pf_rd_p=00d8f370-c2ec-4432-aa57-10d669af24cb&pf_rd_r=DGMRQ5Y8G2EMRHEWAQXN&pd_rd_wg=C8IfU&pd_rd_r=244e2db9-84c6-4b92-9acb-afa4e756efed&pd_rd_i=B0BZWZJXWN&psc=1

[33] "OVONIC 4S Lipo Battery 35C 2200 mAH 14.8V Lipo Battery with XT60 Connector for Airplane RC Quadcopter Helicopter FPV Drone," Amazon. Retrieved from https://www.amazon.com/dp/B08R71SWJ3?psc=1&ref=ppx_pop_dt_b_product_details

[34] "Matek Systems 2.4G ExpressLRS ELRS ELRS-R24-D Diversity Rx Receiver Support CRSF Protocol for Micro Carbon Fiber Long Range FPV Racing Quadcopter Quad Frame kit RC Drone Frame," Amazon. Retrieved from https://www.amazon.com/dp/B09NY89VHP?ref_=ppx_hzsearch_conn_dt_b_fed_asin_title_1

[35] "FPV Camera RunCam Phoenix 2 SE - Special Edition Micro Drone Camera With lens hood 5.8ghz FOV160°Global WDR 8.6g for RC FPV Car Plane Racing Drone," Amazon. Retrieved from https://www.amazon.com/dp/B0BQ2FVKWN?ref_=ppx_hzsearch_conn_dt_b_fed_asin_title_1

[36] "HGLRC Zeus350mW VTX M2 M3 16x16 20x20 25.5x25.5 5.8GHz Built-in Microphone Switchable FPV Transmitter VTX Betaflight for FPV Racing Drone Quad (SMA)," Amazon. Retrieved from https://www.amazon.com/dp/B08MQ4ZDVF?ref_=ppx_hzsearch_conn_dt_b_fed_asin_title_1

[37] "HobbyPark Nylon Micro Control Horns 20x11mm 4 Holes for RC Airplane Remote Control Foam Electric Park Flyers Parts," Amazon. Retrieved from https://www.amazon.com/Hobbypark-Control-Airplane-Remote-Electric/dp/B019I79ZG0

[38] “The difference between tree support and linear support in 3d printing settings,” Flashforge, 2016. Retrieved from https://www.flashforge.com.hk/blog/the-difference-between-tree-support-and-linear-support-in-3d-printing-settings2981816

[39] “Rafts, Skirts and Brims!” Simplify3D. Retrieved from https://www.simplify3d.com/resources/articles/rafts-skirts-and-brims/

Appendix A. Weight Sizing MATLAB Code

```
%% Weight Sizing
% By: Aaron Do
clear
clc
format shortG

% Aircraft Payload + Crew (Open to interpretation)
    Wcrew = 0;    % Newtons [0 kg]
    Wpayload = 10; % Newtons [1 kg]  % Sensors

% Guess for gross takeoff weight
% Update this value based on results (Iterative Design)
    W0guess = 56.45; % Newtons [5 kg] (12 lbs)

% Raymer Table 3.1: Empty Weight Fraction vs W0
    % UAV-small:
    A = 0.97;
    C = -0.06;
    Kvs = 1;

% Empty weight fraction based on takeoff weight guess and type of aircraft
    We_W0 = A*W0guess^C*Kvs; % Raymer Table 3.1
    g = 9.8; % Gravity [m/s]
    m_b = 0.178; % Battery Mass [kg]
    E_sb = 200; % Wh/kg (LiPo Battery is 100-265)

      eff_b = 0.9; % Battery-to-System Efficiency
      eff_p = 0.7; % Propeller Efficiency
      P_used = 2.2*14.8/1000; % 2.2 Amp & 14.8 V (Full Charge) [kW]
      LD = 10; % Assumed Lift-Drag Ratio
      m =  W0guess/g; % mass of AC [kg]
      pW = P_used/m; % Calucated Thrust-to-Weight Ratio

  % Desired Flight Characteristics
      V = 70; % Velocity (km/h)
      h = 100; % height (m)

  % Loiter-Time Endurance
      E_Loiter = 3.6*LD*(E_sb*eff_b*eff_p*m_b)/(g*V*m);
  % Level Flight Range
      R = 3.6*LD*(E_sb*eff_b*eff_p*m_b)/(g*m);
  % Vertical Velocity
      V_V = ((1000*eff_p*pW)/g)-(V/(3.6*LD));

  % Battery Mass Fraction
  % Loiter Battery Mass Fraction (Eq: 20.7)
      BMF_Loiter = (E_Loiter*V*g)/(3.6*E_sb*eff_b*eff_p*LD);
  % Cruise Battery Mass Fraction (Eq: 20.8)
      BMF_Cruise = (R*g)/(3.6*E_sb*eff_b*eff_p*LD);
  % Climb Battery Mass Fraction (Eq: 20.8)
      BMF_Climb = (h*pW)/(3.6*V_V*E_sb*eff_b);

% Total Battery Mass Fraction
    BMF_Total = BMF_Climb + BMF_Cruise + BMF_Loiter

% Calculated takeoff weight
    W0 = (Wcrew + Wpayload) / (1 - BMF_Total - We_W0) % lbs or kg
    PctDiff = (W0-W0guess)/W0guess*100 % percent differeance (to determine accuracy)

```

Appendix B. SOLIDWORKS Mass And CoM Calculations